November 2020

Posttranslational Modification and Protein Disorder Regulate Protein-Protein Interactions and DNA Binding Specificity of p53

Robin Levy
University of South Florida

Posttranslational Modification and Protein Disorder Regulate Protein-Protein Interactions and DNA Binding Specificity of p53

by

Robin Levy

A dissertation submitted in partial fulfillment
of the requirements for the degree of
Doctor of Philosophy
Department of Cell Biology, Microbiology, and Molecular Biology
College of Arts and Sciences
University of South Florida

Major Professor: Gary Wayne Daughdrill, Ph.D.
Younghoon Kee, Ph.D.
Meera Nanjundan, Ph.D.
Sameer Varma, Ph.D.

Date of Approval:
November 9, 2020

Keywords: Intrinsically disordered proteins, phosphorylation, phosphomimetics, NMR, transient secondary structure

Acknowledgments

This work would not have been possible without the guidance of Dr. Gary Daughdrill or through the funding of his grants: National Institutes of Health (NIH) (1R01GM115556-01A1) and (2R01CA14124406-A1). I would also like to thank my academic committee Dr. Younghoon Kee, Dr. Meera Nanjundan and Dr. Sameer Varma for their help, support, and patience. Some of the work presented in this project was done with the help of other lab members like our previous post-doc, Wade Borcherds who carried out some of the NMR experiments. Also a fellow lab member and Ph.D. student, Emily Gregory-Lott, who carried out some of the ITC experiments involving KIX and assisted with data analysis of the DNA binding experiments.

Table of Contents

List of Tables

List of Figures

Abstract

p53 is an intrinsically disordered transcription factor that suppresses tumor development by arresting the cell cycle and promoting DNA repair. p53 deletions or mutations can lead to cancer due to the inability of cells to respond to stress. The protein levels and post-translational modification state of p53 changes in response to cellular stress like DNA damage. Previous studies have shown that p53 can undergo coupled folding and binding with the E3 ubiquitin ligase, Mdm2, and the histone deacetylase, p300. In normal cells, p53 is kept at a low level by Mdm2, which marks it with ubiquitin, targeting p53 for proteasome degradation. In turn, p53 activates the transcription of Mdm2. This negative feedback loop not only regulates p53 levels but also the fate of the cell. In stressful conditions, such as DNA damage, p53 levels increase within the nucleus, where it becomes active and induces cell growth arrest or apoptosis.

p53 consists of discrete domains that participate in sequence-specific DNA binding, tetramerization, and transcriptional activation. p53 contains two transactivation domains (TAD1 and TAD2), that contain multiple phosphorylation sites. The disordered p53 transactivation domain (p53TAD) contains specific levels of transient helical secondary structure that are necessary for its binding to the negative regulators, Mdm2 and MdmX. The interactions of p53 with Mdm2 and MdmX are also modulated by posttranslational modifications (PTMs) of p53TAD including phosphorylation at S15, T18 and S20 that inhibits p53-Mdm2 binding. It is unclear whether the levels of transient secondary structure in p53TAD are changed by phosphorylation or other PTMs. We used

phosphomimetic mutants to determine if adding a negative charge at positions 15 and 18 has any effect on the transient secondary structure of p53TAD and protein-protein binding. Using a combination of biophysical and structural methods, we investigated the effects of single and multisite phosphomimetic mutations on the transient secondary structure of p53TAD and its interaction with Mdm2, MdmX, and the KIX domain. The phosphomimetics reduced Mdm2 and MdmX binding affinity by 3-5-fold, but resulted in minimal changes in transient secondary structure, suggesting that the destabilizing effect of phosphorylation on the p53TAD-Mdm2/MdmX interaction is primarily electrostatic. Phosphomimetics had no effect on the p53-KIX interaction, suggesting that increased binding of phosphorylated p53 to KIX may be influenced by decreased competition with p53 negative regulators.

Previous studies have shown that there is an intramolecular interaction between p53TAD and the DNA binding domain of p53 and that this interaction can reduce sequence-specific DNA binding. We aim to determine whether mutations within TAD2 combined with site-specific phosphorylation can decrease p53-DNA binding. Two consecutive hydrophobic residues within TAD2 (W53, F54), which are surrounded by acidic amino acids, are essential for the activity of the transactivation domain. We will determine the effect that these mutated sites have on DNA binding. Using biophysical methods, we investigated the effects of point mutations and phosphomimetic mutations on the interaction between p53 and DNA. Our binding data shows that phosphomimicry of the p53TAD decreases DNA binding affinity, while substituting the hydrophobic residues, (W53, F54), with acidic residues within TAD2 of p53 increases DNA binding. By determining the impact that phosphorylation has on the binding affinity of p53 we will

identify a new understanding of the structure and function of not just p53 but other intrinsically disordered proteins.

Chapter One: Introduction of intrinsically disordered proteins

General characteristics

Many proteins are classified as ordered proteins, capable of forming stable secondary, tertiary and even quaternary structures. These proteins have adopted these complex folded structures in order to perform cellular functions. In the past two decades, a group of proteins have emerged that do not have these following characteristics. These proteins, called intrinsically disordered proteins (IDP), are highly dynamic and lack a fixed or ordered structure. They form specific heterogeneous conformational ensembles that fluctuate over time [6-10]. IDPs are structurally very different from ordered proteins and tend to have distinct properties in terms of function, sequence, interactions, evolution and regulation [9, 11, 12]. A polypeptide's function is determined by its amino acid sequence. The composition of amino acid residues in ordered proteins varies greatly from that of disordered proteins [13, 14]. Unlike ordered proteins, IDPs tend to have a higher proportion of residues with charged and polar side chains which allow for the repulsion of neighboring amino acids [13, 14]. They also have a lower number of residues that contain hydrophobic and bulky aromatic side chains [14]. All of these differences help prevent the formation of a compact structure and aids in maintaining their flexibility [14]. IDPs also tend to have lower sequence complexity than ordered proteins [15-18]. These different characteristics allow for the identification of disordered regions through the use of algorithms with 75-80% accuracy [15-18].

IDPs are widespread throughout nature and regulate many biological processes such as transcription, translation, cell signaling, and cell proliferation. A higher percentage of IDPs can be found more in eukaryotes than in prokaryotes or archaea [19, 20]. The enrichment of IDPs within eukaryotes has been predicted to be due to increased cellular organization [10, 20, 21]. Over one-third of eukaryotic proteins have been predicted to have disordered regions of 30 residues or longer [9, 19, 22].

Structure and function

Amino acid residue composition of IDPs varies greatly when compared to ordered proteins [23]. IDPs contain a low level of sequence complexity which exhibits a high level of polar-charged residues and a low level of hydrophobic residues [14, 24]. Intrinsically disordered regions (IDR) contain numerous structure interrupting amino acid residues like prolines and glycines [14]. These amino acids aid in extending IDRs which allow binding partners access to numerous attachment points. IDRs contain less bulky aromatic amino acids than ordered regions and longer insertion and deletion regions [25]. In aqueous solutions, all proteins maintain some degree of flexibility [26]. The presence of a high level of polar-charged residues in IDPs allows for the repulsion of neighboring amino acid residues, which aid in the prevention and destabilization of the formation of a compact structure, thus maintaining their flexibility [23]. The flexibility of IDRs allows binding to multiple protein partners, which is a common feature of IDPs [26]. Due to the constant variation of structure conformations within IDPs, they do not maintain an equilibrium state of their atoms and bond angles, thus making the phi and psi dihedral angles flexible, which suggests that IDPs exist in a random coil state [8, 27]. IDPs cover a range of different states from fully folded to partially folded [11, 22, 28, 29]. In addition to a lack of

hydrophobic residues, most IDPs contain a large number of charged residues than ordered proteins [17, 29]. This prevents the collapse of the protein through the repulsion of like charged residues. There are some IDPs that possess a neutral net charge in addition to few hydrophilic amino acid residues and these IDPs exist in collapsed forms [29, 30]. They form random structures but contain no defined secondary structures and are grouped in the pre-molten globule class of IDPs [22, 29, 30]. A special of class of IDPs, termed molten globules, contain a high fraction of hydrophobic residues, but a low level of folding. Within these IDPs energy exists in collapsed forms. They, unlike the pre-molten globule proteins, form stable secondary structures but unstable or no tertiary interactions [29, 31].

Several attempts have been made to organize IDPs into various classes based on varying degrees of dynamic behavior [19, 32]. Due to the different features of IDPs, i.e. being completely unstructured, having some transient secondary structure, or being configured in such a manner that ordered regions are joined together by flexible linkers, it is difficult to group these proteins based on their structure, sequence, biophysical and functional features [12]. Instead they are grouped into classes based on their evolution, function, and protein interactions [12].

Even though IDPs do not form stable structures they make up a large class of proteins that are functionally relevant. Many IDPs form numerous transient secondary structures and are known to go through various amounts of PTMs [33-35]. Despite their lack of structural stability, many IDPs undergo coupled folding and binding processes when they are bound to their targets [10, 33, 34]. This coupled folding and binding is key to the functional role IDPs play in cellular functions such as signaling and ligand

recognition and binding, in addition to harboring PTMs and acting as protein network hubs [33, 34].

Posttranslational modifications

Posttranslational modifications regulate the activity of IDPs [36, 37]. IDPs contain an enormous amount of PTMs which suggests that IDPs play an important role in cell signaling and regulation. Due to the increased flexibility of IDPs, as previously described, protein modifiers like phosphatases, ubiquitinases, and kinases have easier access to recognition and binding sites [38]. This flexibility also allows IDPs to take on various conformations which enables the binding of multiple partners over a short sequence, in addition to allowing IDPs to overcome steric hindrances in large complexes due to the IDP being able to wrap around its binding partner [8, 19]. These features of IDPs make them ideal for cellular processes involving PTMs, which require the binding of a protein to multiple macromolecules like protein modifiers [19]. PTMs of proteins can lead to conformational changes in IDRs and disorder to ordered transitions, and vice versa. This in turn can affect the binding and function of ordered and disordered proteins [39]. It is common for disordered regions to contain numerous phosphorylation sites. During phosphorylation, the phosphate group contains a double negative charge that affects protein conformation mainly due to the electrostatic effects that occur between the phosphate and surrounding charged atoms of the protein [35, 40]. These conformational changes can be local and/or long-range, effect protein-protein interactions, and increase or decrease levels of disorder [35].

Coupled folding and binding

Many IDPs undergo coupled folding and binding when they are bound to their targets [10]. This process involves the binding and folding of IDPs when they encounter their binding partner. The coupled folding and binding process is best explained through two models, conformational selection and induced fit [26, 41]. The conformational selection model is based on the hypothesis that an IDP will fluctuate between different conformational states that resemble the bound state leading to the binding of its protein partner [41]. In this model, the conformation of the IDP is selected by the binding partner in which the IDP will fold and then bind [41]. The induced fit model proposes an opposite type of interaction where the IDP first binds to the protein partner making multiple weak interaction conformations, then proceeds to fold into a tighter final bound state, in which it uses the binding partner as a template [41].

Evolution of intrinsically disordered proteins

As compared to ordered proteins, IDPs tend to evolve faster due to the numerous amino acid substitutions, insertions and deletions, and repeat expansions they encounter [42-44]. Even with the many amino acid substitutions, IDPs remain unaffected due to having fewer long-range intramolecular interactions and the lack of a hydrophobic core unlike that of ordered proteins [45]. In spite of the high mutation rates of IDPs, certain hydrophobic residues that they do contain like proline, leucine, phenylalanine, and tryptophan are highly preserved suggesting their importance in IDP binding and function [13, 19]. The evolutionary characteristics of IDPs may affect the evolution of PTMs that are found within IDPs compared to those found within ordered proteins [42]. As more information regarding the comparisons between homologous IDP families is discovered,

more insight into their flexibility, coupled folding and binding, and overall function can be provided.

Role in diseases

There are many diseases that are associated with IDPs and proteins containing IDRs. Aggregates of α-synuclein protein are accumulated in Parkinson's disease, Alzheimer's disease, and Down's syndrome [46-48]. Other IDPs associated with neurodegenerative diseases include amyloid-β and tau proteins which are also involved in Alzheimer's disease, prions which are associated with bovine spongiform encephalopathy, and ataxin which plays a major role in spinocerebellar ataxia [49, 50]. Other pathogenic IDPs involved in human diseases are amylin (type II diabetes), HIV-1 Rev protein (AIDS) and CFTR (cystic fibrosis) [51-53]. A previous study found that within an ordered/disordered protein, mutations within the IDRs can result in disease due to the loss of PTM sites as well as the conversion from disorder to order [54]. This study showed several mutations of IDPs that were associated with human diseases and are predicted to cause disorder to order conversions such as tumor suppressor p53, Troponin I3, Breast cancer type 1 susceptibility protein, and methyl CpG binding protein 2 [54].

p53 protein

p53 is an intrinsically disordered protein that acts as a tumor suppressor and cell cycle regulator. p53 plays a vital role in protection from the development of cancer which may arise from different types of cellular stress. The p53 pathway is frequently targeted for genetic alterations in cancer. Approximately half of all human tumors express defective p53 that have been mutated in its DNA-binding domain making it inactive as a transcription factor [55]. Breast cancer, soft tissue, and bone sarcoma account for over

50% of tumors in p53 mutation carriers, followed by adrenocortical carcinomas and brain tumors [56]. This transcription factor is activated following stress in which it regulates multiple downstream genes that are necessary for cell cycle control, antiangiogenesis, senescence, and apoptosis.

Structure

Understanding the structure of p53 is imperative to understanding its function. p53 contains a natively disordered N-terminal transactivation domain (TAD), which can be divided into two separate domains, TAD1 and TAD2. Following the TAD1 and TAD2 regions is a proline-rich region (PRR), which is connected to the structured DNA-binding domain (DBD) and the tetramerization domains (TD), which are connected to one another by a flexible linker region. The final domain of p53 is the regulatory carboxyl terminus (REG), which is similar to the TAD region in that it is also intrinsically disordered (see Figure 1). The TAD regions are essential for p53 transcriptional activity. They link gene recognition with expression by binding directly to the transcriptional coactivators p300/CREB-binding protein (CBP) as well as to other components of the basal

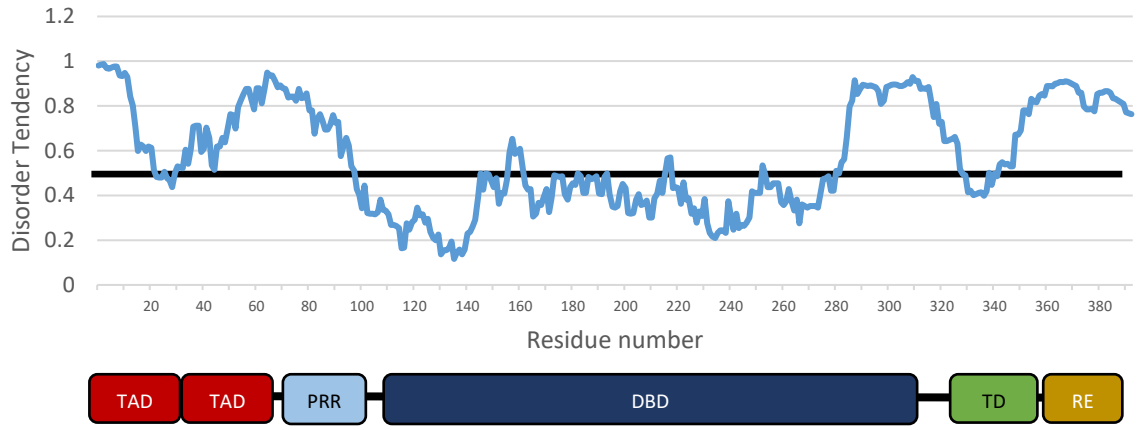

Figure 1 – Human p53 domain structure. IUPred disorder prediction plot (top). Domain structure of p53 corresponding to the residue positon of the overlaid plot (bottom). Values above 0.5 are predicted to be disordered.

transcription machinery [57, 58]. The TAD1 region becomes helical upon Taz2, Mdm2 and MdmX binding while the TAD2 region forms a helical structure upon binding to the replication protein A and transcription factor II H protein [59-63].

Regulation

In normal cells, p53 is present at low concentrations whereas, under the condition of cellular stress, such as DNA damage, p53 accumulates in the nucleus, where it is active [64]. The activation of p53 can lead to different responses depending on the type of cellular stress. DNA damage results in growth arrest in order for DNA to be repaired or apoptosis [65]. Cells that lack functional p53 are unable to respond to stress appropriately and this leads to the mutations and the development of cancer [66]. Under normal cellular conditions, mouse double minute 2 homolog (Mdm2) is continuously degrading p53, thus keeping p53 at low levels. p53 can transcriptionally activate Mdm2 resulting in the inhibition of p53 activity by Mdm2. In turn Mdm2 functions as an E3 ubiquitin ligase that recognizes the N-terminal TAD of p53 in which it is able to target p53 for degradation [67, 68]. Expression of Mdm2 initiates a negative feedback loop that regulates p53 and thus controls the fate of the cell [69-71]. Mdm2 also acts as an inhibitor of p53 transcriptional activation by binding to the p53TAD and inhibiting p53 mediated transactivation [72]. Mdm2 is also able to inhibit p53 transcriptional activity through its ability to transport p53 out of the nucleus to the cytoplasm due to its nuclear export signal [73, 74]. Mouse double minute 2 homolog, Mdm4, also known as MdmX is an additional Mdm2 family member that was also discovered to be an important negative regulator of p53. MdmX lacks the ubiquitin E3 ligase activity and is unable to target p53 for ubiquitin-proteasome-dependent proteolysis. However, MdmX is able to directly bind to p53 and inhibit its transcriptional

activity which is a function that has been found to be independent of Mdm2 [75-77]. MdmX can also stabilize Mdm2 by inhibiting the auto-degradation of Mdm2, which will increase Mdm2 accumulation and lead to increased degradation of p53 [78, 79].

Function

The model of p53 activation (see Figure 2) shows that cellular stress like DNA damage, activates signaling pathways that lead to the phosphorylation of the TAD regions which inhibit Mdm2 and MdmX binding. Some cellular stressors that can lead to p53 activation are X-ray and UV radiation, low pH, chemotherapeutic DNA damaging drugs, nitrous oxide, microtubule disruption, and prevention of RNA or DNA synthesis [1]. Since different cellular stresses elicit different kinases, p53 is able to produce a specific response based on which residues are modified and how they are modified [78-80]. Some of the heavily studied PTMs within p53 are within the Mdm2/MdmX binding site (See Figure 3). Numerous residues, serine and threonine, within the TAD are phosphorylated in cells immediately following DNA damage [80-82]. Loss of S15 phosphorylation has been shown to extend the half-life of p53 [83]. It is commonly known that the phosphorylation of S15 and T18 play a critical role in preventing the interaction with Mdm2 [80, 84-87]. S33 is phosphorylated in response to UV and ionizing radiation [88]. There has also been evidence that suggests p53 N-terminal phosphorylation can initiate C-terminal acetylation of the protein [88, 89]. The full schematic of p53 regulation is quite

complex and has yet to be completely understood, but the main mechanisms seem to involve the interactions between p53, Mdm2, MdmX and the PTMs [74, 90].

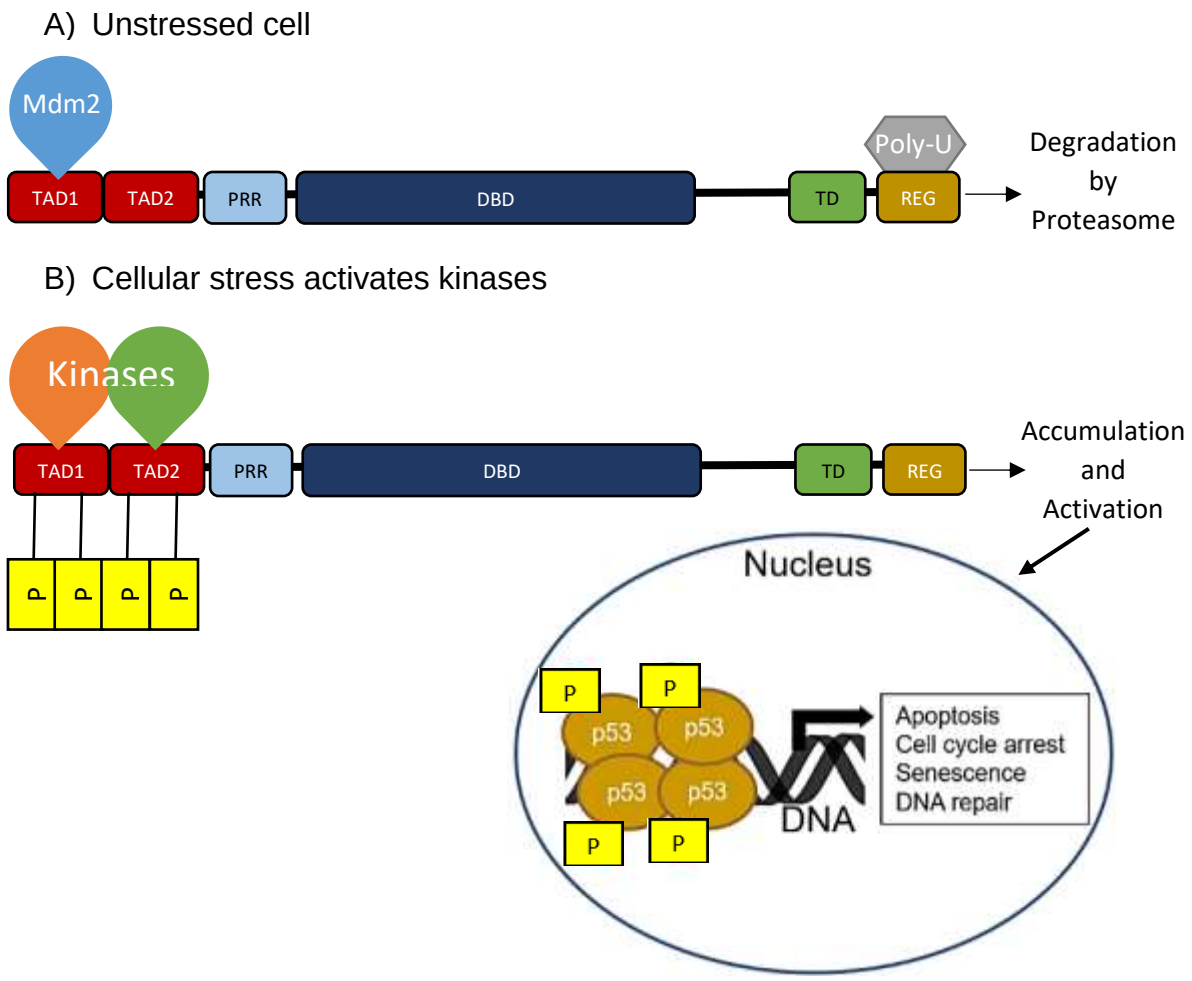

Figure 2 – Model of p53 regulation. A. In normal cells, p53 is regulated and kept at a low level by the E3 ubiquitin ligase MDM2, which marks it for ubiquitination leading to p53 degradation. In turn, p53 activates the transcription of MDM2. In stressful conditions, such as DNA damage, p53 level increase within the nucleus, where it becomes active and induces cell growth arrest or apoptosis. B. During cellular stress the activation of p53 occurs via several posttranslational modifications including phosphorylation by kinases such as ATM, ATR, Chk1 and MAPKs. This interrupts the Mdm2 binding leading to the accumulation of p53 and its transactivation activity and possible cytoplasmic roles. Figure adapted from Toledo et al. [3].

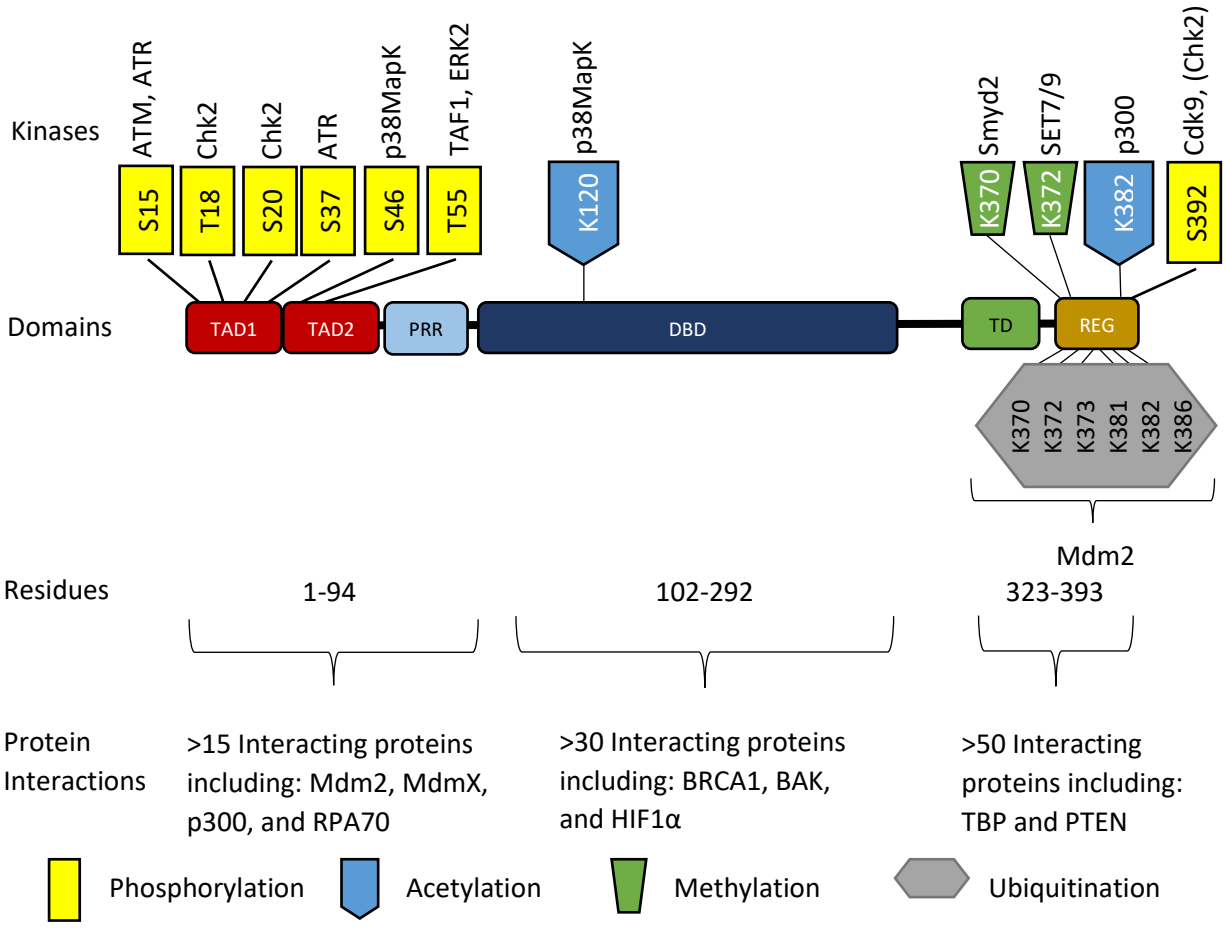

Figure 3 – Well-known human p53 PTM sites and binding partners. The domains of p53 are shown together with PTM sites and modifying kinases. Figure adapted from Meek et al. [4].

Binding partners

As shown in Figure 3, p53 has many binding partners. Some of the most relevant partners for this study, which are also some of the most studied partners are CREB-binding protein (CBP)/p300, Mdm2 and its homologue MdmX. As a dimer, Mdm2 functions as an E3 ubiquitin ligase. The p53 binding domain on Mdm2 is localized at the N-terminus, from residues 1–118 or 19–102 [80, 81]. Mdm2 also contains an acidic domain and a RING finger domain located at the C-terminal end of Mdm2 which houses its ubiquitination function [80, 82, 83]. MdmX also functions as a dimer and has similar

domain structure to that of Mdm2, although it contains much less E3 ubiquitin ligase function. As previously discussed, Mdm2 and MdmX play important roles in regulating p53.

The phosphorylation of p53 at residue S15 increases interaction with CBP [84-86]. CBP is a transcriptional coactivator and histone acetyltransferase that facilitates transcription initiation of p53 target genes and stabilizes p53 by acetylating its lysines that would otherwise be ubiquitinated by Mdm2 [87, 88]. CBP contains four domains, KIX, TAZ1, TAZ2, and IBiD, capable of binding to p53 within the TAD1 and TAD2 regions. It has been proposed that all four domains may bind tetrameric p53 in the nucleus to facilitate transcription initiation [89, 90]. Phosphorylation of the TAD1 region of p53 increases binding affinity with the KIX, TAZ1, and TAZ2 domains of CBP [85, 91]. Thus, CBP competes with Mdm2 and MdmX for binding to p53 [90].

Thermodynamics of DNA binding specificity

The protein-DNA interaction is an intricate phenomenon that does not rely only on structural analysis but involves thermodynamic factors to stabilize the bound complex against the unbound complex. Protein–DNA interactions occur in one of two ways, either through specific interaction, or non-specific interaction [92, 93]. In protein-DNA interactions, the indirect and direct DNA specific base sequences are recognized through hydrophobic interactions, the van der Waals attractions, and the non-specific electrostatic interactions between the phosphate backbone of the DNA and the protein's basic residues [92]. The most intensively studied proteins that interact with DNA are transcription factors. These proteins are able to make multiple contacts with the DNA bases within the major groove of DNA where the bases are more accessible. This allows

them to read the DNA sequence, which explains the binding specificity these transcription factors have with DNA [93].

Full-length p53 contains two independently folding domains, the DBD and the TD [94]. The high number of mutations within the sequence-specific DBD of p53 speaks to the importance of DNA binding in the ability of p53 to transactivate genes [95, 96]. p53 polypeptides that contain both the DBD and the TD form stable p53-DNA complexes in solution, having nanomolar affinity for sequence-specific DNA [97]. Inclusion of the N-terminal domain of p53 increases p53 DNA binding specificity, which is essential for p53's ability to differentiate the promoter sites of target genes [98].

Evolution of p53

p53 is well-conserved throughout evolution. The TAD region however is not as well conserved as the ordered DBD region, which is common among IDRs. Compared to IDPs, ordered proteins with just 30% sequence similarity usually have nearly identical folds and functions [99, 100]. When looking at the p53 family, there are 3 members: p53, p63, and p73 (Figure 4). Previous studies claim p63 to be the ancestral member while p53 is the most recent member of the family [5, 101]. All 3 members contain an acidic N-terminal domain, DBD, TD, and REG. Unlike p53, the p63 and p73 genes contain a C-terminal sterile alpha motif (SAM) domain [101]. Figure 4 shows the structural alignment for the domains and the approximate sequence similarity of the homologues. Such strong similarities would suggest that the family would share functions. They all act as transcription factors and have similar gene targets [101]. However, there are differences between the genes. The TDs are similar between all three genes, however, p63 and p73 are not able to oligomerize with p53 even though they are able to form oligomers with

each other [102]. p63 and p73 are both involved in the regulation of the cell cycle and the induction of apoptosis, but unlike p53, p73 is rarely mutated in tumors and thus seems to lack the effectiveness to induce apoptosis when compared to p53 [103].

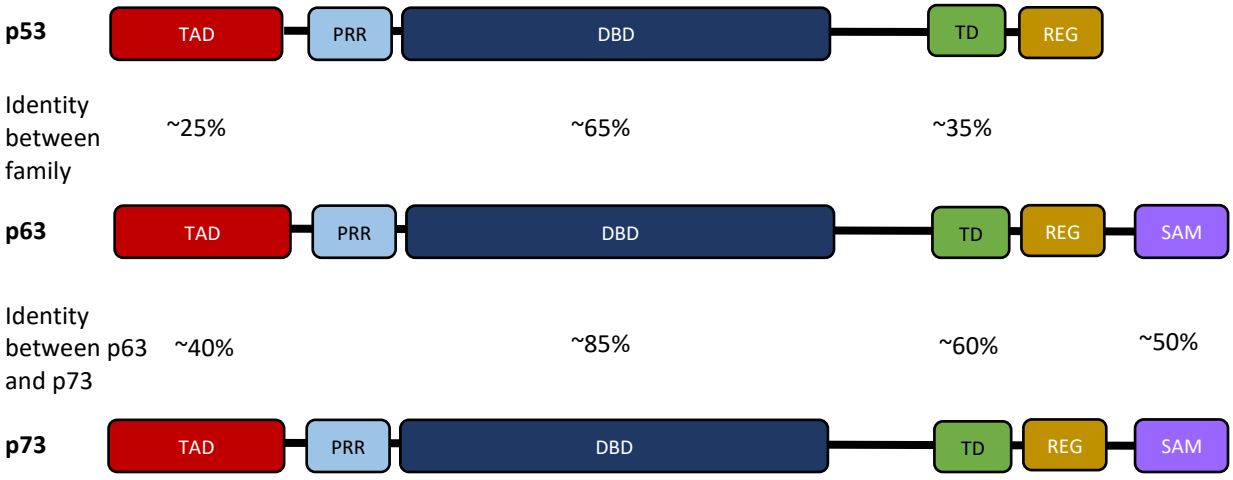

Figure 4 – p53 family domain structures. Comparison of the domain structures within the p53 family. Figure adapted from Yang et al. [5].

Significance and IDP model protein

p53 can be a useful model for studying IDPs. In its monomeric state full-length p53 is predicted to have 50% disorder. The areas where most of this disorder is found is within the TAD, TD and REG domains, while the DBD is considered to be ordered within the monomeric state [95, 98, 104]. The TAD region contains transient helical structures and numerous ligand binding sites [105-107]. The TAD domain of p53 contains many PTM sites that regulate the binding events within the p53TAD [4, 90, 108, 109]. The Mdm2 binding site within p53 displays the strongest tendencies for secondary structure and forms a stable alpha helix when bound by its Mdm2/MdmX protein partners [51, 89, 101]. Another major binding site is the DNA binding domain which participates in DNA binding but also intramolecular binding to the N-terminal of p53 [102]. Long range interactions that affect DNA binding have been observed between the disordered TAD and the

ordered DBD regions of p53 [95, 98, 104]. The acidic domain of Mdm2 and MdmX inhibit p53 DNA binding by interacting with the p53 DNA binding domain [104, 105].

Studying the TAD domain of p53 will help to improve our understanding of the structure and function of not just p53 but other IDPs. Studying p53TAD allows us to further understand a family of disordered regions that should have conserved function based on the p53 sequence similarities which would allow for the observation across a large range of sequence conservation. In addition to this, p53TAD serves as a great model for understanding coupled folding and binding due to two binding sites that show coupled folding and binding but differ in sequence identity, dynamic behavior, and structure. Understanding the behavior of p53 and the secondary intramolecular and intermolecular interactions that p53 is involved with will aid in understanding the regulation of p53 along with similar phenomena in complexes containing multidomain IDRs.

Chapter Two: Effects of phosphorylation on the structure of p53 transactivation domain (p53TAD) and binding partners

Note to the readers: This chapter is comprised of prior published data, used with the permission of the publishers [110].

Rationale

The disordered p53 transactivation domain (p53TAD) contains specific levels of transient helical secondary structure that are necessary for its binding to its negative regulators, Mdm2 and MdmX. The interactions of p53 with Mdm2 and MdmX are also modulated by posttranslational modifications (PTMs) of p53TAD including phosphorylation at S15, T18 and S20 that inhibits p53-Mdm2 binding. It is unclear whether the levels of transient secondary structure in p53TAD are changed by phosphorylation or other PTMs. We used phosphomimetic mutants to determine if adding a negative charge at positions 15 and 18 has any effect on the transient secondary structure of p53TAD and protein-protein binding. The phosphomimetics reduced Mdm2 and MdmX binding affinity by 3-5-fold, but resulted in minimal changes in transient secondary structure, suggesting that the destabilizing effect of phosphorylation on the p53TAD-Mdm2 interaction is primarily electrostatic. Phosphomimetics had no effect on the p53-KIX interaction, suggesting that increased binding of phosphorylated p53 to KIX may be influenced by decreased competition with its negative regulators.

In this study, we used a combination of biophysical and structural methods to obtain insights into the role of phosphorylation in modulating interactions of p53 with Mdm2, MdmX, and CBP/KIX and the effect of phosphorylation on transient secondary

structure. We assessed the effects of single- and double-site phosphomimetic mutations of p53TAD upon binding to the N-terminal domain of Mdm2, MdmX, and the KIX domain of CBP. Due to the location of S15 and T18 in a region of p53TAD containing transient helical secondary structure and the importance of their phosphorylation for regulation, we engineered p53TAD phosphomimetics, S15D and S15D/T18E, to determine if the phosphomimicry of p53TAD at these sites affects protein-protein binding and changes the levels of transient helical secondary structure. Our data shows that multisite phosphomimicry reduces the binding affinity of p53TAD to Mdm2 and MdmX. In contrast to earlier published results on p53 phosphorylation, single and multisite phosphomimetics of p53TAD have equivalent, small effects on binding with KIX [85, 91, 111]. We observe little, if any, change to the transient secondary structure of p53TAD.

Effects of PTMs on p53TAD and binding partners

Loss-of-function mutations in the p53 pathway frequently arise during cancer development [55, 112, 113]. Approximately half of all human tumors express p53 mutants with reduced DNA-binding affinity which reduces or eliminates transactivation [55, 114]. p53 is a well-known intrinsically disordered protein (IDP) whose disorder is a major component of its functionality [8, 115]. An IDP is a protein that lacks a fixed or ordered structure. IDPs are structurally very different from ordered proteins and tend to have distinct properties in terms of function, sequence, interactions, evolution and regulation [9, 11, 12]. Many IDPs like p53 form transient secondary structures and undergo coupled folding and binding when they are bound to their targets [90, 116, 117]. IDPs cover a range of different states from fully unstructured to partially structured [11, 28, 29]. Modulation of the degree of transient secondary structure affect p53's interactions with

its binding partners [118]. Studies showed that the levels of residual helicity in free p53 TAD are controlled by conserved prolines flanking the Mdm2/MdmX binding site [119]. The mutation of these prolines to alanine resulted in a higher p53TAD helicity and increased Mdm2 binding [119]. Posttranslational modifications (PTMs) also regulate the activity of IDPs [36, 37]. In normal cells, p53 is present at low concentrations due to its interaction with the E3 ubiquitin ligase Mdm2; however, under stress conditions, p53 levels increase as it is phosphorylated, leading to its dissociation from Mdm2, migration to the nucleus, and the transcriptional activation of its target genes [64]. Cells with mutant or deleted p53 are unable to respond to stress appropriately, and this leads to mutations and the development of cancer [66].

Mouse double minute 2 (Mdm2), also known as E3 ubiquitin-protein ligase Mdm2 proto-oncogene, and its homolog Mmd4, also known as MdmX, are negative regulators of p53 [70, 120, 121]. Mdm2 is overexpressed in several human tumor types, such as soft tissue sarcomas as well as breast tumors [122]. p53 levels are suppressed by the Mdm2/MdmX heterodimer which promotes the polyubiquitination of p53 leading to its degradation [75, 78]. Mdm2 and p53 are involved in an auto-regulatory feed-back loop where p53 stimulates the expression of Mdm2; Mdm2, in turn, inhibits p53 activity because it stimulates its degradation [67, 68]. MdmX lacks ubiquitin E3 ligase activity but is able to directly bind to and inhibit p53 activity independently of Mdm2 [75-77]. DNA damage activates kinases that phosphorylate p53 at residues S15, T18 and S20, which stabilize and activate p53 by inhibiting Mdm2 binding [108, 123, 124]. In vitro, p53 phosphorylation affects its interaction with Mdm2, where phosphorylation of S15 and S20 residues individually result in a 2 and 1.5-fold reduction, respectively [91].

Phosphorylation of T18 leads to a 19-22-fold reduction in binding affinity of p53TAD to Mdm2, and one study has described an equivalent effect of phosphorylated T18 on Mdm2 binding to p53 [90, 91, 125]. Dually phosphorylated p53 at S15/T18 results in a binding reduction equivalent to that of T18 alone, suggesting that T18 phosphorylation is the driver of reduced binding affinity of p53 to Mdm2, though the T18 site of p53 cannot be phosphorylated until the S15 site is phosphorylated first [91, 123, 126-129]. T18 phosphorylation creates additional charge-charge repulsion, creating an energetically unfavorable environment for p53 and Mdm2 binding; however, the contribution of phosphorylated p53's structural changes to Mdm2 binding has not been assessed [123, 126-129].

Phosphorylation of p53TAD upon cellular stress leads to increased transcription of its target genes and increased association with its coactivator, CREB binding protein (CBP)/p300 [86]. CBP is a transcriptional coactivator and histone acetyltransferase that facilitates transcription initiation of p53 target genes and stabilizes p53 by acetylating its lysines that would otherwise be ubiquitinated by Mdm2 [87, 88]. CBP contains four domains capable of binding p53TAD, and it has been proposed that all four domains may bind tetrameric p53 in the nucleus to facilitate transcription initiation [89]. Whereas Mdm2 and MdmX interact with p53's TAD1 region, which spans approximately residues 1-40, the KIX, TAZ1, TAZ2, and IBiD domains of CBP interact with both TAD1 and TAD2 of p53, approximately residues 41-60 [90]. Thus, CBP competes with Mdm2 and MdmX for binding to p53, though it has also been shown that CBP and Mdm2 may form a ternary complex with p53 in vitro [90]. Phosphorylation of the TAD1 region of p53 increases binding affinity with the KIX, TAZ1, and TAZ2 domains of CBP, though possibly by

different mechanisms [85, 91]. In this study we focus on KIX, for which the bound state of p53 has not been determined. Phosphorylation of S15 or T18 is reported to result in a 1.7-4-fold increase in binding affinity with KIX, but an increase of 3-11-fold for the same residues when binding to TAZ2. S15/T18 phosphorylation, however, has been reported to result in 16 and 8-fold changes in binding affinity for KIX and TAZ2, respectively [85]. Likewise, where binding of p53 to the KIX domain is controlled by a combination of conformational selection and electrostatic attraction, for example, TAZ2 interaction with the phosphorylated T18 is likely driven by electrostatic attraction [61, 111, 130].

Dipole stabilization of the p53 N-terminal

During phosphorylation the phosphate group contains a double negative charge that affects protein conformation mainly due to the electrostatic effects that occur between the phosphate and surrounding charged atoms of the protein [35, 40]. These conformational changes can be local and/or long-range, affect protein-protein interactions, and increase or decrease levels of disorder [35]. As an extreme example of the effect of phosphorylation of protein-protein interactions, PTM-mediated folding of the IDP 4E-BP2 allows it to regulate translation initiation [37]. Multisite phosphorylation stabilizes 4E-BP2 and decreases affinity to its binding partner elF4E by a factor of 4,000 compared to single-site phosphorylation which only decreased affinity by 100-fold [37]. Phosphorylation of T51 conforms PAGE4 into a more compact structure that still maintains a flexible state for long range interactions. PAGE4 phosphorylation also increases c-Jun transactivation but decreases the affinity of PAGE4 to c-Jun, which is believed to occur due to the compact structure of PAGE4 [131]. This attenuation of binding due to phosphorylation is common between many IDPs, which are known to form

transient secondary structures and undergo coupled folding and binding when they are bound to their targets [9-11]. p53TAD1 forms a short helix when bound to Mdm2 and MdmX anchored via the hydrophobic residues F19, W23, L26, and TAD2 forms a short helix when bound to the TAZ2 domain of CBP anchored around the hydrophobic residues I50, W53 and F54 [62, 85]. Electrostatic interactions control the stability of the helix [132]. Such helices will have a macroscopic helical dipole with a partial positive charge at the N-terminus and a partial negative charge at the C-terminus, which could stabilize the helix dipole [133, 134].

Phosphomimetic mutations of p53

To study the effects of phosphorylation on protein structure and function phosphomimetic mutations have been used extensively. Phosphomimetic mutations are amino acid substitutions (Ser/Thr to Asp or Glu and Tyr to Glu) that mimic the effect of a phosphorylated residue [135-137]. There are no natural amino acid side chains that provide the combination of negative charge with a tetrahedral center. However, there are numerous studies showing partial phenotypes when aspartic acid is substituted for phospho-serine or glutamic acid is substituted for phospho-threonine [86, 138]. In our phosphomimic mutants, the TAD1 helix, which corresponds to residues 19-25, has one or two additional negative charges added towards the N-terminus. The addition of negative charge might be thought to stabilize the helix as seen between antiparallel alpha helices where the close proximity of opposing charges stabilizes each [134]. However, computational studies have predicted that p53 T18 phosphorylation would destabilize the helix by causing a long-range interaction with the K24 residue of p53, interfering with the

D21 interaction with K24 [62]. Relatedly, phosphorylation of S20 is predicted to increase helical propensity by stabilizing the D21-K24 interaction [132].

Transient secondary structure of p53TAD phosphomimetic mutants

We attempted in vitro phosphorylation experiments with NMR labeled p53TAD using DNA-PK and CK1γ2 kinases to determine changes to transient secondary structure but were unable to get 100% phosphorylation at either S15 or T18 compared to that of previous studies (Figure S1) [139]. Therefore, we chose to use phosphomimetic mutations. The phosphorylation of p53 makes it more negatively charged. In studying protein phosphoregulation, it has become common to mutate phosphorylation sites to phosphomimetic residues to attempt to study the constitutively phosphorylated state of the protein [91, 136, 137, 140-144]. We designed p53TAD phosphomimetics (residues 1-73) by mutating S15 to Asp and S15/T18 to Asp/Glu, which will be referred to as S15D and S15D/T18E, respectively. We used NMR spectroscopy to measure any changes in the transient secondary structure of p53TAD wild type (p53TAD) and mutants. An overlay of the ^{1}H-^{15}N heteronuclear single quantum coherence (HSQC) spectra of p53TAD and the phosphomimetics is shown in Figure 5. The labeled peaks show the resonance assignments of p53TAD residues (black peaks). There is hardly any shift in the majority of the residues for the S15D (red peaks) and S15D/T18E (blue peaks) mutants compared to p53TAD. We do see a significant shift at residues that are close to the mutated sites of S15 and T18 suggesting that any structural effects from the mutation(s) will be local.

Secondary chemical shift values were calculated using the prediction of temperature, neighbor and pH-corrected chemical shifts for intrinsically disordered proteins (POTENCI) software (Figure 2). This software calculates residue-specific random coil chemical shifts from an amino acid sequence and these values are subtracted from the NMR-measured chemical shift values to give the corrected secondary chemical shift values [145]. Positive alpha carbon secondary chemical shifts are indicative of alpha helix formation [146, 147]. All of the measured chemical shifts (NH, N, CA, CB, and CO) were used to calculate the distribution of transient secondary structure using the

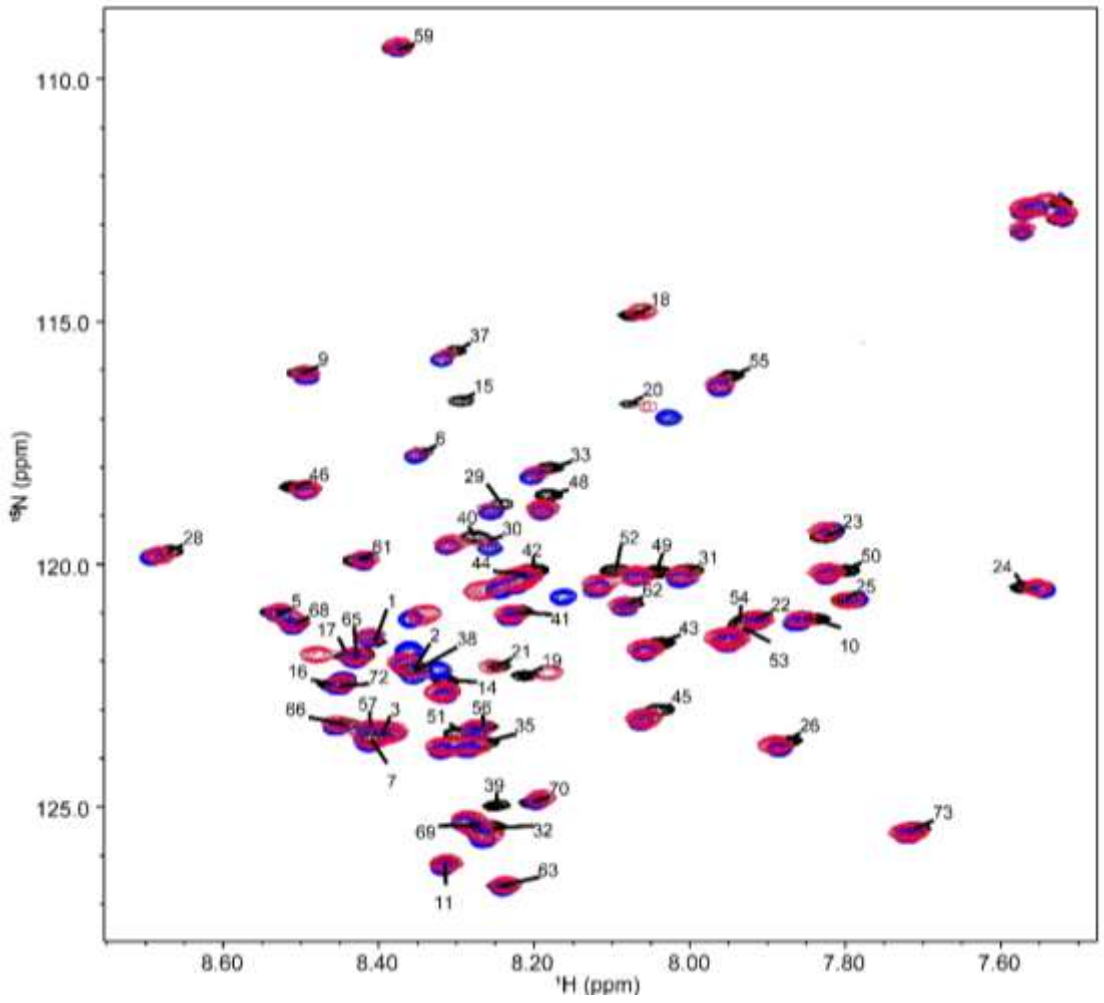

Figure 5 – p53TAD and phosphomimetics. ^{1}H-^{15}N HSQC spectra overlay of ^{15}N-labeled p53TAD (black), ^{15}N-labeled S15D mutant (red), ^{15}N-labeled S15D/T18E mutant (blue).

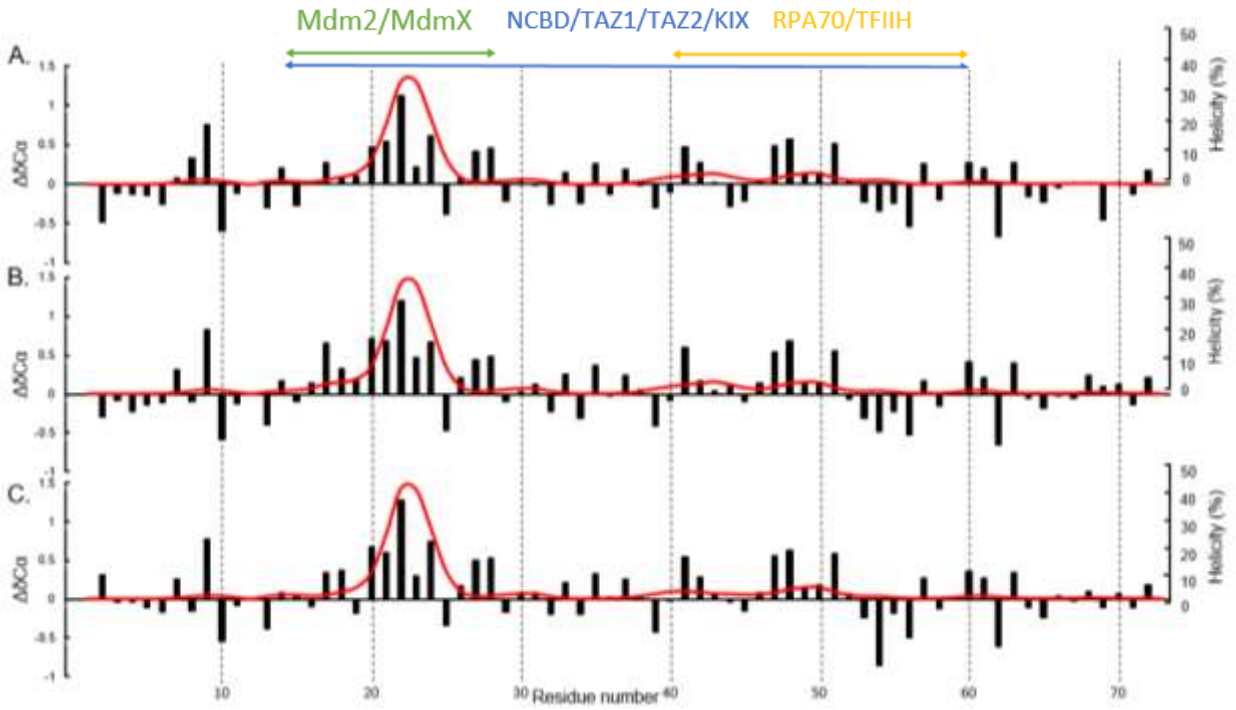

Figure 6 – Residue-specific secondary structure of p53TAD and phosphomimetics. Secondary chemical shift plots and δ2D plot for p53TAD and phosphomimetics determined from NMR spectroscopy. (A) p53TAD (B) S15D (C) S15D/T18E. α-carbon secondary chemical shift (ΔδCα, black bars) and helical δ2D plots (red line) for the p53TAD and phosphomimetics as determined by NMR spectroscopy. Colored bars indicate binding sites for respective protein partners. The α-carbon chemical shifts for p53TAD were collected on a 600 MHz NMR at a digital resolution of 0.31ppm. The alpha carbon chemical shifts for S15D and S15D/T18E were collected on an 800 MHz NMR at a digital resolution of 0.27ppm.

δ2D software [148]. The negative charge produced during phosphorylation affects protein conformation mainly due to the electrostatic effects and these changes can be local and long-range [35, 40]. A short helix compromising residues 19-25 has one or two additional negative charges added towards the N-terminus in our phosphomimetic mutants which might stabilize the helix due to the close proximity of opposing charges. We observed small differences in the transient helical secondary structure between p53TAD, S15D and S15D/T18E (Figure 6). However, of the changes that were present most were within the Mdm2/MdmX binding site. There was a slight increase in helicity for the mutants, with

p53TAD having 36.4% helicity at its highest point and S15D and S15D/T18E having 39.8% and 39.9% helicity at their highest points, respectively, as indicated by the δ2d plots (Figure 6 red line). The reported accuracy of δ2D is 2%. The changes in the secondary chemical shifts, though minimal, were also observed within the Mdm2/MdmX binding site (Figure 6 black bars).

Binding effects of phosphomimetic mutants

Next, we used isothermal titration calorimetry (ITC) to determine the effect of the phosphomimetic mutations on p53TAD binding to Mdm2 (residues 17-125), MdmX (residues 23-111), excluding the N-terminal "lid" and KIX (residues 586-672) (Figure 7) [149-151]. Compared to qualitative methods of measuring protein-protein binding (e.g. immunoprecipitation, western blot, GST pull-down) ITC is a widely used technique for quantitative studies of an extensive variety of biomolecular interactions [119, 152-155]. It is mostly used to observe the binding between molecules like protein and DNA by measuring the binding affinity, enthalpy and stoichiometry of interacting molecules [152]. ITC measures the heat that is either expelled or consumed by the interaction of the molecules present and modern ITC instruments make it possible to measure the differences in heat as small as 0.1μcal (0.4 μJ) [156]. It can simultaneously determine multiple binding parameters in a single experiment and does not require the modification of binding partners with fluorescent tags or through immobilization; ITC measures the affinity of binding partners in their native states. ITC experiments were performed by titrating the p53TAD phosphomimetics into Mdm2, MdmX, and KIX. The ITC experiments were performed in triplicate and the values averaged (Table 1). Data were analyzed with the Origin70 ITC software from MicroCal and the integrated ITC data were fit with single-

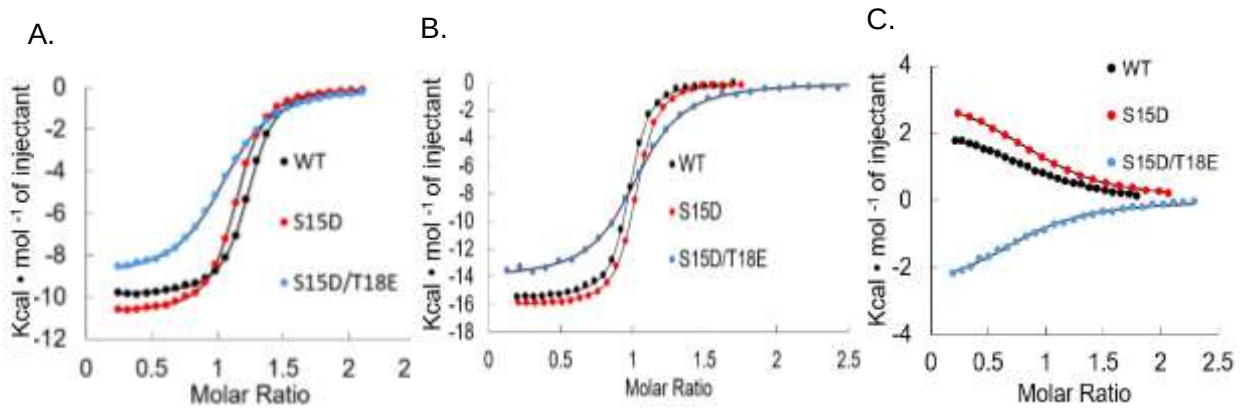

Figure 7 – Binding Isotherms of Mdm2, MdmX and KIX with p53TAD and mutants. Isothermal calorimetry titrations of A. Mdm2 and p53TAD and mutants B. MdmX and p53TAD and mutants and C. KIX and p53TAD and mutants.

site binding models. The stoichiometry ranged from 0.8 to 1.2. A standard deviation was calculated for K_d using data from triplicate measurements. p53TAD and S15D bound Mdm2/MdmX with similar affinities, whereas S15D/T18E displayed a 2.5-4.5-fold reduction with Mdm2 and a 5-fold reduction with MdmX (Figure 7A and 7B). Binding affinity of p53 to KIX was similar between p53TAD and all the phosphomimetics. Binding of p53TAD to KIX was endothermic with similar values for S15D (Figure 7C and Table 1). S15D/T18E, however, was exothermic (Figure 7C and Table 1). Note that all variants of p53 bind to KIX in a reaction that is endothermic at lower temperatures and transitions to exothermic at higher temperatures (Data not shown). Interestingly, the phosphomimetics had no effect on the transient helical secondary structure of p53TAD. Taken together, the results argue that binding affinity between phosphorylated and unphosphorylated p53 to Mdm2/MdmX is primarily controlled by electrostatics whereas the binding to KIX is not improved by increased potential for electrostatic attraction.

Affinities of the p53TAD phosphomimetics for the KIX domain and the N-terminal domains of Mdm2 and MdmX were determined by ITC (Figure 7). For both Mdm2 and MdmX,

Table 1 – ITC values for interactions between Mdm2, MdmX and KIX with p53TAD and mutants.

	Mdm2 into p53TAD	Mdm2 into S15D	Mdm2 into S15D/T18E	MdmX into p53TAD	MdmX into S15D	MdmX into S15D/T18E	KIX into p53TAD	KIX into S15D	KIX into S15D/T18E
K_d (nM)	219.5 ± 0.01	392.5 ± 0.02	1,001 ± 0.02	29 ± 0.004	30 ± 0.002	108 ± 12.5	11,000 ± 2,700	8,200 ± 1,870	8,380 ± 969
ΔG (kCal/mol)	-9.1 ± 0.53	-8.75 ± 0.07	-8.2 ± 0.85	-10.3 ± 0.10	-10.27 ± 0.06	-9.5 ± 0.07	-6.77 ± 0.16	-6.95 ± 0.13	-6.92 ± 0.06
ΔH (kCal/mol)	-9.72 ± 0.20	-11.34 ± 0.83	-8.173 ± 1.20	-16.26 ± 0.91	-16.99 ± 1.41	-14.27 ± 0.19	2.61 ± 0.31	2.93 ± 0.42	-2.82 ± 0.08
TΔS (kCal/mol)	-0.63 ± 0.24	-2.50 ± 0.98	-0.96 ± 0.19	-5.960 ± 0.99	-6.79 ± 1.55	-4.75 ± 0.16	9.38 ±0.17	9.87 ± 0.31	3.96 ± 0.27

S15D showed similar binding to p53TAD. S15D/T18E showed a decrease in binding to Mdm2 and MdmX with binding being 4.5 times and 5 times weaker than p53TAD, respectively (Table 1). Many studies have shown that phosphorylation of S15 and T18 play a critical role in preventing the interaction with Mdm2 [108, 126, 157]. There has been some disagreement in regards to the impact of phosphorylation on binding; there is a good consistency for unphosphorylated peptides (residues 10-57) binding to Mdm2 but there is some variation in the phosphorylated peptides that does not appear to correlate with different techniques or sizes of the peptides being used [85, 90, 158, 159]. Though we do not see much structural change with the phosphomimetics, we do see binding results consistent with other studies that phosphorylated p53 at the same residues. Previous studies showed a 10-20-fold reduction in binding of p53 to Mdm2 due to p53 phosphorylation as compared to our results where we see a 3-5-fold reduction [85, 90, 158-160]. The results of our binding experiments with phosphomimetics are consistent with previous findings suggesting that the phosphorylation of T18 is the driving force for inhibiting Mdm2/MdmX binding [62, 123, 158-161]. Furthermore, there has not yet been a quantitative study of the effect of p53 phosphorylation on MdmX binding. Our results suggest that p53 phosphorylation may in some cases have an equivalent effect on MdmX as on Mdm2.

Binding affinity of p53 to KIX was not significantly altered between p53TAD and the phosphomimetics. We found p53TAD binds to KIX with a K_d of 11μM, similar to values found in previous studies [90, 91, 111]. In contrast to previous studies on p53 phosphorylation, however, these phosphomimetic mutations increased binding affinity for KIX by only 1.3-fold. Phosphorylation of p53 at S15 has been shown to result in a 1.7- 4-

fold increase and S15/T18 phosphorylation results in a 16-fold increase in binding affinity to KIX in vitro [85, 90, 91, 162]. The increase in binding affinity of phosphorylated p53 to the domains of CBP has been attributed to an increase in electrostatic attraction independent of site-specific affinity; however, it is unclear if this trend applies to KIX, which has been suggested to have a relatively weak response to phosphorylation of p53 compared to other CBP/p300 domains [85]. Our results show that an increase in negative charge of p53TAD alone is not sufficient to significantly increase binding affinity for KIX [91]. Instead, it seems that the increase in binding affinity to KIX by p53 phosphorylation may occur by way of a structural change that is not fully replicated in the phosphomimetics produced here. We postulate that the phosphomimetics of p53 created here represent an intermediate phenotype between that of phosphorylated and unphosphorylated p53 and may be useful for future cell and molecular biology studies.

Chapter Three: Intermolecular and intramolecular interactions between phosphorylated p53, DNA and other binding partners

Rationale

There has been much controversy over whether the transactivation domain of p53 (p53TAD) has any effect on DNA binding. TAD1 and TAD2 interact with different transcription factors such as TBP, TFIID, and coactivator p300/CBP. TAD2 contributes significantly to p53 transcriptional activity and it is well known that W53 and F54 are key residues for TAD2 function [89, 163]. Within the past decade studies have shown that the transactivation domain of p53 (p53TAD) interacts with its DNA binding domain [104, 164, 165]. In vivo studies using proteolytic fragment release assays showed that p53TAD bound to DBD at a higher concentration than DBD with C-terminal p53 [98]. This suggests the TAD interacts with DBD more strongly than the C-terminus interacts with DBD [98]. Previous NMR binding experiments have shown that p53TAD interacts with the DBD and binding experiments suggest that p53TAD is also involved in reducing sequence-specific DNA binding by DBD [98, 104, 164]. Some studies suggest that it is not p53TAD that is interacting with the DBD but instead the linker region between the PRR and the DBD [164]. With the differences in results from current studies we decided to investigate the TAD2 region of p53 and its interaction with the DBD.

PTMs of p53TAD are important not only for p53 binding to other partners but also its function. Within p53 TAD1 the Mdm2/MdmX binding site contains some of the more heavily studied PTMs. There has not been as much extensive work put into the understandings of the PTMs within the p53 TAD2 region. We focused our study on the

phosphorylation of p53 TAD2 in particular residue T55. During the recovery from the DNA damage response TAF1 phosphorylation of T55 leads to the dissociation of p53 from DNA [166]. T55 phosphorylation also leads to the dissociation of p53 from the p21 promoter [166]. Mdm2 binding has been shown to be increased in the presence of T55 phosphorylation [167]. The phosphorylation of S46 or T55 increases p53 binding to p62 and Tfb1 subunits of TFIIH [60]. The p53 transactivation domain (p53TAD) that contains T55 interacts with several DNA-binding proteins such as replication protein A, mitochondrial single-stranded DNA-binding protein, and the TfB1 subunit of transcription factor II H [59, 168]. Although there is much evidence that p53 can be phosphorylated at different sites, the results of these site-specific phosphorylation events are still poorly understood. Due to studies like these, we propose that mutations within TAD2 combined with site-specific phosphorylation can decrease p53 binding to DNA and promote binding specificity.

In this study, we investigated the role of phosphorylation in modulating interactions of p53 TAD2 with protein binding partners like Mdm2 and MdmX and the effect of phosphorylation on p53-DNA binding. Due to the importance of T55, W53, and F54 for transcriptional regulation, we engineered a p53TAD phosphomimetic mutant, T55D, and to further determine the role of W53 and F54 in DNA binding we created a NDQS construct where we mutated the tryptophan at residue 53 and the phenylalanine at residue 54 to glutamine and serine respectively [89, 163]. We assessed the effects of phosphomimetic mutations of p53TAD upon binding to the N-terminal domain of Mdm2 and MdmX. Using biophysical methods, we investigated the effects of point mutations and phosphomimetic mutations on the interaction between p53 and DNA. Our binding

data shows that phosphomimicry of the p53 transactivation domain decreases DNA binding affinity, while substituting hydrophobic residues with polar residues within TAD2 of p53 increases DNA binding.

Model for the intramolecular interaction between p53 TAD2 and the DNA binding domain of p53

There has been much controversy over whether the transactivation domain of p53 has any effect on DNA binding. The phosphorylation of T55 increases the negative charges on p53 TAD2, which should increase its affinity for the DBD, thus increasing the inhibitory effect on the DBD for DNA binding. With the inclusion of phosphorylation at T55

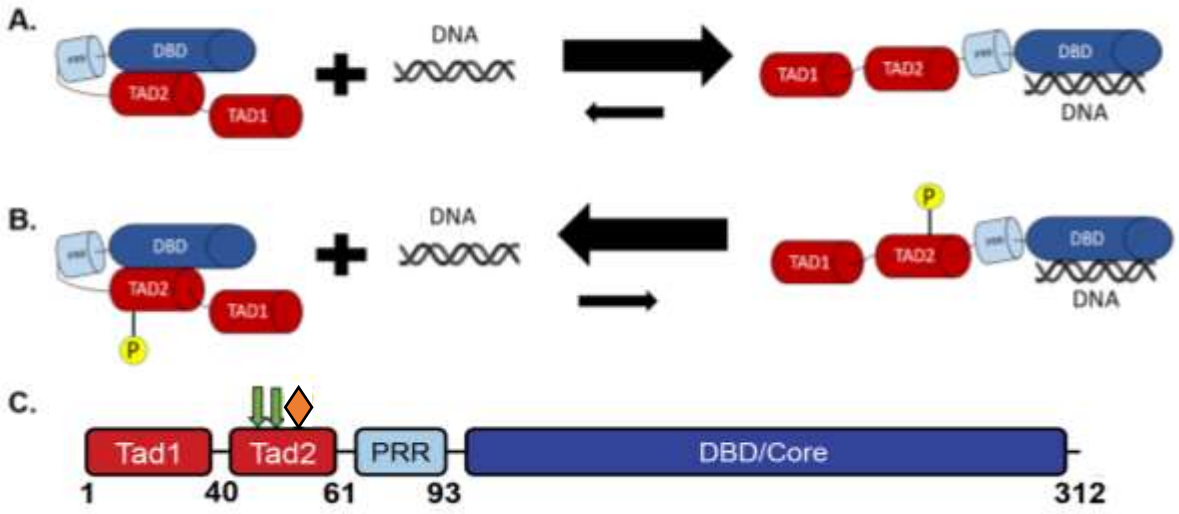

Figure 8 – A model for the interaction between DNA and the p53ND fragment and the schematic of T55D-ND and NDQS mutations. A. The presence of DNA displaces p53TAD from its interaction with DBD with the equilibrium favoring the DNA-bound state. B. Phosphorylation of p53 at T55 or substitution of T55 with the phosphomimetic mutant T55D inhibits binding of DNA to the DBD, where equilibrium favors the intramolecular interaction. C. The schematic shows the phosphorylation of TAD2 as indicated by the orange diamond. We created a phosphomimetic mutation, T55D-ND, within TAD2 at residue 55 mutating it from a threonine to an aspartic acid to mimic the phosphorylation of this site. The green arrows indicate the mutations we made for our NDQS construct where we mutated the tryptophan at residue 53 and the phenylalanine at residue 54 to glutamine and serine respectively.

we propose a model in Figure 8A and B for the interaction between DNA and p53 N-terminal domain (p53ND) and DNA and T55D-ND, respectively. Figure 8A suggests that when residue T55 is not phosphorylated the DNA bound state is more favored, while in Figure 8B we propose that the phosphorylation of T55 will cause a stronger intramolecular interaction between the TAD2 region and the DBD of p53 than that of the p53-DNA bound state, thus inhibiting the binding of DNA. These results are consistent with a model we developed that describes how a direct intramolecular interaction between TAD2 and the DNA binding domain influences DNA binding specificity. As performed in our previous experiments we designed a phosphomimetic mutant to study the phosphorylated state of p53. We created this p53 mutant (residues 1-312) by mutating T55 to Asp, which will be referred to as T55D-ND (Figure 8C). In addition to studying phosphoregulation we also wanted to understand the role that two consecutive hydrophobic residues within TAD2 (W53, F54), played in DNA binding. These residues are surrounded by acidic amino acids and are essential for the activity of the transactivation domain [89, 163]. The second p53 construct we created contained the mutated sites of W53 and F54 to Gln and Ser respectively (Figure 8C). This mutant will be referred to as NDQS.

NMR measurements of structure and dynamics of T55D-ND

We used NMR spectroscopy to measure any changes in the transient secondary structure of p53ND and T55D-ND. An overlay of the ^{1}H-^{15}N heteronuclear single quantum coherence (HSQC) spectra of p53ND and T55D-ND is shown in Figure 9. The labeled peaks show the resonance assignments of the p53ND residues (blue peaks). We used a phosphomimetic mutation to mimic phosphorylated p53 T55 to determine the effects that this site-specific phosphorylation has on the structure of p53 (Figure 9 red peaks).

Secondary chemical shift values were calculated using the prediction of temperature, neighbor and pH-corrected chemical shifts for intrinsically disordered proteins (POTENCI) software (Figure 10A and B black bars). All of the measured chemical shifts (NH, N, CA, CB, and CO) were used to calculate the distribution of transient secondary structure using the δ2D software (Figure 10A and B red line). This data shows that the phosphorylation of residue 55 has little to no effect on the structure of p53 except in the region near the mutated site. Due to a disappearance of peaks occurring near the mutated site we performed NMR titrations to identify the effect this mutant had on DNA binding (Figure

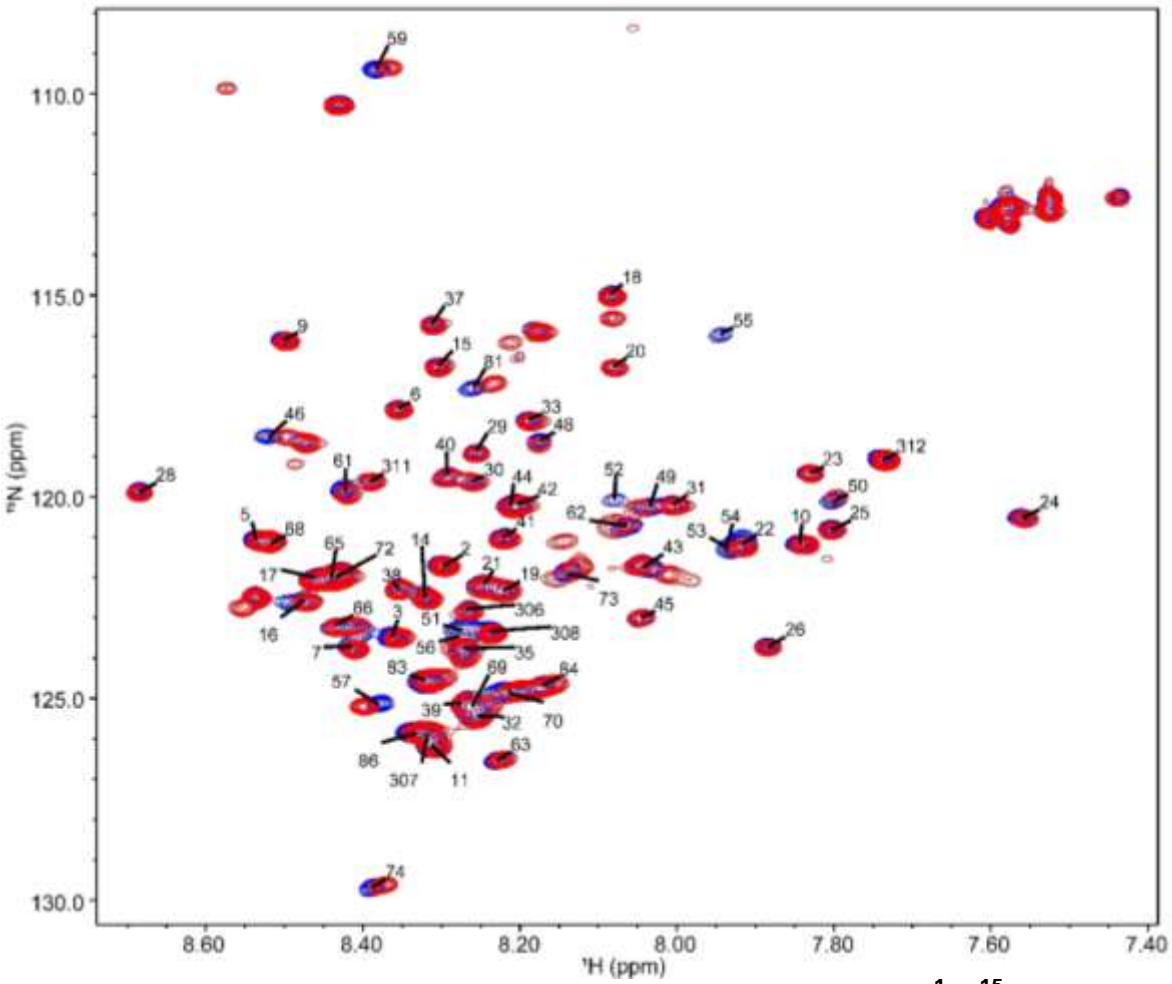

Figure 9 – HSQC spectra of p53ND and T55D-ND mutant. ^{1}H-^{15}N HSQC spectra overlay of ND (blue) and T55D-ND (red).

11).

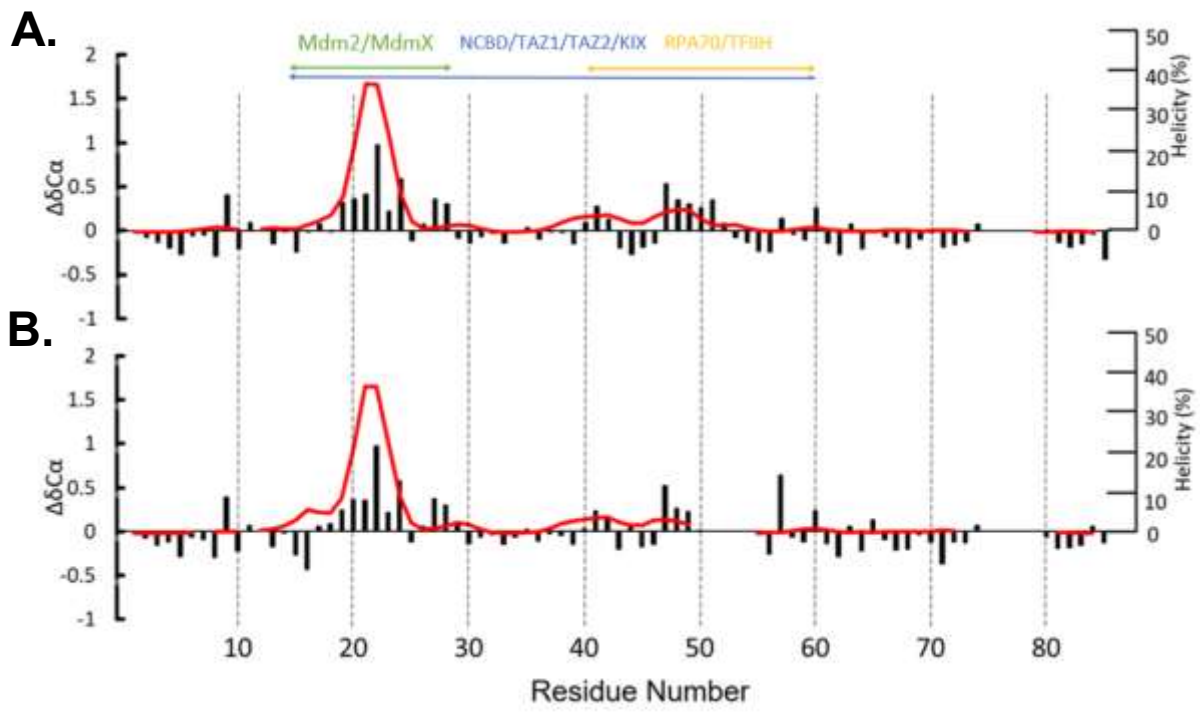

Figure 10 – Residue-specific secondary structure of p53ND and T55D-ND. A. Secondary chemical shift plots and δ2D plot for p53ND. B. Secondary chemical shift plots and δ2D plot for T55D-ND. α-carbon secondary chemical shift (ΔδCα, black bars) and helical δ2D plots (red line) for p53ND and T55D-ND as determined by NMR spectroscopy. Colored bars indicate binding sites for respective protein partners.

We used NMR to investigate the effects of DNA binding on the change in structure of p53ND and T55D-ND (Figure 11). There was no structural change in TAD of T55D-ND; however, the intensity ratios graph, calculated from the values given in the HSQC spectra, shows disappearing peaks for T55D-ND near the mutated site (Figure 11 and 13). As shown by the red numbered residues in Figure 11, the addition of DNA makes this region reappear. A plot of the averaged amide ^{1}H and ^{15}N chemical shift changes between the apo and DNA-bound p53ND and apo and DNA-bound T55D-ND shows the largest chemical shifts are localized in the TAD2 region with maximum shifts observed for residues 52-56 for both p53ND and T55D-ND (Figure 12). There is also significant chemical shift changes within the PRR upon DNA binding, which is consistent with

previously published data that suggests the PRR affects DNA binding [169, 170]. In Figure 13 for p53ND the decrease seen in the TAD2 region suggests an association with the DBD resulting in the lower peak intensities, but the intensity is increased when the TAD2 residues are released from the DBD in the presence of DNA.

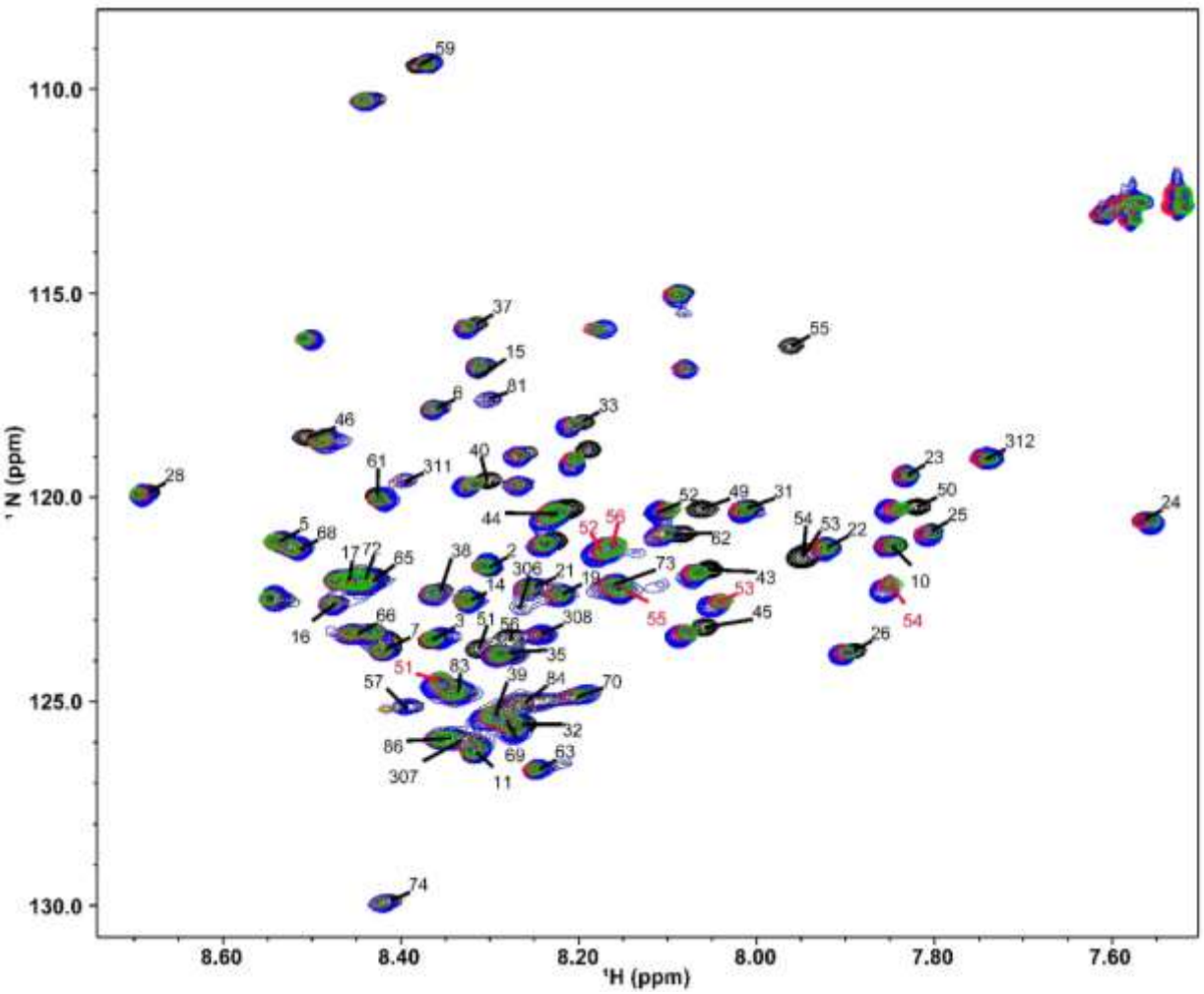

Figure 11 – HSQC spectra of ND and T55D-ND with decreasing amounts of DNA. ^{1}H-^{15}N HSQC spectra overlay of ^{15}N labeled ND with consensus DNA at 100μM (black), ^{15}N labeled T55D-ND with consensus DNA at 150μM (blue), ^{15}N labeled T55D-ND with consensus DNA at 100μM (red), ^{15}N labeled T55D-ND with consensus DNA at 75μM (green). The red numbers represent the residues that are not present for the T55D-ND unbound spectra.

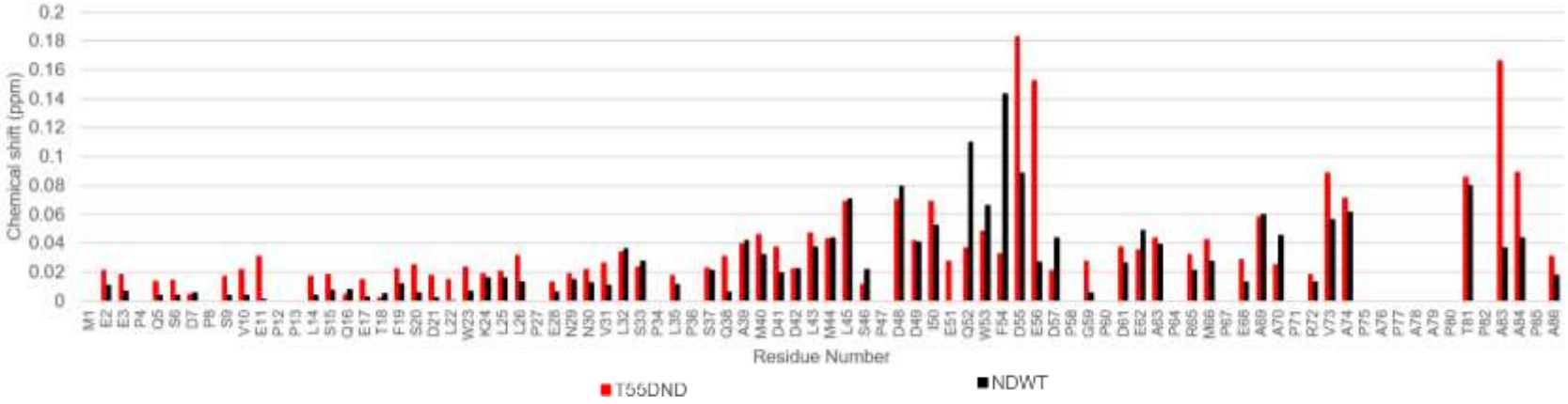

Figure 12 – Chemical shift plot for p53ND and T55D-ND. Plot of the average amide ^{1}H and ^{15}N chemical shift changes for TAD and PRR for the apo vs. DNA bound for p53ND (black bars) and T55D-ND (red bars).

Secondary chemical shift values were calculated using the prediction of temperature, neighbor and pH-corrected chemical shifts for intrinsically disordered proteins (POTENCI) software (Figure 11) [145-147]. All of the measured chemical shifts (NH, N, CA, CB, and CO) were used to calculate the distribution of transient secondary structure using the δ2D software [156].

PTM and DNA Binding specificity of p53ND mutants

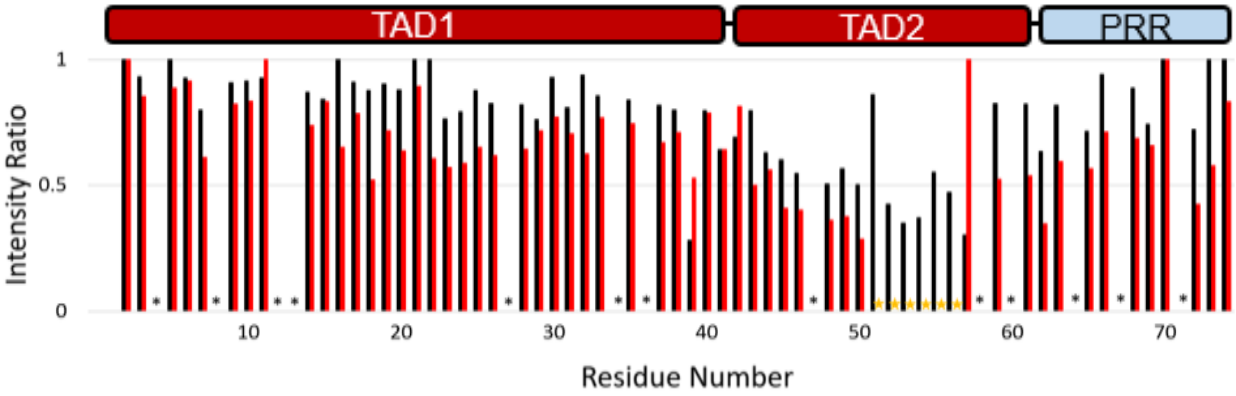

Figure 13 – Intensity ratio of ND and T55D-ND bound and unbound to DNA. The intensity ratios for TAD residues (1-74) were calculated from the values given for the HSQC spectra of ND (black bars) bound and unbound to DNA, T55D-ND (red bars) bound and unbound to DNA, and unassigned peaks are represented by asterisks. The graph for T55D-ND shows disappearing peaks (yellow stars) near the mutated site.

Recent studies showed that the presence of the N-terminal of p53 decreases DNA binding affinity but increases binding specificity [98]. ITC was used to determine the effect of mutations within the p53 N-terminal domain on DNA binding by titrating samples of either the DBD, p53ND, T55D-ND, or NDQS with a 20-bp DNA fragment containing the consensus binding site or a scrambled binding site (Table 2). Figure 14 shows the heat traces from the ITC experiments. The presence of the N-terminal of p53 decreases binding affinity of the DBD for consensus DNA by 29-fold and 39-fold for scramble DNA. The phosphorylation of residue T55 within p53 decreases binding affinity of ND and DBD for consensus DNA by more than 2.5-fold and 82-fold, respectively. The NDQS construct

decreases binding affinity of DBD for consensus DNA by 14-fold and 63-fold for scramble DNA. NDQS is also increased in binding affinity for consensus DNA by 2-fold compared to ND. These results suggest that phosphorylating p53 T55 decreases DNA binding and that residues 53 and 54 aid in the inhibition of DNA binding. The T55D-ND mutant shows a decrease in DNA binding specificity compared to the other constructs we used. This can be estimated by taking the ratio of K_d values for scrambled and consensus DNA. For the p53ND, this ratio is 6.94, for the DBD, it is 3.42, for NDQS the ratio is 15.1, and for T55D-ND the ratio is 3.4. This is an important finding as a decrease in binding specificity would hinder the ability of p53 to discriminate the promoter sites of target genes.

Controlling for DNA quality

In performing any experiments it is always important to make sure that results are reproducible. In this study we performed numerous ITC binding experiments with multiple molecules. After performing a few experiments months apart we noticed some inconsistencies with the data. We performed ITC experiments with differing concentrations of consensus and scramble DNA and a few of the p53 constructs we created. When comparing to the ITC results to DNA:protein concentration ratios we found that for the consensus DNA:p53ND results, there was an increase in the enthalpy (ΔH), entropy (TΔS), ΔG, and K_d values that shared a trend of increasing to the concentration ration of about 2.5-2.7 and then gradually decreasing even with the increasing concentration ratios (Figure 15). For the consensus DNA:DBD results there is an immediate increase to about the 2.7 ratio and then a plateau that occurs for the ΔG and K_d values and a slight increase that occurs for ΔH and TΔS as the concentration ratio reaches 3.7 (Figure 16). When the ITC values for consensus DNA:T55D-ND were

Table 2 – ITC results of DNA binding affinity to p53 constructs. DNA binding affinity of ND (1–312), DBD (94–312), T55D-ND (1-312), and NDQS (1-312) to the consensus DNA binding site and control scrambled DNA as determined by ITC.

	DBD with consensus	DBD with Scramble	ND with consensus	ND with Scramble	T55D-ND with consensus	T55D-ND with Scramble	NDQS with consensus	NDQS with Scramble
K_d (nM)	6.24 ± 1.09	21.37 ± 3.43	192.49 ± 9.35	1335.23 ± 71.13	534.93 ± 29.96	1821.90 ± 113.92	90.04 ± 5.50	1358.70 ± 70.43
Stoichiometry	0.24 ± 0.01	0.24 ± 0.01	0.21 ± 0.002	0.27 ± 0.007	0.25 ± 0.001	0.22 ± 0.005	0.22 ± 0.001	0.23 ± 0.001
ΔG (kCal/mol)	-11.2 ± 0.09	-10.48 ± 0.1	-8.80 ± 0.59	-8.01 ± 0.03	-8.55 ± 0.04	-7.83 ± 0.04	-9.61 ± 0.04	-8.00 ± 0.03
ΔH (kCal/mol)	-16.05 ± 0.18	-15.7 ± 1.50	-9.17 ± 0.48	-9.75 ± 0.85	-5.21 ± 0.13	-6.66 ± 0.10	-8.27 ± 0.20	-9.43 ± 0.11
TΔS (kCal/mol)	-4.85 ± 0.13	-5.22 ± 1.41	-0.37 ± 0.23	-1.74 ± 0.88	3.35 ± 0.14	1.17 ± 0.11	-1.34 ± 0.16	-1.42 ± 0.14

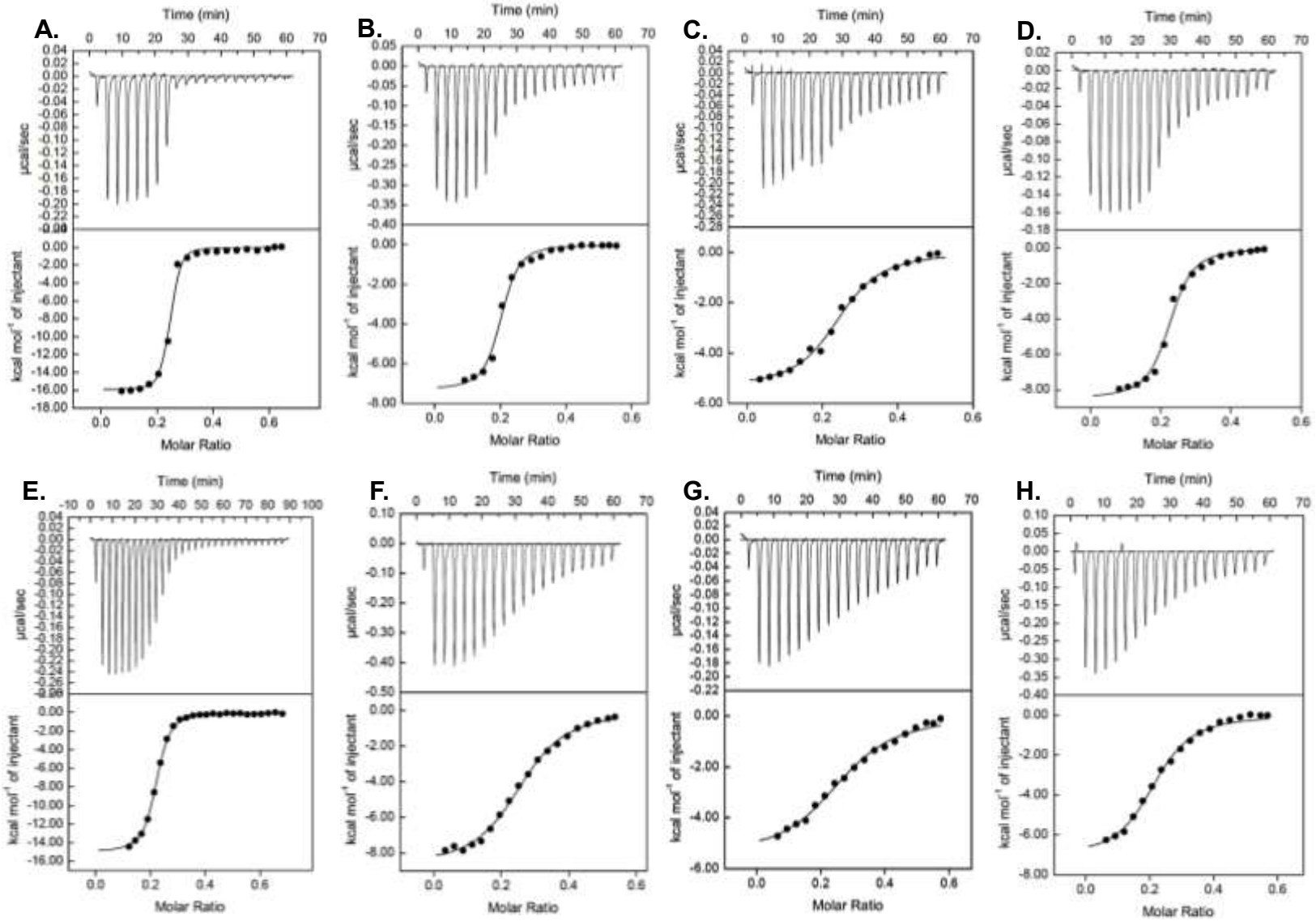

Figure 14 – Binding Isotherms of DNA and p53 constructs. Isothermal calorimetry titrations of A. Consensus DNA into DBD. B. Consensus DNA into p53ND. C. Consensus DNA into T55D-ND. D. Consensus DNA into NDQS. E. Scramble DNA into DBD. F. Scramble DNA into p53ND. G. Scramble DNA into T55D-ND. H. Scramble DNA into NDQS.

analyzed we noticed an increase in all of the values and then a decrease around the 2.5 ratio and then another increase at the end as the concentration ratio continued to increase (Figure 17). In addition to these varying results we tried to repeat previously performed experiments and received very different results especially when working with scrambled DNA (Table 3 and 4). The scramble DNA sample that was currently being used was desalted or salt free. For the consensus DNA we were using a High performance liquid chromatography (HPLC) purified sample. Desalting, or a salt free purification is a very basic process of purification. Excess salt is removed from the sample using normal phase chromatography. This process yields a salt-free sample that is useful for robust techniques, but is unable to remove failed sequences that can possibly form during oligo synthesis. The HPLC method purifies large amounts of oligonucleotides at high purity and even removes shortmers and failed sequences from the sample. Once we noticed the difference in DNA purity we performed the p53ND experiments with HPLC scramble DNA and received the values shown in Table 2.

Table 3 – Previously published ITC results of DNA binding affinity to p53 constructs. DNA binding affinity of ND (1–312), DBD (94–312) to the consensus DNA binding site and control scrambled DNA as determined by ITC.

	p53 ND with Consensus	p53 ND with Scramble	DBD with Consensus	DBD with Scramble
K_d (nM)	188 ± 44.6	1540 ± 392	7.27 ± 2.5	25.4 ± 1.1
Stoichiometry	0.24 ± 0.01	0.26 ± 0.01	0.24 ± 0.01	0.24 ± 0.01
ΔG kcal/mol	-9.18 ± 0.14	-7.94 ± 0.16	-11.1 ± 0.20	-10.4 ± 0.03
ΔH kcal/mol	-9.6 ± 0.28	-9.2 ± 0.35	-16 ± 0.81	-15.6 ± 0.40
TΔS kcal/mol	-0.42 ± 0.41	-1.26 ± 0.47	-4.9 ± 0.67	-5.2 ± 0.42

Table 4 – ITC results of DNA binding affinity to p53 constructs. DNA binding affinity of ND (1–312), DBD (94–312) to the consensus DNA binding site and control scrambled DNA as determined by ITC using lower purity scramble DNA samples.

	ND with Consensus	ND with Scramble	DBD with Consensus	DBD with Scramble
K_d (nM)	252.94 ± 72.08	471.75 ± 91.44	6.5 ± 1.12	47.78 ± 3.86
Stoichiometry	0.19 ± 0.002	0.27 ± 0.007	0.24 ± 0.01	0.21 ± 0.01
ΔG kcal/mol	-9.02 ± 0.19	-8.64 ± 0.11	-11.1 ± 0.10	-9.98 ± 0.04
ΔH kcal/mol	-8.95 ± 0.30	-3.35 ± 0.16	-14.54 ± 0.56	-15.41 ± 0.54
TΔS kcal/mol	0.07 ± 0.50	5.29 ± 0.22	-3.38 ± 0.46	-5.43 ± 0.59

Effect of p53 binding partners on p53-DNA binding

We were interested in how posttranslational modifications affect p53 and its interaction with DNA and other binding partners like Mdm2. We performed ITC to determine the effects p53-DNA binding would have on Mdm2 binding. This experiment was performed by first preforming the titration between p53ND, T55D-ND, and NDQS with consensus DNA, and then titrating Mdm2 into the preformed p53-DNA complex. Table 5 shows that the addition of Mdm2 does not seem to affect the binding of p53ND and NDQS with DNA with the K_d values for the ternary complex being similar to the values for Mdm2 binding to p53ND and NDQS. This suggests that Mdm2 binding is not being inhibited. The phosphorylation of p53 T55 seems to reduce the binding of Mdm2 this could possibly be due to the binding of p53 TAD2 to DBD. This intramolecular binding could be limiting access to the p53 TAD1 domain where Mdm2 binding site is located.

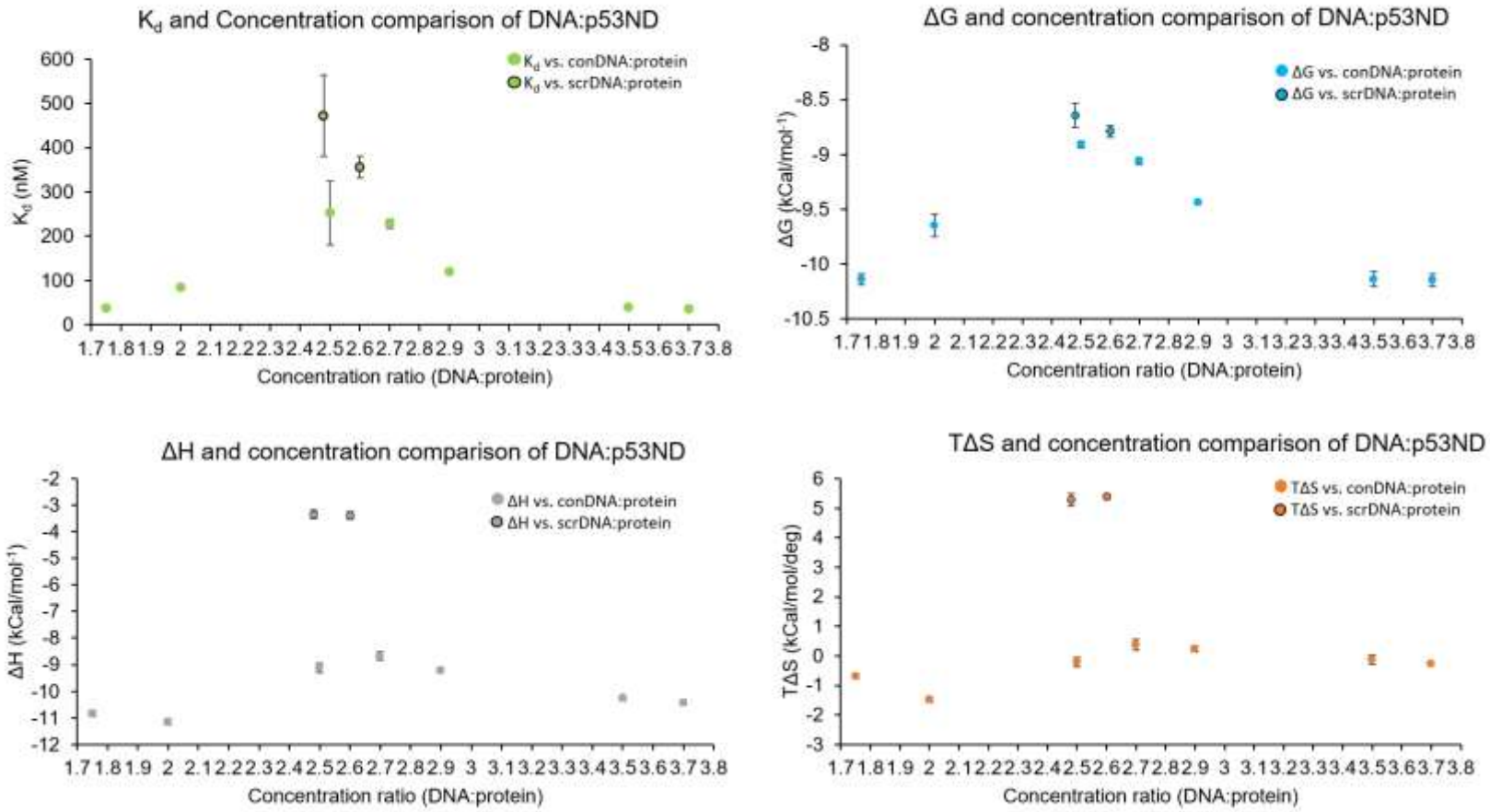

Figure 15 – ITC results compared to the concentration ratio of DNA:p53ND titrated. Titration results of consensus and scramble DNA into p53ND. All circles with no border represent titrations performed with consensus DNA and p53ND. Circles with a black border represent titrations performed with scramble DNA and p53ND. Error bars were calculated from triplicate measurements.

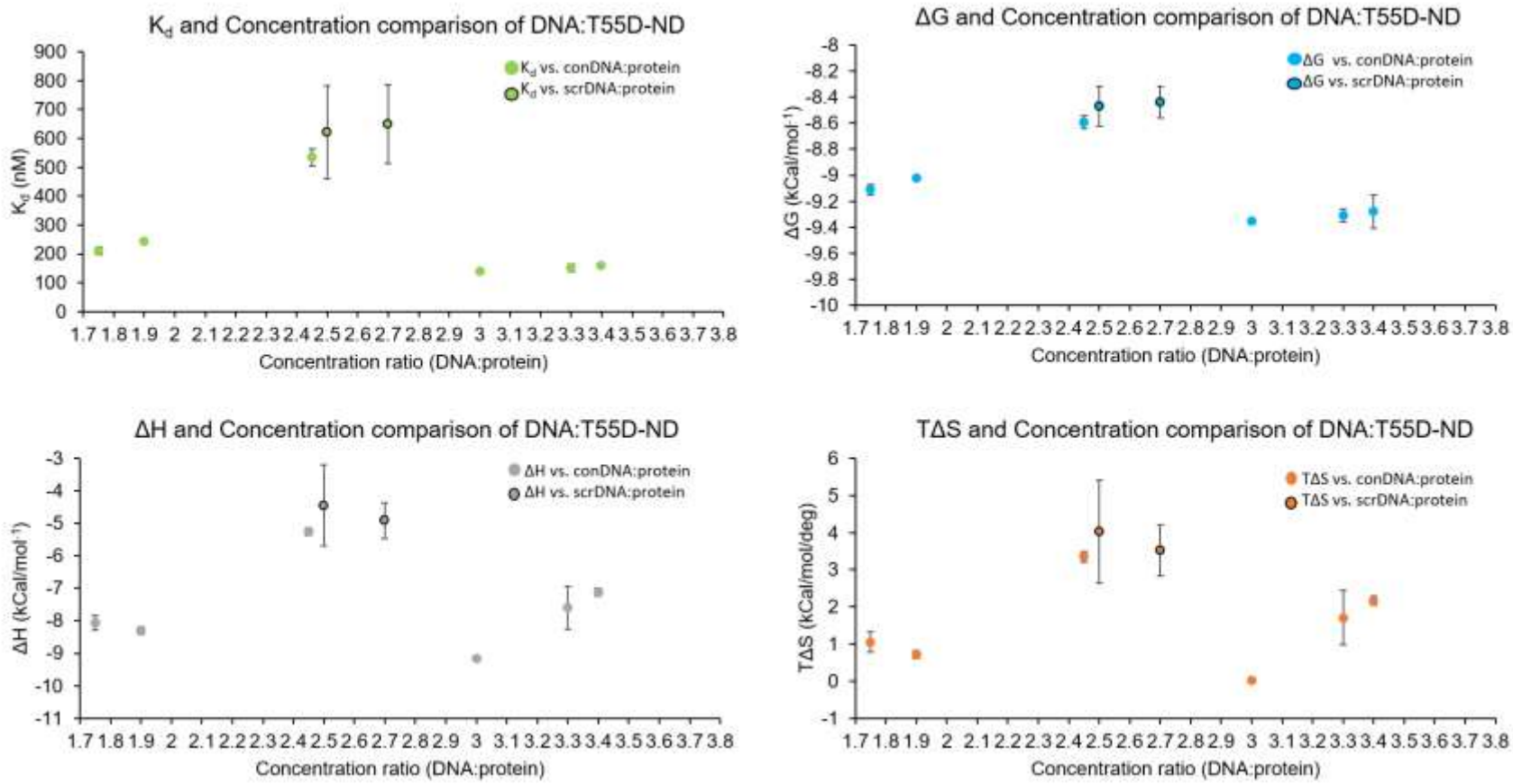

Figure 16 – ITC results compared to the concentration ratio of DNA:DBD titrated. Titration results of consensus and scramble DNA into DBD. All circles with no border represent titrations performed with consensus DNA and DBD. Circles with a black border represent titrations performed with scramble DNA and DBD. Error bars were calculated from triplicate measurements.

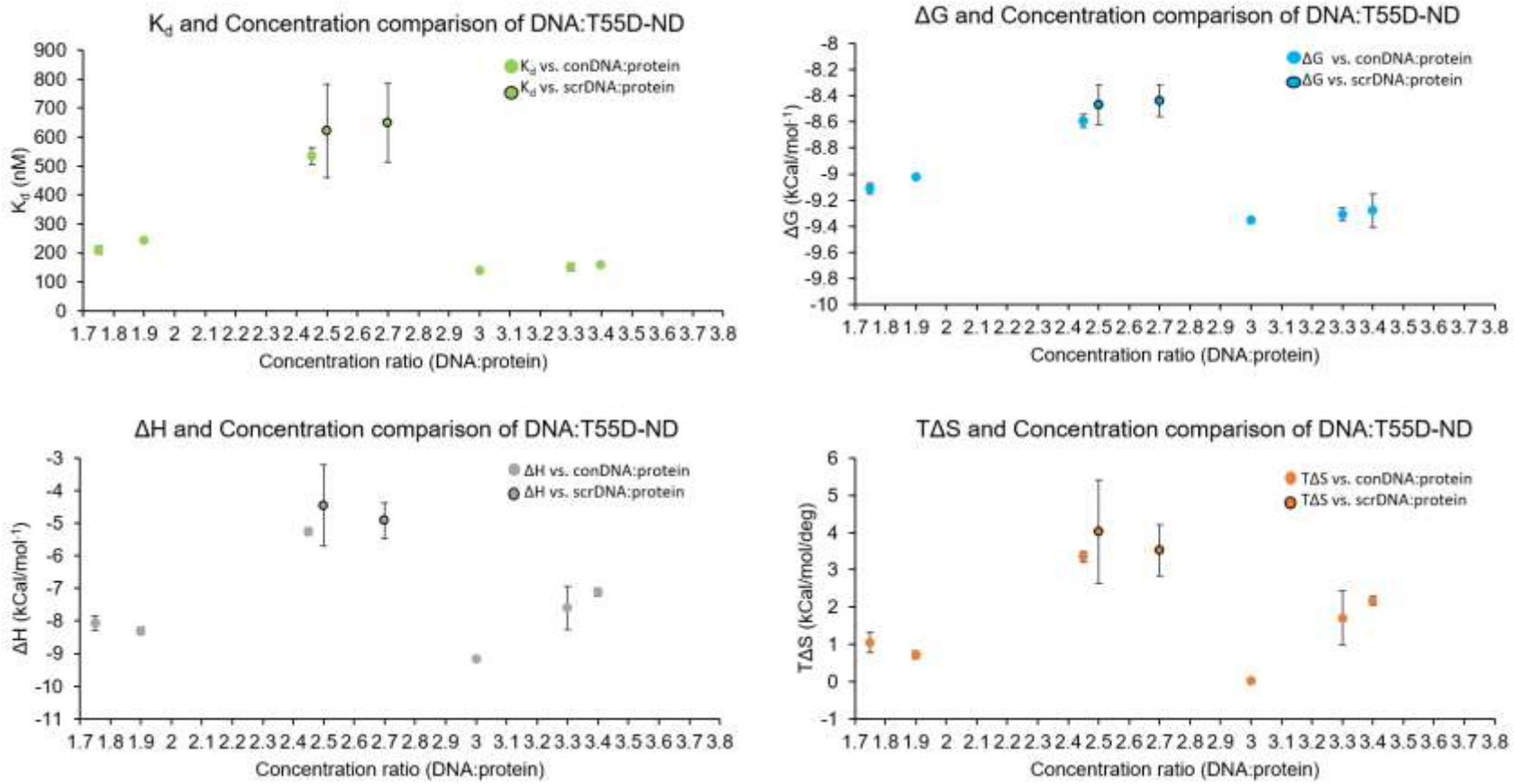

Figure 17 – ITC results compared to the concentration ratio of DNA:T55D-ND titrated. Titration results of consensus and scramble DNA into DBD. All circles with no border represent titrations performed with consensus DNA and DBD. Circles with a black border represent titrations performed with scramble DNA and DBD. Error bars were calculated from triplicate measurements.

Table 5 – ITC results of ND and mutants with consensus DNA and the ternary complex of p53-Mdm2-consensus DNA. DNA binding affinity of ND (1–312), T55D-ND (1-312), and NDQS (1-312) to the consensus DNA binding site and Mdm2 (17-125) as determined by ITC.

	Consensus DNA into p53 ND	Mdm2 into p53 ND	Mdm2 into p53 ND-DNA complex	Consensus DNA into T55D-ND	Mdm2 into T55D-ND	Mdm2 into T55D-ND-DNA complex	Consensus DNA into NDQS	Mdm2 into NDQS	Mdm2 into NDQS-DNA complex
K_d (nM)	143.63 ± 4.44	171.9 ± 33.08	153.62 ± 1.08	509.93 ± 86.97	293.67 ± 0.01	510.40 ± 76.56	94.7 ± 3.75	119.77 ± 4.34	112.3 ± 16.53
Stoichiometry	0.218 ± 0.001	0.956 ± 0.03	0.203 ± 0.004	0.254 ± 0.01	0.909 ± 0.05	0.216 ± 0.01	0.217 ± 0.001	0.982 ± 0.002	0.196 ± 0.01
ΔG (kCal/mol)	-9.46 ± 0.24	-9.02 ± 0.06	-9.29 ± 0.006	-8.59 ± 1.03	-8.58 ± 0.60	-8.59 ± 0.08	-9.34 ± 0.03	-9.44 ± 0.02	-9.48 ± 0.09
ΔH (kCal/mol)	-9.26 ± 0.25	-7.23 ± 0.12	-5.42 ± 0.28	-5.83 ± 0.46	-6.25 ± 0.53	-4.56 ± 0.20	-7.48 ± 0.11	-7.21 ± 0.09	-6.56 ± 0.40
TΔS (kCal/mol)	0.20 ± 0.02	1.82 ± 0.08	3.87 ± 0.28	2.76 ± 0.57	1.50 ± 0.16	4.02 ± 0.14	1.04 ± 0.13	1.23 ± 0.10	2.92 ± 0.47

Chapter Four – Concluding statements

Preservation of p53 transient secondary structure

Through the use of phosphomimetic mutations we investigated the role of phosphorylation on the binding of p53 with Mdm2, MdmX, and CBP/KIX and the effect of phosphorylation on the transient secondary structure of p53. By increasing negative charge of neighboring residues at the positive end (N-terminus) of the helical dipole formed by p53 in the bound state with Mdm2, we expected a stabilization of the dipole in accordance with what is seen in antiparallel helix interactions [134]. This change should also increase the levels of transient helical secondary structure in unbound p53, which we did not observe. Conversely, simulations suggest that phosphorylation of T18 has a destabilizing effect on the helix in the bound state [123]. Our results show that neither an increase nor decrease in transient helicity occurs for S15D or S15D/T18E. Though the phosphomimetics of p53TAD did not show any major changes in structure it is important to note that there were some minor chemical shifts (Figure 5 and 6). The most noticeable shifts were within the Mdm2/MdmX binding site (Figure 6). Small shifts that were seen outside of the Mdm2/MdmX binding site were less than the combined digital resolution of the HSQC experiments. This suggests that any effects were local with no long-range changes in structure, which is an expected result for a disordered protein such as p53.

The binding affinity of p53 to Mdm2 and MdmX was decreased in the presence of the double phosphomimetic mutant, S15D/T18E (Figure 18B). The change in binding affinity for Mdm2 and MdmX is more dramatic than that seen for KIX both here and in

previously published studies, suggesting that where Mdm2 and MdmX compete with CBP for binding to p53, phosphorylation of p53 may encourage binding to CBP through a decrease in Mdm2 and MdmX binding more so than through an increase in CBP binding [85, 91]. Additionally, there could be other factors at play that facilitate binding in vivo.

DNA binding specificity of p53

The p53 N-terminal region performs several important functions. TAD1 and TAD2 interact with different transcription factors such as TBP, TFIID, and coactivator p300/CBP [86]. TAD2 contributes significantly to p53 transcriptional activity and it is well known that W53 and F54 are key residues for TAD2 function [89, 163]. There has been much controversy over whether the transactivation domain of p53 has any effect on DNA binding. Within the past decade studies have shown that the transactivation domain of p53 interacts with the DNA binding domain. Recent studies suggest that p53TAD is also involved in increasing DNA binding specificity [98, 104]. We investigated the effects of point mutations and phosphomimetic mutations on the interaction between p53 and DNA. Our NMR data showed a disappearance of peaks near the mutated site in the absences of DNA but a reappearance of the peaks as we increased DNA concentration (Figure 11, 12 and 13). The disappearance of the peaks within the TAD2 region of T55D-ND indicates that this region is involved in some sort of intramolecular interaction with the DBD and that DNA expels the TAD2 region of T55D-ND from the DBD which causes the peaks to reappear in the presence of DNA. This data indicates that a change in structural confirmation is not the cause of the T55D-ND inhibition of DNA binding but instead that this could possibly be due to electrostatic shielding. Our binding data suggests that the intramolecular interaction between p53TAD and DBD inhibits DNA binding and increases

sequence specificity (Table 2). The NDQS construct increased DNA binding which suggests that residues 53 and 54 play a role in inhibiting DNA binding (Figure 18A). The inhibition of DNA binding is more pronounced with the phosphorylation of residue T55 (Table 2). Furthermore, TAD2 may use multiple weak interactions with the DBD to cause a large effect on DNA binding affinity, which has been suggested in polyvalency models [171].

p53-DNA interaction effects on protein-protein binding affinity

Mouse double minute 2 homolog (MDM2) also known as E3 ubiquitin-protein ligase MDM2 is a protein that in humans is encoded by the MDM2 gene [120]. MDM2 is an important negative regulator of the p53 tumor suppressor and they are both a part of an auto-regulatory feedback loop [70]. The disordered p53 transactivation domain (p53TAD) contains specific levels of transient helical secondary structure that are necessary for its binding to Mmd2. The interactions of p53 with Mdm2 are also modulated by posttranslational modifications of p53TAD. It is unclear whether phosphorylated p53 bound to DNA can effect Mdm2 binding. We used binding experiments to assess how posttranslational modifications effect p53 and its interaction with DNA and Mdm2 binding. Using our p53ND fragment, phosphomimetic mutant T55D-ND and our NDQS mutant we found that there was very little effect on DNA binding when Mdm2 was added to a preformed complex of p53ND with DNA and NDQS with DNA (Table 5 and Figure 18C). The binding results for the ternary complex was similar to that of Mdm2 binding to p53ND and NDQS alone without the presence of DNA. For the T55D-ND with DNA complex there seemed to be a decrease in Mdm2 binding compared to the other p53 fragments (Figure 18D). This could be due to the intramolecular interaction between TAD2 to DBD when

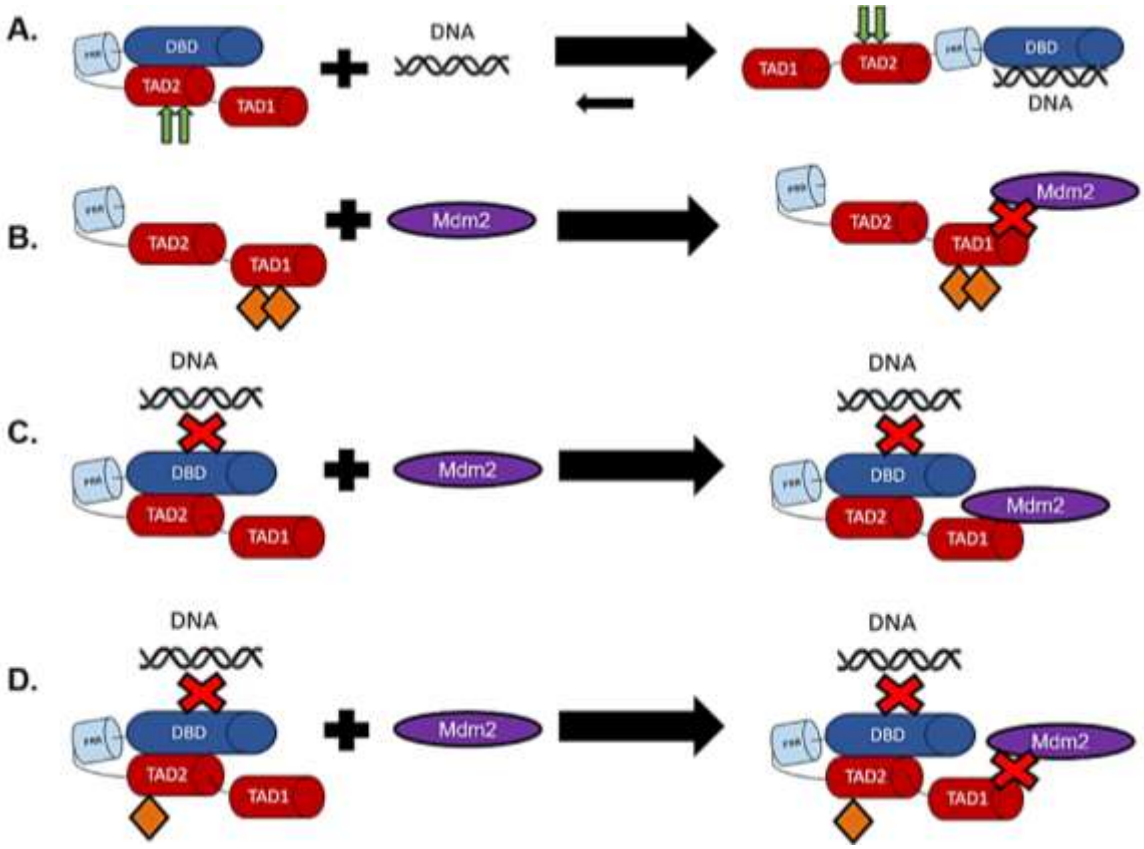

Figure 18 – Schematic of p53ND mutant effects on DNA and protein-protein binding affinity. A. The NDQS mutant results in the equilibrium favoring the DNA-bound state. The green arrows indicate the mutations we made for our NDQS construct. B. The schematic shows that the S15D/T18E (residues 1-73) phosphomimetic mutation of TAD1 inhibits Mdm2 binding. C. The p53ND construct does not affect DNA and Mdm2 binding. D. The T55D-ND phosphomimetic mutant inhibits DNA and Mdm2 binding. Phosphomimetic mutations are indicated by the orange diamonds.

T55 is phosphorylated. These results suggests that the phosphorylation of p53 T55 inhibits Mdm2 binding by restricting access to the TAD1 region of p53.

Concluding statements and future directions

In this report we have shown that PTMs and changes in protein disorder have an effect on binding affinity of protein-protein interactions and DNA binding specificity. We mimicked a state of phosphorylation through the use of phosphomimetic mutants that we created to test the effects of phosphorylation on protein-protein binding and DNA binding. In creating these mutants we in turn increased the negative charge associated with

specific domains of the mutant fragments. This allowed us to also look at the effect of protein disorder on protein structure and protein-DNA interactions. Our structural data did not show any significant changes in structure with these mutants but there were a few notable changes that were localized to the Mdm2/MdmX binding site. We showed that the multi-site phosphorylation of p53TAD decreased binding to Mdm2 and MdmX. In contrast, binding to KIX was unaffected by the mutants which suggests that p53 may utilize certain PTMs like phosphorylation to enforce competitive binding between protein binding partners like Mdm2/MdmX and CBP/p300.

We generated an additional phosphomimetic mutant to investigate the effects of phosphorylation on DNA binding and protein-protein interactions. In addition to that we also wanted to determine the effects on phosphorylation on the intramolecular binding between the transactivation domain and the DNA binding domain of p53 that appears to regulate the DNA binding specificity of p53. Our NMR data showed that the mutation we created for our phosphomimetic mutant had no effect on the structure of our p53 construct, T55D-ND. We did however notice that residues near the mutated site were not visible. With the addition of DNA the missing peaks on the NMR spectra reappeared. This suggested that the T55D-ND mutant was engaging in some type of interaction at the mutated site and in the presence of DNA this interaction is inhibited freeing the mutated site from its previous interaction. Binding data showed that the phosphomimetic mutation of p53 T55 had little effect on Mdm2 and MmdX binding. This was expected as this mutation was not within the Mdm2/MdmX binding site and was thus not expected to interrupt this binding. Our structural data in combination with our binding data suggest

that the intramolecular interaction between phosphorylated p53 TAD2 and DBD inhibits DNA binding and the presence of the p53TAD increases DNA binding specificity.

In performing the DNA binding experiments we came across some inconsistencies with our data which lead us to believe it had to do with the purity of our DNA samples. Our numerous attempts to reproduce results was hindered by the purification technique of our DNA samples. We found that even though we were using a non-consensus DNA sample, the desalting/salt free purification was interfering with the binding of our protein and actually increasing the binding affinity between our protein and the non-consensus DNA which is the opposite reaction we expected. With a more purified sample of DNA we were finally able to reproduce our results which are consistent with previously reported studies.

In the future we plan to work with the desalting/salt free DNA to further understand why this particular purification method produced such inconsistent results. We also would like to investigate the effect of changes in ionic strength and how salt dependence affects p53-DNA binding. This could also give insight into the results received from the desalting/salt free purification. We would like to continue our work with identifying effects of p53-DNA binding on protein-protein interactions by testing other p53 binding partners like MdmX, KIX, TAZ1, and TAZ2. In doing this we will also be utilizing other techniques such as fluorescence anisotropy to study these molecular interactions.

Chapter Five: Methods/Protocols

Site directed mutagenesis

You will need:

-Forward and Reverse primers incorporating mutation

-QuickChange II (Agilent Technologies) kit

-Unmutated plasmid

-NZY+ Broth

Preparation of PCR reactions

Thaw reagents on ice

Prepare control reaction in a sterile microcentrifuge tube by adding:

- 2.5µl of 10X reaction buffer
- 2µl of (10ng) of pWhitescript 4.5-kb control plasmid (5ng/µl)
- 0.625µl (125ng) of oligonucleotide control primer #1 [34-mer (100ng/µl)]
- 0.5µl of dNTP mix
- 18.75µl of double-distilled water (ddH_2O) to a final volume of 25µl

Prepare the sample reaction(s) by setting up a range of sample reactions using various concentrations of template plasmid (e.g., 2.5, 5, 10, 25) while keeping the primer concentration constant.

To each microcentrifuge tube add:

- 2.5µl of 10X reaction buffer
- X µl @ ____ng of respective plasmid to respective tube

- 0.5µl (125ng) of Forward mutant primer
- 0.5µl (125ng) of Reverse mutant primer
- 0.5µl of dNTP mix
- Bring to a final volume of 25µl with ddH_2O

Then add

- 0.5µl of *PfuTurbo* DNA polymerase (2.5U/µl) to each sample reaction and control tube

Thermal cycling

Set up thermal cycler program using the following table:

Table 6 – Thermocycler program for site directed mutagenesis

Segment	**Cycles**	**Temperature(°C)**	**Time (Seconds)**
1	1	95	30
2	30	95	30
		55	60
		68	60/kb of plasmid

Types of mutation desired	**Number of cycles**
Point mutations	12
Single amino acid changes	16
Multiple amino acid deletions or insertions	18

- Store on ice or in fridge until DpnI digestion

DpnI digestion

The DpnI enzyme recognizes the methylated DNA of the template plasmids and cleaves it in many places thus leaving only the mutated products of the PCR reaction intact.

- Add 0.5µl of DpnI enzyme (10U/µl) to each sample reaction and control tube
- Spin down the reaction mixtures in each tube
- Incubate each tube at 37°C for 1 hour with agitation

Transformation

The plasmids are transformed into XL-1 Blue supercompetent cells. These cells were chosen for increased competency and their lack of certain recombinase enzymes preventing the accumulation of mutations within plasmids. This allows for the long term storage of stocks of transformed cells in frozen glycerol.

- Add 25µl of XL-1 Blue supercompetent cells to a sterile microcentrifuge tube
- Add 0.5µl of the DpnI digested sample to respective tubes and gently tap/flick to mix
    - 0.5µl of pUC18 control plasmid can also be added to 25 µl of XL-1 Blue supercompetent cells to verify the transformation efficiency
- Incubate on ice for 30 minutes
- Heat shock at 42°C for 30 seconds
- Incubate on ice for 2 minutes
- Add 125µl of NXY+ Broth preheated to 42°C to each tube
- Incubate for 1 hour at 37°C while shaking at 225-250rpm

- For the mutagenesis and transformation controls, plate the entire volume of cells on LB–ampicillin agar plates containing 80µg/ml X-gal and 20mM IPTG
- For the pUC18 control transformation, plate 5µl of cells on LB–ampicillin agar plates containing 80µg/ml X-gal and 20mM IPTG (to help spread the sample place a 200µl pool of NZY+ broth on the agar plate, pipet the 5 µl of the transformation reaction into the pool, then spread the mixture)
- For the sample reactions, plate the entire volume of each transformation reaction on agar plates containing the appropriate antibiotic for the plasmid vector
- Incubate agar plates overnight (>16hours) at 37°C

For the mutagenesis and transformation controls, there should be 50-800 colonies with 80% that are blue. For the pUC18 control transformation, there should be >250 colonies with >98% that are blue. For the sample reactions, there should be 10-1000 colonies present.

Minipreps

You will need:

-Fresh transformants (no older than 1 week)

-Enough buffer and columns in the Thermo Scientific GeneJET Plasmid Miniprep kit for the number of reactions

-Sterile microcentrifuge tubes for plasmid product

-Overnight cultures

- Add 5ml of LB Broth + appropriate antibiotic for the plasmid vector to the respective number of sterile labeled 15ml Falcon tubes for the respective number of reactions
- Pick selected colonies from transformed plates and inoculate the respective labeled tube
- Incubate tubes overnight at 37°C while shaking at 150-170rp

  For pelleting and lysis:

  - Centrifuge the 15ml Falcon tubes containing the 5ml overnight cultures for 5 minutes at 5,000rpm and discard the supernatant
  - For each tube resuspend the pelleted cells in 250µl of the Resuspension Solution (Buffer P1) which should be stored in the fridge
  - Transfer each cell suspension to a sterile microcentrifuge tube
  - Add 250µl of the Lysis Solution (Buffer p2) and mix thoroughly by inverting the tube 4-6 times until the solution becomes slightly clear and viscous
  - Add 350µl of the Neutralization Solution (Buffer N3) and mix thoroughly by inverting the tube 4-6 times gently to avoid localized precipitation

    DNA purification by spin column
  - Centrifuge each tube for 5 minutes at 13,000rpm and transfer the supernatant (Avoid the white precipitate) to the supplied GeneJET spin column
  - Centrifuge each tube for 1 minute and 13,000rpm and discard the flow-through and reconnect the column
  - Add 500µl of the Wash Solution (Buffer PB) to each column

- Centrifuge each tube for 1 minute at 13,000rpm and discard the flow-through and reconnect the column
- Wash samples a second time by adding 500µl of the Wash Solution (Buffer PB) to each column
- Centrifuge each tube for 1 minute at 13,000rpm and discard the flow-through and reconnect the column
- Repeat the previous step to make sure all of the Wash Solution is removed
- Transfer each column to a sterile microcentrifuge tube
- Add 50µl of Elution Buffer (Buffer EB) to the center of the column (make sure not to touch the membrane)
- Incubate at room temperature for 2 minutes
- Centrifuge each column for 2 minutes at 13,000rpm

DNA purity and sequencing

A nanodrop should be used to measure the concentration and purity of the plasmid DNA. The purity is determined by the ratios of the absorbance at various wavelengths. The ratio of 260nm/230nm estimates the organic solvent contamination and a ratio of greater than 2.0 is desired. The ratio of 260nm/280nm estimates the protein contamination and a ratio of greater than 1.8 is desired. Plasmids should be stored in the fridge (-20°C) until later use. To verify plasmid integrity the plasmid samples should be run on a 1% agarose gel in Tris Boric EDTA (TBE) at 100 Volts for 2 hours.

Plasmid samples that have adequate purity and integrity are shipped to Eurofins MWG Operon for sequencing to confirm that the plasmid has the correct sequence.

Protein purification and Sample preparation

All orthologues that contained a His-tag were expressed using Novagen's pET Vector System, specifically pET-28A plasmid seen in Figure 19. The vector contains a Kanamycin resistance selection site and a T7 promoter followed by a six-histidine tag,

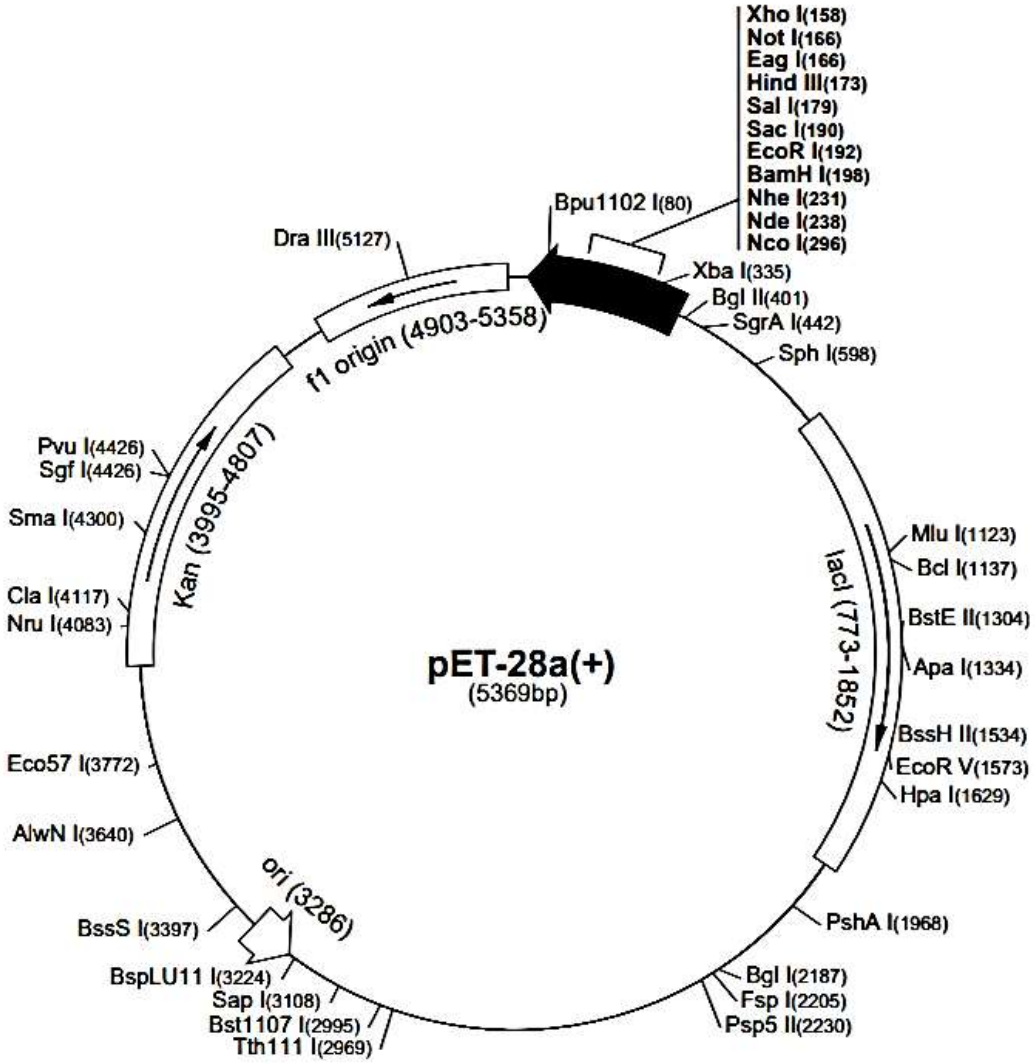

Figure 19 – pET-28A vector [2]. All sequences containing a His-tag were inserted between the Nde I and Xho I restriction sites of this vector.

thrombin cleavage site, and multiple cloning site for expression, purification, and cloning purposes. All orthologues that contained a GST-tag were expressed using SigmaAldrich's

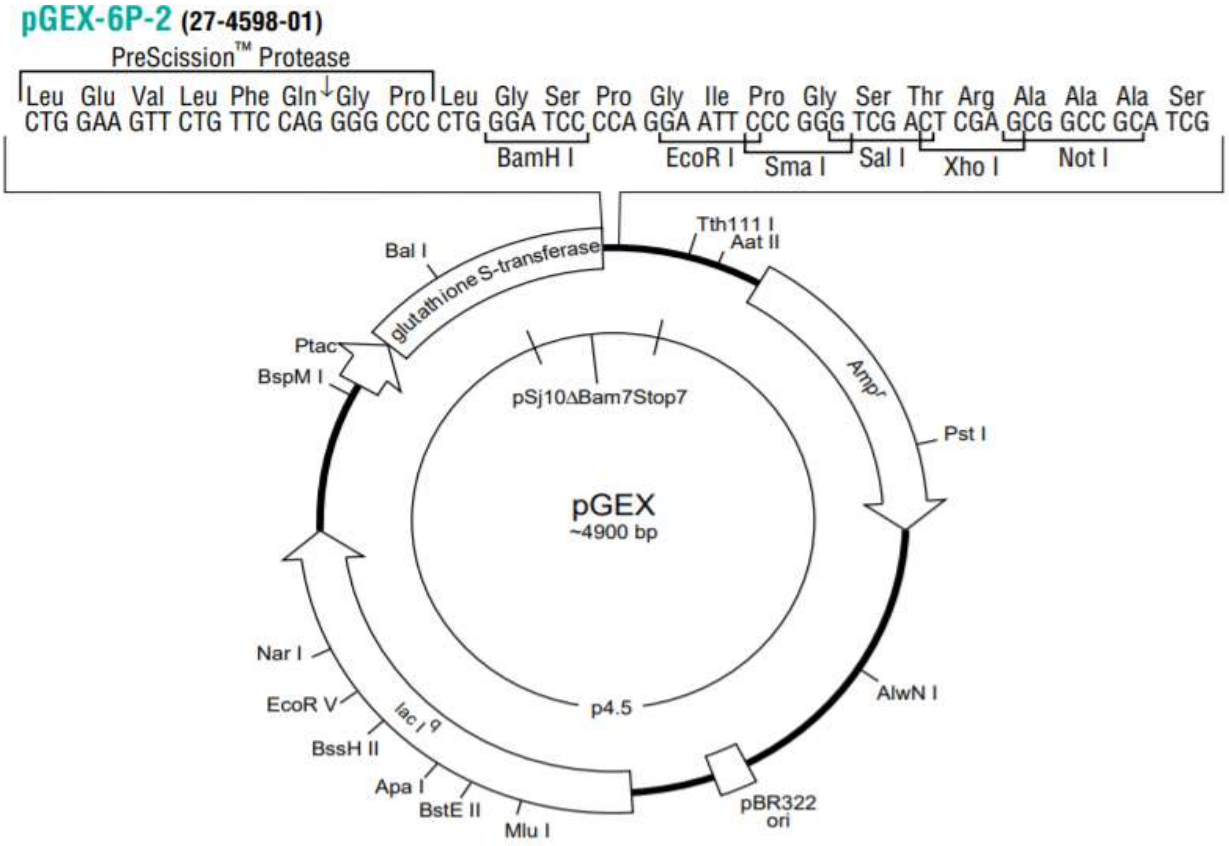

Figure 20 – pGEX vector [1]. All sequences containing a GST-tag were inserted between the BamH I and Xho I restriction sites of this vector

pGEX Vector System, specifically pGEX-6p-2 plasmid seen in Figure 20. The vector contains a Ampicillin resistance selection site and a tac promoter, that is induced by the lactose analog isopropyl β-D-thiogalactoside (IPTG). This vector also contains an internal lacIq gene. The lacIq gene product is a repressor protein that binds to the operator region of the tac promoter, which prevents expression until it is induced by IPTG. This maintains control over the expression of the insert. The plasmids are transformed into BL21 (DE3) chemically competent *E. coli* cells using standard heat shock and SOC recovery protocols. These cells contain the T7 polymerase gene which is regulated by the *lac*UV5 promotor which allows lactose or IPTG to induce the expression of the T7 polymerase. All of our sequences have been codon optimized**.**

Transformation

- Add 20µl of BL21 (DE3) cells from New England Biolabs to 2µl of 1ng/µl of desired plasmid in a sterile microcentrifuge tube
    - For the control, only add the cells not plasmid
- Incubate on ice for 15 minutes
- Heat shock at 42°C for 30 seconds
- Incubate on ice for 2 minutes
- Add 100µl of SOC media (or NXY+ Broth) preheated to 37°C to each tube
- Incubate tubes for 1 hour at 37°C while shaking at 200-220rpm
- Plate the entire volume of each transformation reaction on agar plates containing the appropriate antibiotic for the plasmid vector
- Incubate agar plates overnight (>16hours) at 37°C

Expression and Lysis

All cell growth experiments were performed in M9 media. In order to make ^{15}N-labeled or ^{15}N- and ^{13}C-labeled samples 1g/L of ^{15}N-labeled ammonium chloride and/or 0.2% (w/v) ^{13}C-labeled glucose were added in the place of nitrogen and carbon sources (Cambridge Isotopes). Preparing Stock Salt Solutions for pET-28A vector samples:

To make 2L of 10X M9 Salts:

- 120g – Na_2HPO_4
- 60g – KH_2PO_4
- 10g – NaCl
- bring to 2L with ddH_2O
- pH to 7.1 with HCl and filter sterilize

Make and filter sterilize the following solutions separately with ddH_2O:

- 1M $MgSO_4$
- 20% Destrose- Glucose
- 50mM $CaCl_2$
- 289.5M $FeCl_3$ (in 0.1M HCl to prevent precipitation)
- 5mg/ml Vitamin B (protect from light and store at 4°C)

Preparing 2L of M9 Media for pET-28A vector samples:

- To 1.7L ddH_2O add 200ml of 10X M9 salts
- 4ml 1M $MgSO_4$
- 4ml 50mM $CaCl_2$
- 2ml 0.01M $FeCl_3$
- 400µl Vitamin B (5mg/ml stock)
- If working with a double labeled sample take a 2ml sample of contents already mixed before adding the labeled glucose. If the sample is not labeled continue adding contents below.
- Add 4g of dry Dextrose-Glucose (20ml of 20% stock)
- pH between 7.3-7.5 (7.35 is the optimal pH that reduces salt precipitation)

- Add 2ml of M9 media to sterile 15ml Falcon tube and label this control “Glucose only”
  - Add 2g Ammonium Chloride (NH4Cl)
  - pH between 7.3-7.5 (7.35 is the optimal pH that reduces salt precipitation)
  - Add 2ml of M9 media to sterile 15ml Falcon tube and label this control “Glucose + Nitrogen”

- Add 1mL of antibiotic of choice (pET-28A vector is Kanamycin resistant)
- Add 2ml of M9 media to sterile 15ml Falcon tube and label this control ‘”Antibiotic added”
- Bring to 2L with ddH_2O and filter sterilize into 2 1L bottles
- Inoculate the controls labeled “Glucose only” and “Glucose + Nitrogen” with freshly transformed colonies (no older than 1 week)
- Incubate all controls overnight at 37°C while shaking at 150-170rpm
- Add 25ml of the M9 Media from each 1L bottle to a flask and inoculate the flask with freshly transformed colonies (no older than 1 week)
- Incubate the flask overnight at 37°C while shaking at 150-170rpm
- Place the remaining amount of M9 Media in a 37°C incubator overnight

Expression of pET-28A vector samples

- Check the controls to make sure there is minimal growth in the control labeled “Glucose only”, growth in the control labeled “Glucose + Nitrogen”, and no growth in the control labeled “Antibiotic added”
- Measure the OD@600nm (flow path of 1cm) of the overnight cultures in the flasks (should be over 1.00)
- Place the remaining M9 Media that was stored in the incubator into 2 large flasks that were placed in a 37°C incubator shaking at 150-170rpm
- Inoculate the media to a starting point of 0.04 OD
- Monitor the OD periodically (usually doubles every hour)
- Once the OD of 600 is reached, place 300µl of the culture into a microcentrifuge tube and centrifuge for 2 minutes at 12,000rpm and discard the supernatant. This

pre-induction sample will be stored for SDS-PAGE analysis to compare to samples taken during and post-induction to determine conditions necessary for maximum protein expression.

    - For KIX, once the OD of 600 is reached, place culture in a 15°C incubator shaking at 150-170rpm. Place 300µl of the culture into a microcentrifuge tube and centrifuge for 2 minutes at 12,000rpm and discard the supernatant.

- Induce culture with 1mM IPTG final concentration
- When working with a new mutant take 300µl samples of the culture each hour for SDS-PAGE analysis. p53TAD constructs showed maximum expression at 6 hours. KIX fully expresses after 22 hours.
- Pellet cultures at 8,000rpm for 5 minutes each spin
- Remove supernatant after each spin and when the entire culture has been pelleted, freeze pellet at -80°C for no more than 1 month before purification

Preparing Stock Salt Solutions for pGEX vector samples:

To make 0.1L of Metal Stock Solution:

- 8ml – concentrated HCl
- 5g – $FeCl_2 \cdot 2H_2O$
- 184mg – $CaCl_2 \cdot 2H_2O$
- 4mg – H_3BO_3
- 40mg – $MnCl_2 \cdot 4H_2O$
- 18mg – $CoCl_2 \cdot 6H_2O$
- 4mg – $CuCl_2 \cdot 2H_2O$
- 340mg – $ZnCl_2$

- 605mg – $Na_2 MoO_4 \cdot 2H_2O$
- Fill to 100ml with ddH_2O

To make “O” solution:

- 10ml – Metal Stock Solution
- 26.8g – $MgCl_2 \cdot 6H_2O$
- Fill to 500ml with ddH_2O

To make “S” solution:

- 4.8g – K_2SO_4
- Fill to 100mL with ddH_2O

To make “Salt” solution:

- 16.5g – KH_2PO_4 (MONOBASIC)
- 87.7g – K_2HPO_4 (DIBASIC)
- 18.25g – NaCl
- Fill to 500mL with ddH_2O
- pH to 7.5

Preparing 2L of M9 Media for pGEX vector samples:

- To 1880ml of ddH_2O add 80ml of “Salt” solution
- 2ml “S” solution
- 4ml “O” solution
- 400µl Vitamin B (5mg/mL stock)
- If working with a double labeled sample take a 2mL sample of contents already mixed before adding the labeled glucose. If the sample is not labeled continue adding contents below.

- Add 4g of dry Dextrose-Glucose (20ml of 20% stock)
- pH between 7.3-7.5 (7.35 is the optimal pH that reduces salt precipitation)
- Add 2ml of M9 media to sterile 15ml Falcon tube and label this control "Glucose only"
- Add 2g Ammonium Chloride (NH_4Cl)
- pH between 7.3-7.5 (7.35 is the optimal pH that reduces salt precipitation)
- Add 2ml of M9 media to sterile 15ml Falcon tube and label this control "Glucose + Nitrogen"
- Add 1mL of antibiotic of choice (pGEX vector is Ampicillin resistant)

- Add 2ml of M9 media to sterile 15ml Falcon tube and label this control '"Antibiotic added"
  - Bring to 2L with ddH_2O and filter sterilize into 2 1L bottles
  - Inoculate the controls labeled "Glucose only" and "Glucose + Nitrogen" with freshly transformed colonies (no older than 1 week)
  - Incubate all controls overnight at 37°C while shaking at 150-170rpm
  - Add 25ml of the M9 Media from each 1L bottle to a flask and inoculate the flask with freshly transformed colonies (no older than 1 week)
  - Incubate the flask overnight at 37°C while shaking at 150-170rpm
  - Place the remaining amount of M9 Media in a 37°C incubator overnight

Expression of pGEX vector samples

- Check the controls to make sure there is minimal growth in the control labeled "Glucose only", growth in the control labeled "Glucose + Nitrogen", and no growth in the control labeled "Antibiotic added"

- Measure the OD@600nm (flow path of 1cm) of the overnight cultures in the flasks (should be over 1.00)
- Place the remaining M9 Media that was stored in the incubator into 2 large flasks that were placed in a 37°C incubator shaking at 150-170rpm
- Inoculate the media to a starting point of 0.04 OD
- Monitor the OD periodically (usually doubles every hour)
- For Mdm2/MdmX constructs, once the OD of 600 is reached, place flasks in a 15°C incubator shaking at 150-170rpm. Place 300µl of the culture into a microcentrifuge tube and centrifuge for 2 minutes at 12,000rpm and discard the supernatant. For p53ND constructs, once the OD of 500 is reached add 200µl of 100mM $ZnCl_2$ per liter of culture and transfer culture to cold incubator set to 15°C and continue growing the culture until the OD of 600 is reached. Place 300µl of the culture into a microcentrifuge tube and centrifuge for 2 minutes at 12,000rpm and discard the supernatant. The pre-induction sample will be stored for SDS-PAGE analysis to compare to samples taken during and post-induction to determine conditions necessary for maximum protein expression.
- For Mdm2/MdmX constructs, induce culture with 1mM IPTG final concentration. For the p53ND constructs, wait 15-30 minutes then induce culture with 1mM IPTG final concentration.
- For the Mdm2/MdmX constructs, the culture will express for 18 hours. For the p53ND constructs, the culture will express for 20 hours.
- Pellet cultures at 8,000rpm for 5 minutes each spin

Remove supernatant after each spin and when the entire culture has been pelleted, freeze pellet at -80°C for no more than 1 month before purification

Nickel column and Thrombin cleavage

To prepare the Nickel column buffers for samples containing a His-tag:

To make 2L of Nickel Lysis buffer:

- To 800ml of ddH_2O add 50mM Sodium Phosphate Monobasic Monohydrate (13.79g)
- 300mM NaCl (35.064g)
- 10mM Imidazole (1.36g)
- 0.02% Sodium Azide (2mL of 20% stock)
- Bring to 2L with ddH_2O
- pH to 8 and filter sterilize into 2 1L bottles

To make 1L of Nickel Elution buffer:

- To 800ml of ddH_2O add 50mM Sodium Phosphate Monobasic Monohydrate (6.895g)
- 300mM NaCl (17.532g)
- 250mM Imidazole (17.02g)
- 0.02% Sodium Azide (1mL of 20% stock)
- Bring to 1L with ddH_2O
- pH to 8 and filter sterilize into a 1L bottle

To make 2L of Gel Filtration buffer:

- To 800ml of ddH_2O add 50mM Sodium Phosphate Monobasic Monohydrate (13.79g)

- 300mM NaCl (35.064g)
- 1mM EDTA (4mL of 500mM stock)
- 0.02% Sodium Azide (2mL of 20% stock)
- Bring to 2L with ddH_2O
- pH to 7 and filter sterilize into 2 1L bottles

Lysis, Pre-Cleave Nickel column, Thrombin cleavage, Post-Cleave Nickel column, and Size Exclusion column

- After expression, suspend pellets in 25mL of Nickel lysis buffer containing 1 protease inhibitor tablet (SigmaAldrich) per liter of culture
- Lyse with a French Press pressure cell using a minimum pressure of 20,000psi.
- Centrifuge the sample at 38,720g for 1hr to isolate the soluble fraction
- Filter the supernatant and add to a column containing 30ml of Ni-NTA Superflow resin (Qiagen). All buffers used on the Ni-NTA column were run at a flow rate of 3ml/min. Table 7 shows the program guidelines of the pre-cleave Nickel column.

Table 7 – Nickel column (pre-cleave) program guidelines

Step	Equilibrate	Inject	Wash	Elute	Reequilibrate
Volume	1 CV*	1 CV* + Sample Volume	2 CV*	3 CV*	3CV*
Buffer	Lysis	Lysis	85% lysis and 15% elution mixed by the FPLC system	Elution	Lysis

*The column volume (CV) is 30ml of Ni-NTA Superflow resin (Qiagen) that is used.

- Analyze fractions of peaks seen on the chromatogram using PAGE and combine the fractions containing the protein

- Concentrate combined sample in an Amicon Ultra-15 3K centrifugal filter device until it reaches a final volume of 8ml.
- Dialyze sample overnight into gel filtration buffer using 3500Da MWCO dialysis tubing (FisherBrand).
- Remove HIS-tag from protein with the Sigma-Aldrich Thrombin CleanCleave Kit (RECOMT).
    - Wash Thrombin beads with dialysate from dialyzed sample, and place the mixture in a 15ml Falcon tube
    - Centrifuge tube for 5 minutes at 1000rpm at 4°C
    - Discard supernatant and wash beads again with fresh dialysate
    - Centrifuge tube for 5 minutes at 1000rpm at 4°C
    - Discard supernatant and wash beads again with fresh dialysate
    - Centrifuge tube for 5 minutes at 1000rpm at 4°C
    - Before adding the dialyzed sample to the thrombin bead remove 15-30µl of the pre-cleaved sample for SDS-PAGE analysis and comparison with the post-cleave sample.
    - Discard supernatant and add dialyzed sample to Thrombin beads.
    - Place the tube on platform rocker for 4 hours (p53TAD WT) or overnight (other p53TAD mutants) and for 2 hours for KIX.
    - Run the solution through the Thrombin column to retrieve the cleaved sample in a fresh 15ml Falcon tube and rinse the tube with the dialysate to collect residual protein in the tube to run through the Thrombin column.

- Place 2ml of the dialysate in the column to collect in a waste collection tube.
- Add 2ml of the Thrombin Regeneration Buffer 1 to the column and allow it to flow through to the waste collection tube.
- Add 2ml of the Thrombin Regeneration Buffer 2 to the column and allow it to flow through to the waste collection tube.
- Add another 2ml of the Thrombin Regeneration Buffer 2 to the column and allow it to flow through to the waste collection tube.
- Add 2ml of the Thrombin Storage Buffer to the column and allow it to flow through to the waste collection tube.
- Cap the column and add 2ml of the Thrombin Storage Buffer to the column and mix to loosen the beads then transfer them to the provided Thrombin kit container and store in -20°C.

- Verify the completion of the cleavage reaction by taking a 15-30µl sample for SDS-PAGE analysis.
- Concentrate combined sample in an Amicon Ultra-15 3K centrifugal filter device until it reaches a final volume of ~4-6ml.
- Load concentrated sample onto 120ml of GE HiLoad 16/60 Superdex 75 resin (size exclusion column). The 2ml injection volumes should be run at a flow rate of 1ml/min. Table 8 shows the program guidelines of the column.

Table 8 – GE HiLoad 16/60 Superdex 75 column program guidelines

Step	**Equilibrate**	**Inject**	**Elute**	**Reequilibrate**	**Inject**	**Elute**
Volume	1.25 CV*	2ml	1.5 CV*	0.25 CV*	2ml	1.5CV

*The column volume (CV) is 120ml of GE HiLoad 16/60 Superdex 75 column that is used.

- Analyze fractions of peaks seen on the chromatogram using SDS-PAGE and combine those fractions containing the protein.
- Concentrate combined sample in an Amicon Ultra-15 3K centrifugal filter device until it reaches a final volume of ~5ml.
- Dialyze samples in NMR buffer or ITC buffer overnight using 3500Da MWCO dialysis tubing (FisherBrand).

To prepare 1L of NMR buffer p53TAD constructs:

- 50mM Sodium Phosphate Monobasic Monohydrate (6.895g)
- 50mM NaCl (2.922g)
- 1mM EDTA (2mL of 500mM stock)
- 0.02% Sodium Azide (1mL of 20% stock)
- Bring to 2L with ddH_2O
- pH to 8 and filter sterilize into 1L bottle

To prepare 2L of ITC buffer for p53TAD constructs:

- 50mM Sodium Phosphate Monobasic Monohydrate (13.79g)
- 150mM NaCl (17.532g)
- 1mM EDTA (4mL of 500mM stock)
- 0.02% Sodium Azide (2mL of 20% stock)
- Bring to 2L with ddH_2O
- pH to 8 and filter sterilize into 2 1L bottles

Finally concentrate to desired NMR or ITC concentration or freeze with 50% glycerol in -80°C.

Glutathione S-transferase, Anion Exchange, and size exclusion columns

To prepare the GST column buffers for samples containing a GST-tag:

To make 2L of GST-A buffer for Mdm2/MdmX:

- 25mM Tris Base (6.057g)
- 25mM Tris Hydrochloride (7.88g)
- 300mM NaCl (35.064g)
- 1mM DTT (0.3085g)
- 0.02% Sodium Azide (2mL of 20% stock)
- 2.5mM EDTA (10mL of 500mM stock)
- Bring to 2L with ddH_2O
- pH to 7.4 and filter sterilize into 2 1L bottles

To make 0.250L of GST-B buffer for Mdm2/MdmX:

- 25mM Tris Base (0.757g)
- 25mM Tris Hydrochloride (0.985g)
- 300mM NaCl (4.383g)
- 1mM DTT (0.0385g)
- 10mM Reduced Glutathione (0.768g)
- 0.02% Sodium Azide (250µL of 20% stock)
- 2.5mM EDTA (1.25mL of 500mM stock)
- Bring to 0.250L with ddH_2O
- pH to 7.4 and filter sterilize into a 250ml bottle

To make 2L of Gel Filtration buffer for Mdm2/MdmX:

- 50mM Sodium Phosphate Monobasic Monohydrate (13.79g)

- 300mM NaCl (35.064g)
- 1mM EDTA (4mL of 500mM stock)
- 0.02% Sodium Azide (2mL of 20% stock)
- Bring to 2L with ddH_2O
- pH to 7 and filter sterilize into 2 1L bottles

To make 2L of GST-A buffer for p53ND constructs:

- 25mM Tris Base (6.057g)
- 25mM Tris Hydrochloride (7.88g)
- 300mM NaCl (58.44g)
- 1mM DTT (0.3085g)
- 0.02% Sodium Azide (2mL of 20% stock)
- 20μM $ZnCl_2$ (400μl of 100mM stock)
- Bring to 2L with ddH_2O
- pH to 7.4 and filter sterilize into 2 1L bottles

To make 0.250L of GST-B buffer for p53ND constructs:

- 25mM Tris Base (0.757g)
- 25mM Tris Hydrochloride (0.985g)
- 300mM NaCl (7.305g)
- 1mM DTT (0.0385g)
- 10mM Reduced Glutathione (0.768g)
- 0.02% Sodium Azide (250μL of 20% stock)
- 20μM $ZnCl_2$ (50μl of 100mM stock)
- Bring to 0.250L with ddH_2O

- pH to 7.4 and filter sterilize into a 250ml bottle

To make 2L of Anion Exchange Load buffer for p53ND constructs:

- 20mM Tris Base (4.85g)
- 0.02% Sodium Azide (2mL of 20% stock)
- 20μM $ZnCl_2$ (400μl of 100mM stock)
- 1mM DTT (0.3085g)
- Bring to 2L with ddH_2O
- pH to 7 and filter sterilize into 2 1L bottles

To make 1L of Anion Exchange Elution buffer for p53ND constructs:

- 20mM Tris Base (2.425g)
- 1M NaCl (58.44g)
- 0.02% Sodium Azide (1mL of 20% stock)
- 1mM DTT (0.154g)
- 20μM $ZnCl_2$ (200μl of 100mM stock)
- Bring to 1L with ddH_2O
- pH to 7 and filter sterilize into a 1L bottle

To make 2L of Gel Filtration buffer for p53ND constructs:

- 50mM Sodium Phosphate Monobasic Monohydrate (13.79g)
- 300mM NaCl (35.064g)
- 0.02% Sodium Azide (2mL of 20% stock)
- 2mM DTT (0.617g)
- Bring to 2L with ddH_2O
- pH to 7 and filter sterilize into 2 1L bottles

Lysis, GST column, Anion Exchange column and Size Exclusion column

- After expression, suspend pellets in 25mL of GST-A buffer containing 1 protease inhibitor tablet (SigmaAldrich) per liter of culture.
- Lyse with a French Press pressure cell using a minimum pressure of 20,000psi.
- Centrifuge the sample at 38,720g for 1hr to isolate the soluble fraction.
- Filter the supernatant and apply to a column containing 10ml Glutathione Sepharose 4 Fast Flow resin. The injection volumes should be run at a flow rate of 2ml/min and the buffers are run at 4.5ml/min. Table 9 shows the program guidelines of the column.

Table 9 – GST column (pre-cleave) program guidelines

Step	**Equilibrate**	**Inject/flow-through**	**Wash**	**Elute**	**Reequilibrate**
Volume	2 CV*	25ml	2.5 CV*	3.5 CV*	1.25 CV*
Buffer	Lysis	Lysis	Lysis	Elution	Lysis

*The column volume (CV) is 25ml Glutathione Sepharose 4 Fast Flow resin that is used.

- Analyze fractions of peaks seen on the chromatogram using PAGE and combine the fractions containing the protein.
- Dialyze the sample overnight into GST-A buffer using 3500Da MWCO dialysis tubing (FisherBrand) and add a 1:100 ratio of HRV3C protease to cleave the GST tag.
- Apply to a column containing 25ml Glutathione Sepharose 4 Fast Flow resin. The injection volumes should be run at a flow rate of 0.1ml/min and the buffers are run at 4ml/min. Table 10 shows the program guidelines of the column.

Table 10 – GST column (post-cleave) program guidelines

Step	Equilibrate	Inject/flow-through	Wash	Elute	Reequilibrate
Volume	2.5 CV*	50ml	3.5 CV*	2.5 CV*	1.25 CV*
Buffer	Lysis	Lysis	Lysis	Elution	Lysis

*The column volume (CV) is 25ml Glutathione Sepharose 4 Fast Flow resin that is used.

- Analyze fractions of peaks seen on the chromatogram using PAGE and combine the fractions containing the protein
- Concentrate combined sample in an Amicon Ultra-15 3K centrifugal filter device until it reaches a final volume of ~10-14ml (make sure not to exceed 100uM protein concentration of the protein will precipitate)
- For Mdm2/MdmX, load sample onto a GE HiLoad 16/60 Superdex 75 column. The 2ml injection volumes should be run at a flow rate of 1.5ml/min. Table 11 shows the program guidelines of the column.

Table 11 – GE HiLoad 16/60 Superdex 75 column program guidelines

Step	Equilibrate	Inject	Elute	Reequilibrate	Inject	Elute
Volume	1.25 CV*	2ml	1.5 CV*	0.25 CV*	2ml	1.5CV

*The column volume (CV) is 30mL of GE HiLoad 16/60 Superdex 75 column that is used.

- For p53ND constructs, after the GST post-cleave column, dialyze the sample overnight into Anion Exchange Load buffer using 3500Da MWCO dialysis tubing (FisherBrand)
- Apply to a column containing 10ml Anion Exchange column. The injection volumes should be run at a flow rate of 4ml/min and the buffers are run at 5ml/min. Table 12 shows the program guidelines of the column.

Table 12 – Anion Exchange column program guidelines

Step	Equilibrate	Inject	Wash	Elute	Reequilibrate
Volume	2 CV*	5 CV*	3 CV*	18 CV* gradient, 4 CV*	3 CV*
Buffer	Lysis	Lysis	Lysis	Gradient 10%-40% Elution, 100% Elution	Lysis

*The column volume (CV) is 10ml Anion Exchange column that is used.

- Analyze fractions of peaks seen on the chromatogram using PAGE and combine the fractions containing the protein
- Concentrate combined sample in an Amicon Ultra-15 3K centrifugal filter device until it reaches a final volume of ~6-10ml (make sure not to exceed 100uM protein concentration of the protein will precipitate)
- For p53ND constructs, load sample onto a GE HiLoad 16/60 Superdex 75 column. The 2ml injection volumes should be run at a flow rate of 1.5ml/min. Table 13 shows the program guidelines of the column

Table 13 – GE HiLoad 16/60 Superdex 75 column program guidelines

Step	Equilibrate	Inject	Elute	Reequilibrate	Inject	Elute
Volume	1.25 CV*	2ml	1.5 CV*	0.25 CV*	2ml	1.5CV

*The column volume (CV) is 30mL of GE HiLoad 16/60 Superdex 75 column that is used.

- Analyze fractions of peaks seen on the chromatogram using SDS-PAGE and combine those fractions containing the protein
- Concentrate combined sample in an Amicon Ultra-15 3K centrifugal filter device until it reaches a desired concentration that does not exceed 100uM
- Dialyze sample in NMR buffer or ITC buffer overnight using 3500Da MWCO dialysis tubing (FisherBrand)

To prepare 1L of NMR buffer for p53ND constructs:

- 50mM Sodium Phosphate Monobasic Monohydrate (6.895g)

- 50mM NaCl (2.922g)
- 0.02% Sodium Azide (1mL of 20% stock)
- Bring to 2L with ddH_2O
- pH to 8 and filter sterilize into 1L bottle

To prepare 2L of low ionic strength (85mM) ITC buffer:

- 10mM Sodium Phosphate Monobasic Monohydrate (13.79g)
- 150mM NaCl (17.532g)
- 0.02% Sodium Azide (2mL of 20% stock)
- 8mM β-mercapthoethanol (1.25ml of 100% stock)
- Bring to 2L with ddH_2O
- pH to 8 and filter sterilize into 2 1L bottles

Finally concentrate to desired NMR or ITC concentration or freeze with 50% glycerol in -80°C.

Sodium Dodecyl Sulphate – Polyacrylamide Gel Electrophoresis (SDS-PAGE)

Preparing a 6%-16% gradient gel:

To make 250ml of 4X Lower Gel Buffer:

- 1.5M Tris Base (45.427g)
- 0.4% SDS (1g)
- Fill to 250mL with ddH_2O water
- pH 8.8

To make 250ml of 4X Upper Gel Buffer:

- 0.5M Tris Base (15.142g)

- 0.4% SDS (1g)
- Fill to 250mL with ddH_2O water
- pH 6.8

To make Lower gel 6% solution in a 15ml Falcon tube:

- 1.25ml 4X LOWER gel buffer
- 2.94ml ddH_2O
- 750µl of 40% Acrylamide
- Mix well by pipetting
- 50µl 10% APS
- Mix well by pipetting
- 5µl TEMED (Add when ready to create gel)
- Mix well by pipetting

To make Lower gel 16% solution in a 15ml Falcon tube:

- 1.25 mL 4X LOWER gel buffer
- 1.695mL ddH_2O
- 2mL 40% Acrylamide
- Mix well by pipetting
- 50µL 10% APS
- Mix well by pipetting
- 5µL TEMED (Add when ready to create gel)
- Mix well by pipetting

To make Upper gel 4% solution in 15ml Falcon tube:

- 1ml 4X UPPER gel buffer

- 2.556mL ddH_2O
- 400µl 40% Acrylamide
- Mix well by pipetting
- 40µl 10% APS
- Mix well by pipetting
- 4µl TEMED (Add when ready to create top layer of gel)
- Mix well by pipetting

To prepare gel:

- Add 1ml of the 16% LOWER gel to the gel apparatus
- Add 1ml of 6% LOWER gel to the tube containing the remaining 16% LOWER gel and mix by pipetting or inverting, be careful not to create too many bubbles
- Add 1ml of the mixed LOWER gel solution to the gel apparatus
- Add 1ml of 6% LOWER gel to the tube containing the remaining 16% LOWER gel and mix by pipetting or inverting, be careful not to create too many bubbles
- Add 1ml of the mixed LOWER gel solution to the gel apparatus
- Add 1ml of 6% LOWER gel to the tube containing the remaining 16% LOWER gel and mix by pipetting or inverting, be careful not to create too many bubbles
- Add 1ml of the mixed LOWER gel solution to the gel apparatus
- Add 200µl of isopropanol to the top of the gel gradient SLOWLY as to no disturb the gel solution

- Allow the LOWER gel to solidify then pour off the isopropanol.
- Add 2-3ml of 4% UPPER gel to the gel apparatus and place comb in the gel apparatus and wipe off excess UPPER gel that is displaced
- Allow the UPPER gel to solidify then remove comb

If making gels for storage wrap in a damp paper towel and store in the fridge for no longer than a week. When running samples set the power supply to 195 Volts for 45 minutes.

Examples of gels and chromatograms

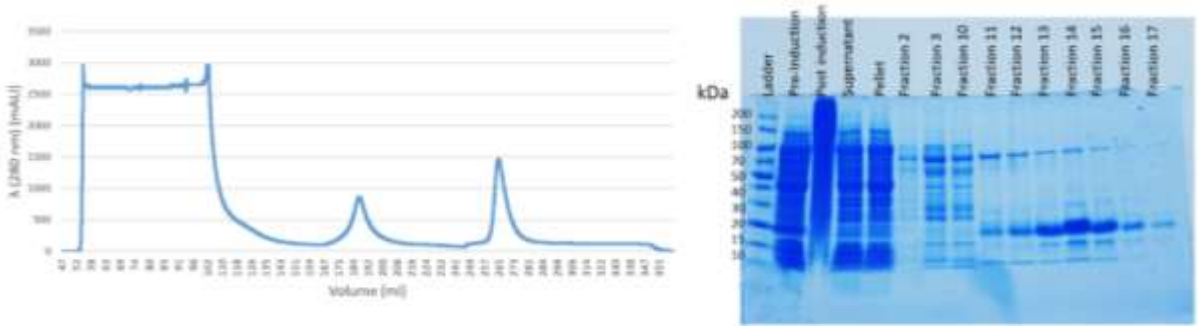

Figure 21 – p53TAD Nickel Pre-Cleave column chromatogram and SDS-PAGE gel.

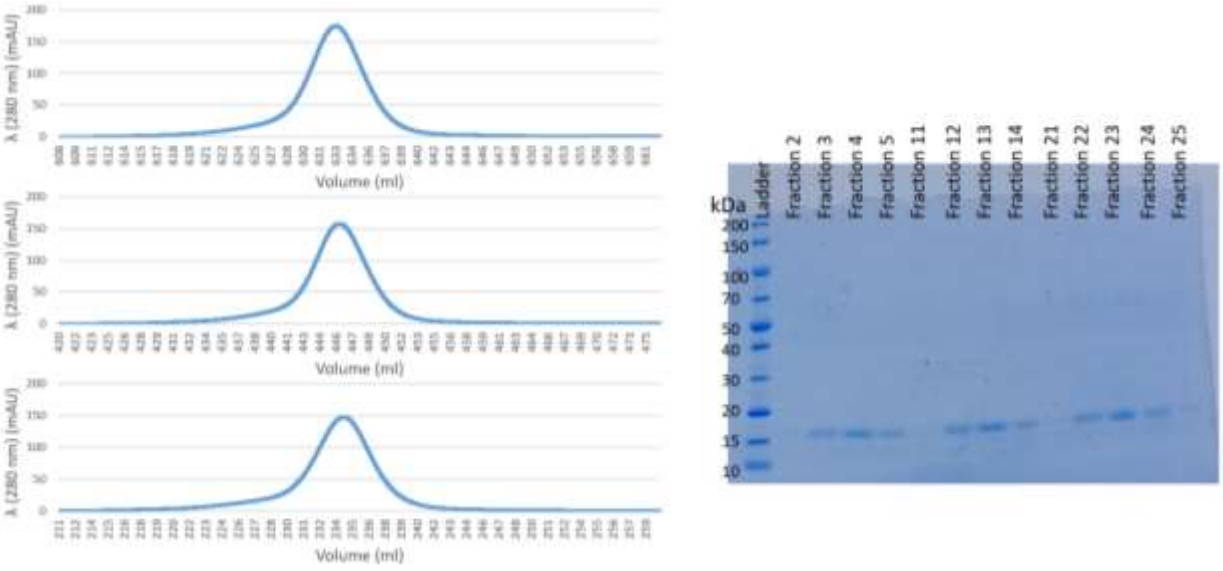

Figure 22 – p53TAD SEC column chromatogram and SDS-PAGE gel.

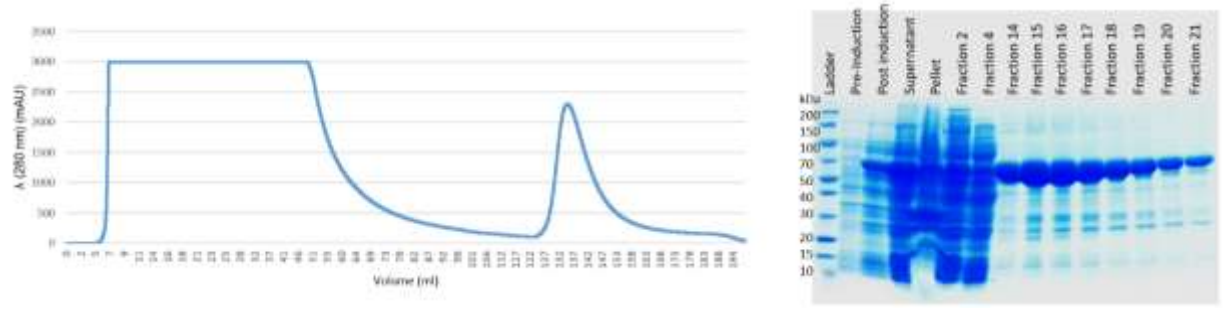

Figure 23 – p53ND GST Pre-Cleave column chromatogram and SDS-PAGE gel.

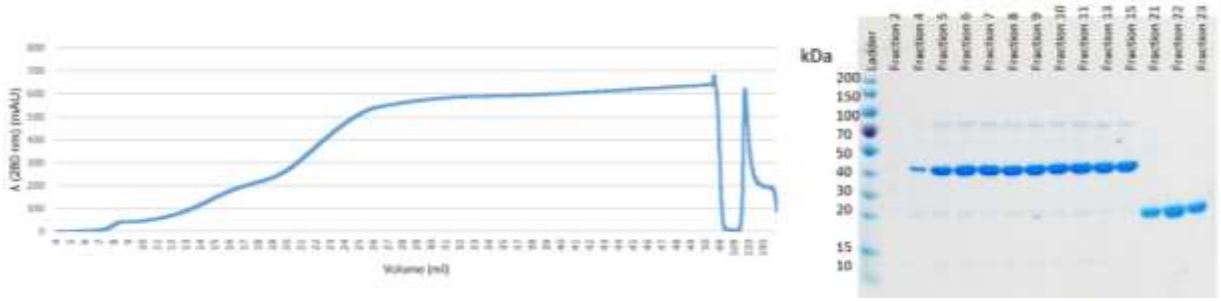

Figure 24 – p53ND GST Post-Cleave column chromatogram and SDS-PAGE gel.

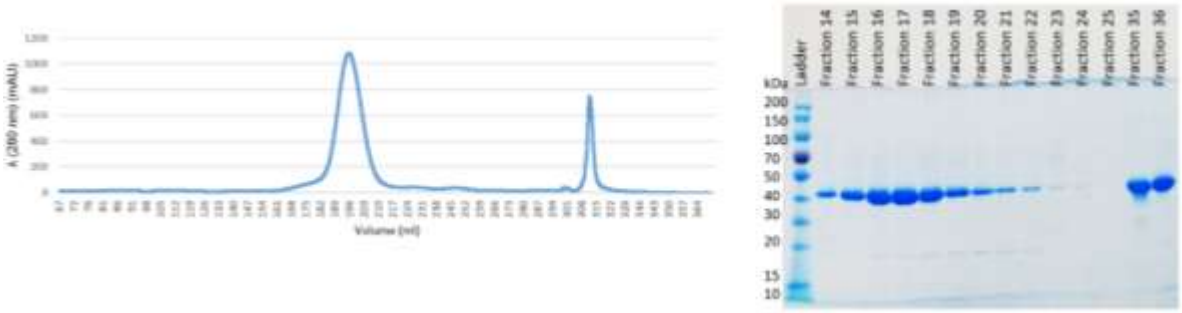

Figure 25 – p53ND Anion Exchange column chromatogram and SDS-PAGE gel.

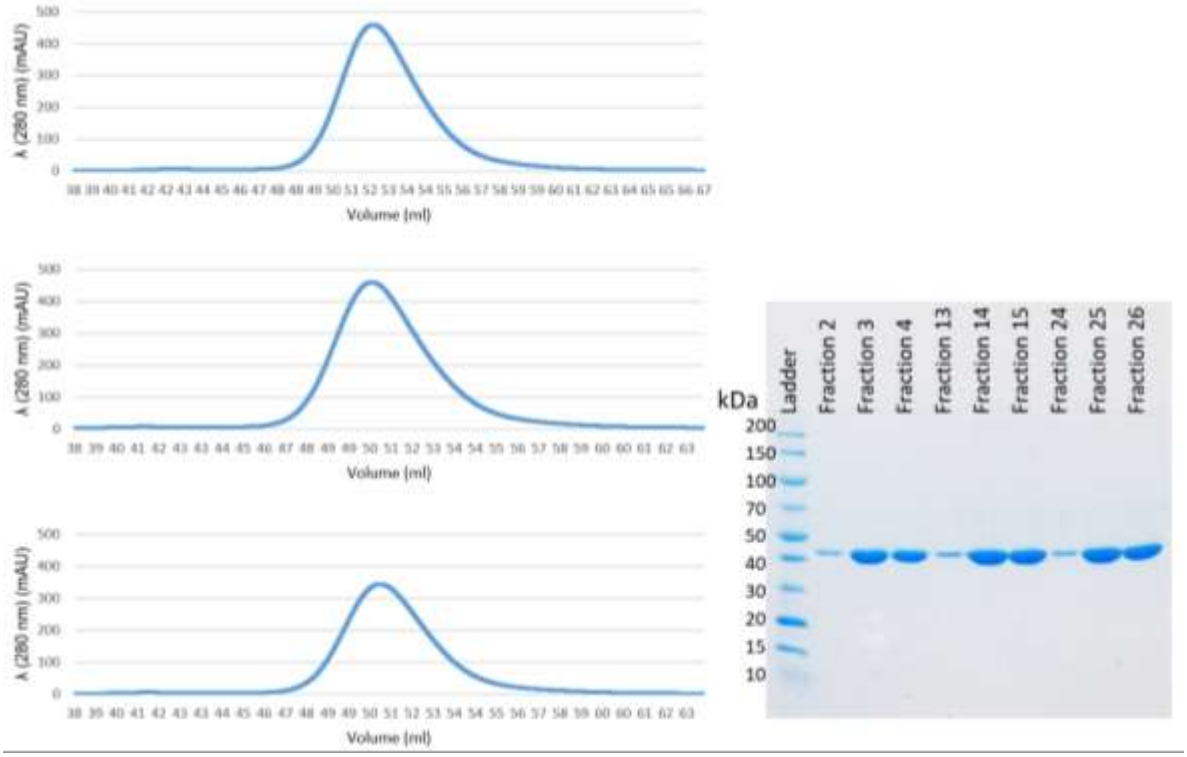

Figure 26 – p53ND SEC column chromatogram and SDS-PAGE gel.

Concentration determination

Sample concentrations were determined using the extinction coefficients as calculated by the ProtParam program available at www.expasy.org (ref#). UV measurements were obtained using an ND-1000 nanodrop (Thermo Fischer). Concentration of the sample is calculated from the absorbance value at 280nm using the Beer's Law Equation i.e., Absorbance = e*L*c where 'e' is the molar extinction coefficient, 'L' is the path length of the cell holder and 'c' is the concentration of the protein. Table 14 lists the extinction coefficients for the proteins used.

Table 14 – Protein Extinction Coefficients

Protein	Number of Amino Acids	Extinction Coefficient (Pre-cleave)	Extinction Coefficient (Post-cleave)
p53TAD WT (residues 1-73)	73	11,000	11,000
p53TAD S15D (residues 1-73)	73	11,000	11,000
p53TAD S15D/T18E (residues 1-73)	73	11,000	11,000
Mdm2 (residues 17–125)	109	53,290	10,430
MdmX (residues 23-111)	89	50,310	7,350
KIX (residues 586-672)	87	13,000	13,000
DBD (residues 94-312)	227	61,770	18,910
NDWT (residues 1-312)	312	78,270	35,410
T55D-ND (residues 1-312)	312	78,270	35,410
NDQS (residues 1-312)	312	78,270	35,410

Nuclear Magnetic Resonance

Assignments and Chemical shifts

NMR experiments were performed using uniformly ^{15}N- and ^{13}C-labeled samples at 50μM, at 25°C on a Varian VNMRS 800 MHz spectrometer equipped with a triple-resonance pulse field Z-axis gradient cold probe. To make the amide ^{1}H and ^{15}N as well as ^{13}Cα, ^{13}Cβ, and ^{13}CO resonance assignments, sensitivity-enhanced ^{1}H–^{15}N HSQC and three-dimensional HNCACB and HNCO experiments were performed on the uniformly ^{15}N- and ^{13}C-labeled samples in 90% H_2O/8% D_2O in NMR buffer for p53ND constructs. For the HNCO the Varian VNMRS 600 MHz spectrometer with a triple resonance pulse field Z-axis gradient cold probe was used. The sweep widths were 9689.9 (t_3) Hz × 3770.1 (t_2) Hz × 1944.5 (t_1) Hz, and complex data points were 1024 (t_3) Hz × 64 (t_2) Hz × 32 (t_1) Hz. For p53TAD the HSQC and the HNCACB were performed on the 600 MHz spectrometer. The sweep widths and complex points for the HSQC were 7225.4 (t_2) Hz × 1500 (t_1) Hz and 1024 (t_2) Hz × 128 (t_1) Hz, respectively. The HNCACB experiment, data were acquired in the 1H, 13C, and 15N dimensions using 7225.4 (t_3) Hz × 12063.8 (t_2) Hz × 1500 (t_1) Hz sweep widths and 1024 (t_3) Hz × 128 (t_2) Hz × 32 (t_1) Hz complex

data points. For p53TAD S15D the HSQC was performed on the 600 MHz spectrometer and the HNCACB was performed on the 800 MHz spectrometer. The sweep widths and complex points for the HSQC were 7266 (t_2) Hz × 1943.2 (t_1) Hz and 1024 (t_2) Hz × 128 (t_1) Hz, respectively. The HNCACB experiment, data were acquired in the 1H, 13C, and 15N dimensions using 9689.9 (t3) Hz × 14074.9 (t_2) Hz × 1944.3 (t_1) Hz sweep widths and 1024 (t_3) Hz × 128 (t_2) Hz × 32 (t_1) Hz complex data points. For p53TAD S15D/T18E the HSQC and the HNCACB were performed on the 800 MHz spectrometer. The sweep widths and complex points for the HSQC were 9689.9 (t_2) Hz × 1944.4 (t_1) Hz and 1024 (t_2) Hz × 128 (t_1) Hz, respectively. The HNCACB experiment, data were acquired in the 1H, 13C, and 15N dimensions using 9689.9 (t_3) Hz × 14074.9 (t_2) Hz × 1944.3 (t_1) Hz sweep widths and 1024 (t_3) Hz × 128 (t_2) Hz × 32 (t_1) Hz complex data points. For p53NDWT the HSQC and the HNCACB were performed on the 800 MHz spectrometer. The sweep widths and complex points for the HSQC were 19,379.8 (t_2) Hz × 2754.5 (t_1) Hz and 1024 (t_2) Hz × 128 (t_1) Hz, respectively. The HNCACB experiment, data were acquired in the 1H, 13C, and 15N dimensions using 9689.9 (t_3) Hz × 14074.9 (t_2) Hz × 2754.4 (t_1) Hz sweep widths and 1024 (t_3) Hz × 128 (t_2) Hz × 32 (t_1) Hz complex data points. For p53NDWT with conDNA the HSQC and the HNCACB were performed on the 800 MHz spectrometer. The sweep widths and complex points for the HSQC were 9689.9 (t_2) Hz × 2754.5 (t_1) Hz and 1024 (t_2) Hz × 128 (t_1) Hz, respectively. The HNCACB experiment, data were acquired in the 1H, 13C, and 15N dimensions using 9689.9 (t_3) Hz × 14074.9 (t_2) Hz × 2754.4 (t_1) Hz sweep widths and 1024 (t_3) Hz × 128 (t_2) Hz × 32 (t_1) Hz complex data points. For p53T55D-ND the HSQC and the HNCACB were performed on the 800 MHz spectrometer. The sweep widths and complex points for the HSQC were

9689.9 (t_2) Hz × 2754.5 (t_1) Hz and 1024 (t_2) Hz × 128 (t_1) Hz, respectively. The HNCACB experiment, data were acquired in the 1H, 13C, and 15N dimensions using 9689.9 (t_3) Hz × 14074.9 (t_2) Hz × 1944.3 (t_1) Hz sweep widths and 1024 (t_3) Hz × 128 (t_2) Hz × 32 (t_1) Hz complex data points. For p53T55D-ND with conDNA the HSQC and the HNCACB were performed on the 800 MHz spectrometer. The sweep widths and complex points for the HSQC were 9689.9 (t_2) Hz × 2754.5 (t_1) Hz and 1024 (t_2) Hz × 128 (t_1) Hz, respectively. The HNCACB experiment, data were acquired in the 1H, 13C, and 15N dimensions using 9689.9 (t_3) Hz × 14074.9 (t_2) Hz × 2754.4 (t_1) Hz sweep widths and 1024 (t_3) Hz × 128 (t_2) Hz × 32 (t_1) Hz complex data points. All NMR spectra were processed with NMRFxProcessor and analyzed using NMRView J.

Secondary chemical shifts and Random coil chemical shifts

Secondary chemical shift values were calculated by subtracting the residue-specific random coil chemical shifts in the prediction of temperature, neighbor and pH-corrected chemical shifts for intrinsically disordered proteins (POTENCI) from the measured chemical shifts. Secondary structure populations were calculated with δ2D using the measured proton, nitrogen, and α, β, and carbonyl carbon chemical shifts. The overall helicity was calculated as the mean of the per residue δ2D helical population estimates.

Isothermal Titration Calorimetry

Testing

The p53TAD construct ITC experiments were performed using a GE MicroCal VP-ITC 200 system instrument. All proteins, p53TAD constructs, Mdm2, MdmX, and KIX, were dialyzed against ITC buffer for p53TAD constructs. Experiments were performed at

25°C. The typical concentration of p53TAD constructs (syringe) ranged from 50-500μM and for Mdm2, MdmX and KIX (cell) 5–50μM. Peptide concentrations were determined by absorbance at 280nm. A typical ITC experiment consisted of 1 injection of 5μl, followed by 29 injections of 10μl up to a 2.5-fold molar excess of titrant.

The p53ND construct ITC experiments were performed using a GE MicroCal VP-ITC 200 system instrument. All proteins, p53ND constructs, Mdm2 and MdmX, and DNA were dialyzed against low ionic strength (85mM) ITC buffer. Experiments were performed at 25°C. The typical concentration of p53 constructs (syringe) ranged from 10-150μM and for Mdm2, MdmX and consensus and scramble DNA (cell) 5–150μM. Peptide concentrations were determined by absorbance at 280nm. A typical ITC experiment consisted of 1 injection of 5μL, followed by 19 injections of 15μL up to a 2.5-fold molar excess of titrant. The following double-stranded DNA oligonucleotides were used: consensus 5′ AGACATGCCTAGGACATGCCT and scrambled 5′TGCCGATCAAAACCGATTCG [172].

Analysis

Data were analyzed with the Microcal Origin software (7.0). Data was fit using a nonlinear least square curve-fitting algorithm yielding the stoichiometry, enthalpy, and affinity constants reported for a single binding site. Averages and standard deviations from three different ITC experiments are shown. Integrated ITC data were fit with single-site binding models and the stoichiometry ranged from 0.8 to 2. Errors in K_d were calculated from triplicate measurements.

Literature Cited

1. Market, L. S. "pGEX- 6P- 2." Retrieved March 30, 2020, 2020, from https://www.lifescience-market.com/plasmid-c-94/pgex-6p-2-p-63186.html.
2. Sigma-Aldrich. "pET-28a-c(+) Vectors - Novagen." Retrieved March 30, 2020, 2020, from https://www.emdmillipore.com/US/en/product/pET-28a+-DNA-Novagen,EMD_BIO-69864#anchor_VMAP.
3. Toledo, F. and Wahl, G. M. Regulating the p53 pathway: in vitro hypotheses, in vivo veritas. *Nat Rev Cancer* **2006** *6*(12): 909-923. 10.1038/nrc2012
4. Meek, D. W. and Anderson, C. W. Posttranslational modification of p53: cooperative integrators of function. *Cold Spring Harb Perspect Biol* **2009** *1*(6): a000950. 10.1101/cshperspect.a000950
5. Yang, A.; Kaghad, M., et al. On the shoulders of giants: p63, p73 and the rise of p53. *Trends Genet* **2002** *18*(2): 90-95. 10.1016/s0168-9525(02)02595-7
6. Ptitsyn, O. B.; Bychkova, V. E., et al. Kinetic and equilibrium folding intermediates. *Philos Trans R Soc Lond B Biol Sci* **1995** *348*(1323): 35-41. 10.1098/rstb.1995.0043
7. Uversky, V. N. and Ptitsyn, O. B. Further evidence on the equilibrium "pre-molten globule state": four-state guanidinium chloride-induced unfolding of carbonic anhydrase B at low temperature. *J Mol Biol* **1996** *255*(1): 215-228. 10.1006/jmbi.1996.0018
8. Dunker, A. K.; Brown, C. J., et al. Intrinsic disorder and protein function. *Biochemistry* **2002** *41*(21): 6573-6582.
9. Dunker, A. K.; Silman, I., et al. Function and structure of inherently disordered proteins. *Curr Opin Struct Biol* **2008** *18*(6): 756-764. 10.1016/j.sbi.2008.10.002
10. Dyson, H. J. and Wright, P. E. Intrinsically unstructured proteins and their functions. *Nat Rev Mol Cell Biol* **2005** *6*(3): 197-208. 10.1038/nrm1589
11. Uversky, V. N. Intrinsically disordered proteins and novel strategies for drug discovery. *Expert Opin Drug Discov* **2012** *7*(6): 475-488. 10.1517/17460441.2012.686489
12. van der Lee, R.; Buljan, M., et al. Classification of intrinsically disordered regions and proteins. *Chem Rev* **2014** *114*(13): 6589-6631. 10.1021/cr400525m
13. Romero, P.; Obradovic, Z., et al. Sequence complexity of disordered protein. *Proteins* **2001** *42*(1): 38-48. 10.1002/1097-0134(20010101)42:1<38::aid-prot50>3.0.co;2-3
14. Theillet, F. X.; Kalmar, L., et al. The alphabet of intrinsic disorder: I. Act like a Pro: On the abundance and roles of proline residues in intrinsically disordered proteins. *Intrinsically Disord Proteins* **2013** *1*(1): e24360. 10.4161/idp.24360
15. Dosztanyi, Z.; Csizmok, V., et al. IUPred: web server for the prediction of intrinsically unstructured regions of proteins based on estimated energy content. *Bioinformatics* **2005** *21*(16): 3433-3434. 10.1093/bioinformatics/bti541
16. Dosztanyi, Z.; Meszaros, B., et al. ANCHOR: web server for predicting protein binding regions in disordered proteins. *Bioinformatics* **2009** *25*(20): 2745-2746. 10.1093/bioinformatics/btp518

17. Ferron, F.; Longhi, S., et al. A practical overview of protein disorder prediction methods. *Proteins* **2006** *65*(1): 1-14. 10.1002/prot.21075
18. Obradovic, Z.; Peng, K., et al. Predicting intrinsic disorder from amino acid sequence. *Proteins* **2003** *53 Suppl 6*: 566-572. 10.1002/prot.10532
19. Dunker, A. K.; Lawson, J. D., et al. Intrinsically disordered protein. *J Mol Graph Model* **2001** *19*(1): 26-59. 10.1016/s1093-3263(00)00138-8
20. Ward, J. J.; Sodhi, J. S., et al. Prediction and functional analysis of native disorder in proteins from the three kingdoms of life. *J Mol Biol* **2004** *337*(3): 635-645. 10.1016/j.jmb.2004.02.002
21. Dunker, A. K.; Obradovic, Z., et al. Intrinsic protein disorder in complete genomes. *Genome Inform Ser Workshop Genome Inform* **2000** *11*: 161-171.
22. Uversky, V. N. Natively unfolded proteins: a point where biology waits for physics. *Protein Sci* **2002** *11*(4): 739-756. 10.1110/ps.4210102
23. Uversky, V. N.; Gillespie, J. R., et al. Why are "natively unfolded" proteins unstructured under physiologic conditions? *Proteins* **2000** *41*(3): 415-427. 10.1002/1097-0134(20001115)41:3<415::aid-prot130>3.0.co;2-7
24. Dunker, A. K.; Brown, C. J., et al. Identification and functions of usefully disordered proteins. *Adv Protein Chem* **2002** *62*: 25-49. 10.1016/s0065-3233(02)62004-2
25. Fukuchi, S.; Homma, K., et al. Intrinsically disordered loops inserted into the structural domains of human proteins. *J Mol Biol* **2006** *355*(4): 845-857. 10.1016/j.jmb.2005.10.037
26. Dunker, A. K.; Garner, E., et al. Protein disorder and the evolution of molecular recognition: theory, predictions and observations. *Pac Symp Biocomput* **1998**: 473-484.
27. Dyson, H. J. and Wright, P. E. Insights into the structure and dynamics of unfolded proteins from nuclear magnetic resonance. *Adv Protein Chem* **2002** *62*: 311-340. 10.1016/s0065-3233(02)62012-1
28. Lee, S. H.; Kim, D. H., et al. Understanding pre-structured motifs (PreSMos) in intrinsically unfolded proteins. *Curr Protein Pept Sci* **2012** *13*(1): 34-54.
29. Oldfield, C. J. and Dunker, A. K. Intrinsically disordered proteins and intrinsically disordered protein regions. *Annu Rev Biochem* **2014** *83*: 553-584. 10.1146/annurev-biochem-072711-164947
30. Uversky, V. N. What does it mean to be natively unfolded? *Eur J Biochem* **2002** *269*(1): 2-12. 10.1046/j.0014-2956.2001.02649.x
31. Uversky, V. N.; Narizhneva, N. V., et al. Ligand-free form of human alpha-fetoprotein: evidence for the molten globule state. *FEBS Lett* **1997** *410*(2-3): 280-284. 10.1016/s0014-5793(97)00606-6
32. Marsh, J. A. and Forman-Kay, J. D. Sequence determinants of compaction in intrinsically disordered proteins. *Biophys J* **2010** *98*(10): 2383-2390. 10.1016/j.bpj.2010.02.006
33. Dosztanyi, Z.; Chen, J., et al. Disorder and sequence repeats in hub proteins and their implications for network evolution. *J Proteome Res* **2006** *5*(11): 2985-2995. 10.1021/pr060171o
34. Dunker, A. K.; Cortese, M. S., et al. Flexible nets. The roles of intrinsic disorder in protein interaction networks. *FEBS J* **2005** *272*(20): 5129-5148. 10.1111/j.1742-4658.2005.04948.x

35. Johnson, L. N. and Lewis, R. J. Structural basis for control by phosphorylation. *Chem Rev* **2001** *101*(8): 2209-2242.
36. Bah, A. and Forman-Kay, J. D. Modulation of Intrinsically Disordered Protein Function by Post-translational Modifications. *J Biol Chem* **2016** *291*(13): 6696-6705. 10.1074/jbc.R115.695056
37. Bah, A.; Vernon, R. M., et al. Folding of an intrinsically disordered protein by phosphorylation as a regulatory switch. *Nature* **2015** *519*(7541): 106-109. 10.1038/nature13999
38. Galea, C. A.; Wang, Y., et al. Regulation of cell division by intrinsically unstructured proteins: intrinsic flexibility, modularity, and signaling conduits. *Biochemistry* **2008** *47*(29): 7598-7609. 10.1021/bi8006803
39. Uversky, V. N. Intrinsically disordered proteins from A to Z. *Int J Biochem Cell Biol* **2011** *43*(8): 1090-1103. 10.1016/j.biocel.2011.04.001
40. Stock, J. and Da Re, S. Signal transduction: response regulators on and off. *Curr Biol* **2000** *10*(11): R420-424.
41. Wright, P. E. and Dyson, H. J. Linking folding and binding. *Curr Opin Struct Biol* **2009** *19*(1): 31-38. 10.1016/j.sbi.2008.12.003
42. Brown, C. J.; Johnson, A. K., et al. Evolution and disorder. *Curr Opin Struct Biol* **2011** *21*(3): 441-446. 10.1016/j.sbi.2011.02.005
43. Huntley, M. and Golding, G. B. Evolution of simple sequence in proteins. *J Mol Evol* **2000** *51*(2): 131-140. 10.1007/s002390010073
44. Tompa, P. Intrinsically unstructured proteins evolve by repeat expansion. *Bioessays* **2003** *25*(9): 847-855. 10.1002/bies.10324
45. Lin, Y. S.; Hsu, W. L., et al. Proportion of solvent-exposed amino acids in a protein and rate of protein evolution. *Mol Biol Evol* **2007** *24*(4): 1005-1011. 10.1093/molbev/msm019
46. Breydo, L.; Wu, J. W., et al. Alpha-synuclein misfolding and Parkinson's disease. *Biochim Biophys Acta* **2012** *1822*(2): 261-285. 10.1016/j.bbadis.2011.10.002
47. Uversky, V. N. Neuropathology, biochemistry, and biophysics of alpha-synuclein aggregation. *J Neurochem* **2007** *103*(1): 17-37. 10.1111/j.1471-4159.2007.04764.x
48. Uversky, V. N. Alpha-synuclein misfolding and neurodegenerative diseases. *Curr Protein Pept Sci* **2008** *9*(5): 507-540. 10.2174/138920308785915218
49. Uversky, V. N. Intrinsic disorder in proteins associated with neurodegenerative diseases. *Front Biosci (Landmark Ed)* **2009** *14*: 5188-5238. 10.2741/3594
50. Uversky, V. N. The triple power of D(3): protein intrinsic disorder in degenerative diseases. *Front Biosci (Landmark Ed)* **2014** *19*: 181-258. 10.2741/4204
51. Baker, J. M.; Hudson, R. P., et al. CFTR regulatory region interacts with NBD1 predominantly via multiple transient helices. *Nat Struct Mol Biol* **2007** *14*(8): 738-745. 10.1038/nsmb1278
52. Casu, F.; Duggan, B. M., et al. The arginine-rich RNA-binding motif of HIV-1 Rev is intrinsically disordered and folds upon RRE binding. *Biophys J* **2013** *105*(4): 1004-1017. 10.1016/j.bpj.2013.07.022
53. Uversky, V. N.; Oldfield, C. J., et al. Intrinsically disordered proteins in human diseases: introducing the D2 concept. *Annu Rev Biophys* **2008** *37*: 215-246. 10.1146/annurev.biophys.37.032807.125924

54. Vacic, V. and Iakoucheva, L. M. Disease mutations in disordered regions--exception to the rule? *Mol Biosyst* **2012** *8*(1): 27-32. 10.1039/c1mb05251a
55. Hainaut, P. and Hollstein, M. p53 and human cancer: the first ten thousand mutations. *Adv Cancer Res* **2000** *77*: 81-137.
56. Bouaoun, L.; Sonkin, D., et al. TP53 Variations in Human Cancers: New Lessons from the IARC TP53 Database and Genomics Data. *Hum Mutat* **2016** *37*(9): 865-876. 10.1002/humu.23035
57. Lill, N. L.; Grossman, S. R., et al. Binding and modulation of p53 by p300/CBP coactivators. *Nature* **1997** *387*(6635): 823-827. 10.1038/42981
58. Thut, C. J.; Chen, J. L., et al. p53 transcriptional activation mediated by coactivators TAFII40 and TAFII60. *Science* **1995** *267*(5194): 100-104.
59. Bochkareva, E.; Kaustov, L., et al. Single-stranded DNA mimicry in the p53 transactivation domain interaction with replication protein A. *Proc Natl Acad Sci U S A* **2005** *102*(43): 15412-15417. 10.1073/pnas.0504614102
60. Di Lello, P.; Jenkins, L. M., et al. Structure of the Tfb1/p53 complex: Insights into the interaction between the p62/Tfb1 subunit of TFIIH and the activation domain of p53. *Mol Cell* **2006** *22*(6): 731-740. 10.1016/j.molcel.2006.05.007
61. Feng, H.; Jenkins, L. M., et al. Structural basis for p300 Taz2-p53 TAD1 binding and modulation by phosphorylation. *Structure* **2009** *17*(2): 202-210. 10.1016/j.str.2008.12.009
62. Kussie, P. H.; Gorina, S., et al. Structure of the MDM2 oncoprotein bound to the p53 tumor suppressor transactivation domain. *Science* **1996** *274*(5289): 948-953.
63. Popowicz, G. M.; Czarna, A., et al. Structure of the human Mdmx protein bound to the p53 tumor suppressor transactivation domain. *Cell Cycle* **2008** *7*(15): 2441-2443. 10.4161/cc.6365
64. Oren, M. Regulation of the p53 tumor suppressor protein. *J Biol Chem* **1999** *274*(51): 36031-36034.
65. Vousden, K. H. and Lu, X. Live or let die: the cell's response to p53. *Nat Rev Cancer* **2002** *2*(8): 594-604. 10.1038/nrc864
66. Donehower, L. A.; Harvey, M., et al. Mice deficient for p53 are developmentally normal but susceptible to spontaneous tumours. *Nature* **1992** *356*(6366): 215-221. 10.1038/356215a0
67. Kubbutat, M. H.; Jones, S. N., et al. Regulation of p53 stability by Mdm2. *Nature* **1997** *387*(6630): 299-303. 10.1038/387299a0
68. Haupt, Y.; Maya, R., et al. Mdm2 promotes the rapid degradation of p53. *Nature* **1997** *387*(6630): 296-299. 10.1038/387296a0
69. Lahav, G.; Rosenfeld, N., et al. Dynamics of the p53-Mdm2 feedback loop in individual cells. *Nat Genet* **2004** *36*(2): 147-150. 10.1038/ng1293
70. Picksley, S. M. and Lane, D. P. The p53-mdm2 autoregulatory feedback loop: a paradigm for the regulation of growth control by p53? *Bioessays* **1993** *15*(10): 689-690. 10.1002/bies.950151008
71. Wu, X.; Bayle, J. H., et al. The p53-mdm-2 autoregulatory feedback loop. *Genes Dev* **1993** *7*(7A): 1126-1132.
72. Momand, J.; Zambetti, G. P., et al. The mdm-2 oncogene product forms a complex with the p53 protein and inhibits p53-mediated transactivation. *Cell* **1992** *69*(7): 1237-1245.

73. Roth, J.; Dobbelstein, M., et al. Nucleo-cytoplasmic shuttling of the hdm2 oncoprotein regulates the levels of the p53 protein via a pathway used by the human immunodeficiency virus rev protein. *EMBO J* **1998** *17*(2): 554-564. 10.1093/emboj/17.2.554
74. Tao, W. and Levine, A. J. Nucleocytoplasmic shuttling of oncoprotein Hdm2 is required for Hdm2-mediated degradation of p53. *Proc Natl Acad Sci U S A* **1999** *96*(6): 3077-3080.
75. Shvarts, A.; Steegenga, W. T., et al. MDMX: a novel p53-binding protein with some functional properties of MDM2. *EMBO J* **1996** *15*(19): 5349-5357.
76. Francoz, S.; Froment, P., et al. Mdm4 and Mdm2 cooperate to inhibit p53 activity in proliferating and quiescent cells in vivo. *Proc Natl Acad Sci U S A* **2006** *103*(9): 3232-3237. 10.1073/pnas.0508476103
77. Xiong, S.; Van Pelt, C. S., et al. Synergistic roles of Mdm2 and Mdm4 for p53 inhibition in central nervous system development. *Proc Natl Acad Sci U S A* **2006** *103*(9): 3226-3231. 10.1073/pnas.0508500103
78. Stad, R.; Little, N. A., et al. Mdmx stabilizes p53 and Mdm2 via two distinct mechanisms. *EMBO Rep* **2001** *2*(11): 1029-1034. 10.1093/embo-reports/kve227
79. Gu, J.; Kawai, H., et al. Mutual dependence of MDM2 and MDMX in their functional inactivation of p53. *J Biol Chem* **2002** *277*(22): 19251-19254. 10.1074/jbc.C200150200
80. Chen, J.; Marechal, V., et al. Mapping of the p53 and mdm-2 interaction domains. *Mol Cell Biol* **1993** *13*(7): 4107-4114.
81. Oliner, J. D.; Pietenpol, J. A., et al. Oncoprotein MDM2 conceals the activation domain of tumour suppressor p53. *Nature* **1993** *362*(6423): 857-860. 10.1038/362857a0
82. Brooks, C. L. and Gu, W. p53 ubiquitination: Mdm2 and beyond. *Mol Cell* **2006** *21*(3): 307-315. 10.1016/j.molcel.2006.01.020
83. Chen, J. The Roles of MDM2 and MDMX Phosphorylation in Stress Signaling to p53. *Genes Cancer* **2012** *3*(3-4): 274-282. 10.1177/1947601912454733
84. Lambert, P. F.; Kashanchi, F., et al. Phosphorylation of p53 serine 15 increases interaction with CBP. *J Biol Chem* **1998** *273*(49): 33048-33053.
85. Teufel, D. P.; Bycroft, M., et al. Regulation by phosphorylation of the relative affinities of the N-terminal transactivation domains of p53 for p300 domains and Mdm2. *Oncogene* **2009** *28*(20): 2112-2118. 10.1038/onc.2009.71
86. Dumaz, N. and Meek, D. W. Serine15 phosphorylation stimulates p53 transactivation but does not directly influence interaction with HDM2. *EMBO J* **1999** *18*(24): 7002-7010. 10.1093/emboj/18.24.7002
87. Grossman, S. R.; Perez, M., et al. p300/MDM2 complexes participate in MDM2-mediated p53 degradation. *Mol Cell* **1998** *2*(4): 405-415.
88. Kruse, J. P. and Gu, W. Modes of p53 regulation. *Cell* **2009** *137*(4): 609-622. 10.1016/j.cell.2009.04.050
89. Teufel, D. P.; Freund, S. M., et al. Four domains of p300 each bind tightly to a sequence spanning both transactivation subdomains of p53. *Proc Natl Acad Sci U S A* **2007** *104*(17): 7009-7014. 10.1073/pnas.0702010104
90. Ferreon, J. C.; Lee, C. W., et al. Cooperative regulation of p53 by modulation of ternary complex formation with CBP/p300 and HDM2. *Proceedings of the National Academy of Sciences* **2009** *106*(16): 6591.

91. Lee, C. W.; Ferreon, J. C., et al. Graded enhancement of p53 binding to CREB-binding protein (CBP) by multisite phosphorylation. *Proc Natl Acad Sci U S A* **2010** *107*(45): 19290-19295. 10.1073/pnas.1013078107
92. Oda, M.; Furukawa, K., et al. Thermodynamics of specific and non-specific DNA binding by the c-Myb DNA-binding domain. *J Mol Biol* **1998** *276*(3): 571-590. 10.1006/jmbi.1997.1564
93. Pabo, C. O. and Sauer, R. T. Protein-DNA recognition. *Annu Rev Biochem* **1984** *53*: 293-321. 10.1146/annurev.bi.53.070184.001453
94. Vogelstein, B.; Lane, D., et al. Surfing the p53 network. *Nature* **2000** *408*(6810): 307-310. 10.1038/35042675
95. Levine, A. J. p53, the cellular gatekeeper for growth and division. *Cell* **1997** *88*(3): 323-331. 10.1016/s0092-8674(00)81871-1
96. Pietenpol, J. A.; Tokino, T., et al. Sequence-specific transcriptional activation is essential for growth suppression by p53. *Proc Natl Acad Sci U S A* **1994** *91*(6): 1998-2002. 10.1073/pnas.91.6.1998
97. Weinberg, R. L.; Veprintsev, D. B., et al. Comparative binding of p53 to its promoter and DNA recognition elements. *J Mol Biol* **2005** *348*(3): 589-596. 10.1016/j.jmb.2005.03.014
98. He, F.; Borcherds, W., et al. Interaction between p53 N terminus and core domain regulates specific and nonspecific DNA binding. *Proc Natl Acad Sci U S A* **2019** *116*(18): 8859-8868. 10.1073/pnas.1903077116
99. Chothia, C. and Lesk, A. M. The relation between the divergence of sequence and structure in proteins. *EMBO J* **1986** *5*(4): 823-826.
100. Chothia, C. and Lesk, A. M. The evolution of protein structures. *Cold Spring Harb Symp Quant Biol* **1987** *52*: 399-405. 10.1101/sqb.1987.052.01.046
101. Blandino, G. and Dobbelstein, M. p73 and p63: why do we still need them? *Cell Cycle* **2004** *3*(7): 886-894.
102. Davison, T. S.; Vagner, C., et al. p73 and p63 are homotetramers capable of weak heterotypic interactions with each other but not with p53. *J Biol Chem* **1999** *274*(26): 18709-18714. 10.1074/jbc.274.26.18709
103. Irwin, M.; Marin, M. C., et al. Role for the p53 homologue p73 in E2F-1-induced apoptosis. *Nature* **2000** *407*(6804): 645-648. 10.1038/35036614
104. Krois, A. S.; Dyson, H. J., et al. Long-range regulation of p53 DNA binding by its intrinsically disordered N-terminal transactivation domain. *Proc Natl Acad Sci U S A* **2018** *115*(48): E11302-E11310. 10.1073/pnas.1814051115
105. Krois, A. S.; Ferreon, J. C., et al. Recognition of the disordered p53 transactivation domain by the transcriptional adapter zinc finger domains of CREB-binding protein. *Proc Natl Acad Sci U S A* **2016** *113*(13): E1853-1862. 10.1073/pnas.1602487113
106. Liu, X. and Chen, J. Modulation of p53 Transactivation Domain Conformations by Ligand Binding and Cancer-Associated Mutations. *Pac Symp Biocomput* **2020** *25*: 195-206.
107. Lee, H.; Mok, K. H., et al. Local structural elements in the mostly unstructured transcriptional activation domain of human p53. *J Biol Chem* **2000** *275*(38): 29426-29432. 10.1074/jbc.M003107200
108. Shieh, S. Y.; Ikeda, M., et al. DNA damage-induced phosphorylation of p53 alleviates inhibition by MDM2. *Cell* **1997** *91*(3): 325-334.

109. Dohoney, K. M.; Guillerm, C., et al. Phosphorylation of p53 at serine 37 is important for transcriptional activity and regulation in response to DNA damage. *Oncogene* **2004** *23*(1): 49-57. 10.1038/sj.onc.1207005
110. Levy, R.; Gregory, E., et al. p53 Phosphomimetics Preserve Transient Secondary Structure but Reduce Binding to Mdm2 and MdmX. *Biomolecules* **2019** *9*(3). 10.3390/biom9030083
111. Lee, C. W.; Arai, M., et al. Mapping the interactions of the p53 transactivation domain with the KIX domain of CBP. *Biochemistry* **2009** *48*(10): 2115-2124. 10.1021/bi802055v
112. Blagosklonny, M. V. P53: an ubiquitous target of anticancer drugs. *Int J Cancer* **2002** *98*(2): 161-166.
113. Chene, P. Targeting p53 in cancer. *Curr Med Chem Anticancer Agents* **2001** *1*(2): 151-161.
114. Sigal, A. and Rotter, V. Oncogenic mutations of the p53 tumor suppressor: the demons of the guardian of the genome. *Cancer Res* **2000** *60*(24): 6788-6793.
115. Matas, D.; Sigal, A., et al. Integrity of the N-terminal transcription domain of p53 is required for mutant p53 interference with drug-induced apoptosis. *EMBO J* **2001** *20*(15): 4163-4172. 10.1093/emboj/20.15.4163
116. Oda, K.; Arakawa, H., et al. p53AIP1, a potential mediator of p53-dependent apoptosis, and its regulation by Ser-46-phosphorylated p53. *Cell* **2000** *102*(6): 849-862.
117. Scoumanne, A.; Harms, K. L., et al. Structural basis for gene activation by p53 family members. *Cancer Biol Ther* **2005** *4*(11): 1178-1185.
118. Crabtree, M. D.; Borcherds, W., et al. Conserved Helix-Flanking Prolines Modulate Intrinsically Disordered Protein:Target Affinity by Altering the Lifetime of the Bound Complex. *Biochemistry* **2017** *56*(18): 2379-2384. 10.1021/acs.biochem.7b00179
119. Borcherds, W.; Theillet, F.-X., et al. Disorder and residual helicity alter p53-Mdm2 binding affinity and signaling in cells. **2014** *10*: 1000. 10.1038/nchembio.1668

https://www.nature.com/articles/nchembio.1668#supplementary-information
120. Oliner, J. D.; Kinzler, K. W., et al. Amplification of a gene encoding a p53-associated protein in human sarcomas. *Nature* **1992** *358*(6381): 80-83. 10.1038/358080a0
121. Badciong, J. C. and Haas, A. L. MdmX is a RING finger ubiquitin ligase capable of synergistically enhancing Mdm2 ubiquitination. *J Biol Chem* **2002** *277*(51): 49668-49675. 10.1074/jbc.M208593200
122. Wienken, M.; Dickmanns, A., et al. MDM2 Associates with Polycomb Repressor Complex 2 and Enhances Stemness-Promoting Chromatin Modifications Independent of p53. *Mol Cell* **2016** *61*(1): 68-83. 10.1016/j.molcel.2015.12.008
123. Jabbur, J. R.; Tabor, A. D., et al. Mdm-2 binding and TAF(II)31 recruitment is regulated by hydrogen bond disruption between the p53 residues Thr18 and Asp21. *Oncogene* **2002** *21*(46): 7100-7113. 10.1038/sj.onc.1205856
124. Serrano, M. A.; Li, Z., et al. DNA-PK, ATM and ATR collaboratively regulate p53-RPA interaction to facilitate homologous recombination DNA repair. *Oncogene* **2013** *32*(19): 2452-2462. 10.1038/onc.2012.257
125. Bottger, V.; Bottger, A., et al. Comparative study of the p53-mdm2 and p53-MDMX interfaces. *Oncogene* **1999** *18*(1): 189-199. 10.1038/sj.onc.1202281

126. Baresova, P.; Musilova, J., et al. p53 tumor suppressor protein stability and transcriptional activity are targeted by Kaposi's sarcoma-associated herpesvirus-encoded viral interferon regulatory factor 3. *Mol Cell Biol* **2014** *34*(3): 386-399. 10.1128/MCB.01011-13
127. Dumaz, N.; Milne, D. M., et al. Protein kinase CK1 is a p53-threonine 18 kinase which requires prior phosphorylation of serine 15. *FEBS Lett* **1999** *463*(3): 312-316.
128. Saito, S.; Yamaguchi, H., et al. Phosphorylation site interdependence of human p53 post-translational modifications in response to stress. *J Biol Chem* **2003** *278*(39): 37536-37544. 10.1074/jbc.M305135200
129. McKinney, K. and Prives, C. Efficient specific DNA binding by p53 requires both its central and C-terminal domains as revealed by studies with high-mobility group 1 protein. *Mol Cell Biol* **2002** *22*(19): 6797-6808.
130. Huang, Y.; Gao, M., et al. Deciphering the promiscuous interactions between intrinsically disordered transactivation domains and the KIX domain. *Proteins* **2017** *85*(11): 2088-2095. 10.1002/prot.25364
131. He, Y.; Chen, Y., et al. Phosphorylation-induced Conformational Ensemble Switching in an Intrinsically Disordered Cancer/Testis Antigen. *J Biol Chem* **2015** *290*(41): 25090-25102. 10.1074/jbc.M115.658583
132. Mavinahalli, J. N.; Madhumalar, A., et al. Differences in the transactivation domains of p53 family members: a computational study. *BMC Genomics* **2010** *11 Suppl 1*: S5. 10.1186/1471-2164-11-S1-S5
133. Hol, W. G. The role of the alpha-helix dipole in protein function and structure. *Prog Biophys Mol Biol* **1985** *45*(3): 149-195.
134. Sheridan, R. P.; Levy, R. M., et al. alpha-Helix dipole model and electrostatic stabilization of 4-alpha-helical proteins. *Proc Natl Acad Sci U S A* **1982** *79*(15): 4545-4549.
135. Guerra-Castellano, A.; Diaz-Moreno, I., et al. Structural and functional characterization of phosphomimetic mutants of cytochrome c at threonine 28 and serine 47. *Biochim Biophys Acta* **2016** *1857*(4): 387-395. 10.1016/j.bbabio.2016.01.011
136. Luwang, J. W. and Natesh, R. Phosphomimetic Mutation Destabilizes the Central Core Domain of Human p53. *IUBMB Life* **2018** *70*(10): 1023-1031. 10.1002/iub.1914
137. Pecina, P.; Borisenko, G. G., et al. Phosphomimetic substitution of cytochrome C tyrosine 48 decreases respiration and binding to cardiolipin and abolishes ability to trigger downstream caspase activation. *Biochemistry* **2010** *49*(31): 6705-6714. 10.1021/bi100486s
138. Loughery, J.; Cox, M., et al. Critical role for p53-serine 15 phosphorylation in stimulating transactivation at p53-responsive promoters. *Nucleic Acids Res* **2014** *42*(12): 7666-7680. 10.1093/nar/gku501
139. Theillet, F. X.; Rose, H. M., et al. Site-specific NMR mapping and time-resolved monitoring of serine and threonine phosphorylation in reconstituted kinase reactions and mammalian cell extracts. *Nat Protoc* **2013** *8*(7): 1416-1432. 10.1038/nprot.2013.083
140. Gokirmak, T.; Denison, F. C., et al. Phosphomimetic mutation of a conserved serine residue in Arabidopsis thaliana 14-3-3omega suggests a regulatory role of phosphorylation in dimerization and target interactions. *Plant Physiol Biochem* **2015** *97*: 296-303. 10.1016/j.plaphy.2015.10.022

141. Cheng, Q.; Chen, L., et al. ATM activates p53 by regulating MDM2 oligomerization and E3 processivity. *EMBO J* **2009** *28*(24): 3857-3867. 10.1038/emboj.2009.294
142. Cheng, Q.; Cross, B., et al. Regulation of MDM2 E3 ligase activity by phosphorylation after DNA damage. *Mol Cell Biol* **2011** *31*(24): 4951-4963. 10.1128/MCB.05553-11
143. Nakamizo, A.; Amano, T., et al. Phosphorylation of Thr18 and Ser20 of p53 in Ad-p53-induced apoptosis. *Neuro Oncol* **2008** *10*(3): 275-291. 10.1215/15228517-2008-015
144. Sato, Y.; Kamura, T., et al. Degradation of phosphorylated p53 by viral protein-ECS E3 ligase complex. *PLoS Pathog* **2009** *5*(7): e1000530. 10.1371/journal.ppat.1000530
145. Nielsen, J. T. and Mulder, F. A. A. POTENCI: prediction of temperature, neighbor and pH-corrected chemical shifts for intrinsically disordered proteins. *J Biomol NMR* **2018** *70*(3): 141-165. 10.1007/s10858-018-0166-5
146. Jane Dyson, H. and Ewright, P. (2002). Insights into the structure and dynamics of unfolded proteins from nuclear magnetic resonance. Advances in Protein Chemistry, Academic Press. **62:** 311-340.
147. Borcherds, W. M. and Daughdrill, G. W. Using NMR Chemical Shifts to Determine Residue-Specific Secondary Structure Populations for Intrinsically Disordered Proteins. *Methods Enzymol* **2018** *611*: 101-136. 10.1016/bs.mie.2018.09.011
148. Camilloni, C.; De Simone, A., et al. Determination of secondary structure populations in disordered states of proteins using nuclear magnetic resonance chemical shifts. *Biochemistry* **2012** *51*(11): 2224-2231. 10.1021/bi3001825
149. Bista, M.; Wolf, S., et al. Transient protein states in designing inhibitors of the MDM2-p53 interaction. *Structure* **2013** *21*(12): 2143-2151. 10.1016/j.str.2013.09.006
150. Chan, J. V.; Ping Koh, D. X., et al. Role of the N-terminal lid in regulating the interaction of phosphorylated MDMX with p53. *Oncotarget* **2017** *8*(68): 112825-112840. 10.18632/oncotarget.22829
151. McCoy, M. A.; Gesell, J. J., et al. Flexible lid to the p53-binding domain of human Mdm2: implications for p53 regulation. *Proc Natl Acad Sci U S A* **2003** *100*(4): 1645-1648. 10.1073/pnas.0334477100
152. Pierce, M. M.; Raman, C. S., et al. Isothermal titration calorimetry of protein-protein interactions. *Methods* **1999** *19*(2): 213-221. 10.1006/meth.1999.0852
153. Rajarathnam, K. and Rosgen, J. Isothermal titration calorimetry of membrane proteins - progress and challenges. *Biochim Biophys Acta* **2014** *1838*(1 Pt A): 69-77. 10.1016/j.bbamem.2013.05.023
154. Fraser, J. A.; Madhumalar, A., et al. A novel p53 phosphorylation site within the MDM2 ubiquitination signal: II. a model in which phosphorylation at SER269 induces a mutant conformation to p53. *J Biol Chem* **2010** *285*(48): 37773-37786. 10.1074/jbc.M110.143107
155. Lu, M.; Breyssens, H., et al. Restoring p53 Function in Human Melanoma Cells by Inhibiting MDM2 and Cyclin B1/CDK1-Phosphorylated Nuclear iASPP. *Cancer Cell* **2016** *30*(5): 822-823. 10.1016/j.ccell.2016.09.019
156. Freyer, M. W. and Lewis, E. A. Isothermal titration calorimetry: experimental design, data analysis, and probing macromolecule/ligand binding and kinetic interactions. *Methods Cell Biol* **2008** *84*: 79-113. 10.1016/S0091-679X(07)84004-0

157. Pise-Masison, C. A.; Radonovich, M., et al. Phosphorylation of p53: a novel pathway for p53 inactivation in human T-cell lymphotropic virus type 1-transformed cells. *J Virol* **1998** *72*(8): 6348-6355.
158. Sakaguchi, K.; Saito, S., et al. Damage-mediated phosphorylation of human p53 threonine 18 through a cascade mediated by a casein 1-like kinase. Effect on Mdm2 binding. *J Biol Chem* **2000** *275*(13): 9278-9283.
159. Schon, O.; Friedler, A., et al. Molecular mechanism of the interaction between MDM2 and p53. *J Mol Biol* **2002** *323*(3): 491-501.
160. Yadahalli, S.; Neira, J. L., et al. Kinetic and thermodynamic effects of phosphorylation on p53 binding to MDM2. *Sci Rep* **2019** *9*(1): 693. 10.1038/s41598-018-36589-5
161. Vega, F. M.; Sevilla, A., et al. p53 Stabilization and accumulation induced by human vaccinia-related kinase 1. *Mol Cell Biol* **2004** *24*(23): 10366-10380. 10.1128/MCB.24.23.10366-10380.2004
162. Dornan, D. and Hupp, T. R. Inhibition of p53-dependent transcription by BOX-I phospho-peptide mimetics that bind to p300. *EMBO Rep* **2001** *2*(2): 139-144. 10.1093/embo-reports/kve025
163. Romanova, L. Y.; Willers, H., et al. The interaction of p53 with replication protein A mediates suppression of homologous recombination. *Oncogene* **2004** *23*(56): 9025-9033. 10.1038/sj.onc.1207982
164. Natan, E.; Baloglu, C., et al. Interaction of the p53 DNA-binding domain with its n-terminal extension modulates the stability of the p53 tetramer. *J Mol Biol* **2011** *409*(3): 358-368. 10.1016/j.jmb.2011.03.047
165. Taniguchi, Y. and Kawakami, M. Variation in the mechanical unfolding pathway of p53DBD induced by interaction with p53 N-terminal region or DNA. *PLoS One* **2012** *7*(11): e49003. 10.1371/journal.pone.0049003
166. Wu, Y.; Lin, J. C., et al. Phosphorylation of p53 by TAF1 inactivates p53-dependent transcription in the DNA damage response. *Mol Cell* **2014** *53*(1): 63-74. 10.1016/j.molcel.2013.10.031
167. Cai, X. and Liu, X. Inhibition of Thr-55 phosphorylation restores p53 nuclear localization and sensitizes cancer cells to DNA damage. *Proc Natl Acad Sci U S A* **2008** *105*(44): 16958-16963. 10.1073/pnas.0804608105
168. Rajagopalan, S.; Jaulent, A. M., et al. 14-3-3 activation of DNA binding of p53 by enhancing its association into tetramers. *Nucleic Acids Res* **2008** *36*(18): 5983-5991. 10.1093/nar/gkn598
169. Bista, M.; Freund, S. M., et al. Domain-domain interactions in full-length p53 and a specific DNA complex probed by methyl NMR spectroscopy. *Proc Natl Acad Sci U S A* **2012** *109*(39): 15752-15756. 10.1073/pnas.1214176109
170. Muller-Tiemann, B. F.; Halazonetis, T. D., et al. Identification of an additional negative regulatory region for p53 sequence-specific DNA binding. *Proc Natl Acad Sci U S A* **1998** *95*(11): 6079-6084. 10.1073/pnas.95.11.6079
171. Mittag, T.; Orlicky, S., et al. Dynamic equilibrium engagement of a polyvalent ligand with a single-site receptor. *Proc Natl Acad Sci U S A* **2008** *105*(46): 17772-17777. 10.1073/pnas.0809222105
172. Wang, Y.; Schwedes, J. F., et al. Interaction of p53 with its consensus DNA-binding site. *Mol Cell Biol* **1995** *15*(4): 2157-2165. 10.1128/mcb.15.4.2157

Appendix A – Chemical shifts

Table 1A – Human p53 Wild Type

Residue	AA	CA shift	CB	CO shift	H Shift	N shift
1	M	55.5549	32.8283	175.8920	8.4050	121.4550
2	E	56.1329	30.5079	176.0453	8.3590	122.0190
3	E	54.2873	29.9025	0.0000	8.3760	123.4590
4	P	63.1199	32.1065	176.8751	0.0000	0.0000
5	Q	55.5666	29.8545	175.9810	8.5180	120.9510
6	S	58.1317	63.9449	173.7434	8.3390	117.6980
7	D	52.1294	41.2609	0.0000	8.3920	123.6550
8	P	63.6422	32.1236	177.0966	0.0000	0.0000
9	S	58.9036	63.7779	174.5165	8.4890	116.0160
10	V	61.8362	32.8747	175.7947	7.8290	121.0680
11	E	54.1899	29.7722	0.0000	8.2970	126.1130
12	P	0.0000	0.0000	0.0000	0.0000	0.0000
13	P	62.7182	31.9914	176.9181	0.0000	0.0000
14	L	55.3225	42.4125	177.5845	8.3030	122.4360
15	S	58.0781	63.7501	174.5974	8.2890	116.6600
16	Q	55.9466	29.5310	176.0104	8.4560	122.4920
17	E	56.9176	30.8347	176.5730	8.4370	121.9240
18	T	61.9389	69.7908	174.3486	8.0680	114.8930
19	F	58.0296	39.3997	175.8600	8.2000	122.2970
20	S	58.5535	63.7912	174.4514	8.0640	116.7370
21	D	54.8357	40.7647	176.8248	8.2400	122.1210
22	L	56.4631	41.8072	177.9919	7.9090	121.1440
23	W	57.6586	28.9451	176.6936	7.8160	119.3610
24	K	56.8525	32.8760	176.1503	7.5510	120.4940
25	L	54.8878	42.2861	177.0305	7.7900	120.7780
26	L	53.0063	41.5285	0.0000	7.8810	123.6980
27	P	63.6032	31.9833	177.4341	0.0000	0.0000
28	E	57.0527	29.8791	176.3449	8.6660	119.8080
29	N	53.1270	38.9596	174.7611	8.2490	118.8430
30	N	53.3153	39.0797	174.8766	8.2520	119.5640
31	V	62.4529	32.6242	176.0100	7.9950	120.1720
32	L	54.9271	42.3621	177.0500	8.2470	125.5200
33	S	56.1472	63.3320	0.0000	8.1810	118.0820
34	P	62.9133	32.1037	176.7157	0.0000	0.0000

Table 1A – Human p53 Wild Type (Continued)						
35	L	53.1110	41.6515	0.0000	8.2640	123.7120
36	P	62.9888	32.0416	177.0251	0.0000	0.0000
37	S	58.4488	63.7418	174.6916	8.3000	115.6800
38	Q	55.8041	29.6244	175.5471	8.3400	122.2140
39	A	52.3593	19.3351	177.8114	8.2730	125.2000
40	M	55.5628	32.9049	176.2111	8.2930	119.5410
41	D	54.7256	41.1854	176.1620	8.2180	121.0120
42	D	54.7016	41.0435	176.3868	8.2030	120.1970
43	L	55.4983	42.2339	177.3530	8.0440	121.7310
44	M	55.2107	32.4942	175.8877	8.2130	120.3470
45	L	54.9340	42.6288	177.0532	8.0470	123.1500
46	S	56.0322	63.4948	0.0000	8.4830	118.4350
47	P	63.7181	32.0723	176.9795	0.0000	0.0000
48	D	54.8233	41.1136	176.2168	8.1780	118.8120
49	D	54.6058	41.1968	176.3324	8.0590	120.2100
50	I	61.5962	38.8230	176.4156	7.8120	120.1620
51	E	56.9733	29.9328	176.5569	8.3030	123.7100
52	Q	55.8450	29.5814	175.4430	8.1030	120.3870
53	W	57.1601	29.7164	175.6880	7.9380	121.4910
54	F	57.4842	39.8114	175.3456	7.9400	121.4910
55	T	61.4502	69.9034	173.7619	7.9510	116.2660
56	E	56.1628	30.6199	175.7194	8.2630	123.3580
57	D	52.3353	41.1181	0.0000	8.4000	123.3850
58	P	63.2741	32.2276	177.3178	0.0000	0.0000
59	G	44.5121	0.0000	0.0000	8.3640	109.3270
60	P	63.3628	32.1500	177.0459	0.0000	0.0000
61	D	54.4774	41.0237	176.1261	8.4080	119.8830
62	E	56.0845	30.6590	175.7700	8.0740	120.8390
63	A	50.6220	18.0453	0.0000	8.2270	126.5980
64	P	62.9293	32.0587	176.0104	0.0000	0.0000
65	R	55.8240	30.6872	176.2645	8.4210	121.8890
66	M	53.1630	32.3271	0.0000	8.4400	123.2890
67	P	63.1438	32.0490	176.8751	0.0000	0.0000
68	E	56.4809	30.2332	176.1276	8.5010	121.2070
69	A	52.1209	19.4111	176.9439	8.2640	125.3780
70	A	50.3454	18.1255	0.0000	8.1800	124.8270
71	P	62.9539	32.1336	176.6934	0.0000	0.0000
72	R	56.0627	30.7927	175.5250	8.4420	122.4720
73	V	63.4363	33.3602	0.0000	7.7080	125.5260

Table 1B – p53 S15D

Residue	AA	CA shift	CB	CO shift	H Shift	N shift
1	M	55.6317	32.8530	175.9221	8.3819	121.6523
2	E	56.3124	30.6644	176.1178	8.3439	122.2042
3	E	54.3240	30.1297	0.0000	8.3575	123.6495
4	P	63.0]254	32.0597	176.9554	8.4759	121.0912
5	Q	55.5683	29.6354	176.0171	8.4942	121.1277
6	S	58.2754	64.0893	175.9202	8.3160	117.8762
7	D	52.3624	41.2986	0.0000	8.3768	123.7141
8	P	63.2222	32.2351	177.1384	8.4682	116.2152
9	S	58.9853	63.8122	174.5622	8.4600	116.2307
10	V	61.8579	32.8831	175.8122	7.8265	121.2980
11	E	54.1845	29.6852	0.0000	8.2832	126.3405
12	P	0.0000	0.0000	0.0000	0.0000	0.0000
13	P	62.6227	32.1412	176.9460	8.2903	122.7895
14	L	55.3491	42.6884	177.3523	8.2933	122.7971
15	D	54.2322	41.0524	176.2041	8.3089	121.2192
16	Q	56.2004	29.6557	176.2166	8.2303	120.7265
17	E	57.2989	30.1847	176.8222	8.4497	122.0345
18	T	62.1783	69.7326	174.4750	8.0251	114.9600
19	F	58.1232	39.3800	175.9093	8.1524	122.3981
20	S	58.7939	63.8317	174.5242	8.0189	116.9350
21	D	54.9757	40.7664	176.8545	8.2344	122.2833
22	L	56.5411	41.8248	178.0463	7.8790	121.2964
23	W	57.9051	28.9436	176.7392	7.7833	119.4899
24	K	56.8990	32.7819	176.2130	7.5143	120.6415
25	L	54.8114	42.3063	177.0562	7.7646	120.8973
26	L	53.1322	41.4376	0.0000	7.8560	123.8893
27	P	63.6307	31.9960	177.4575	8.6511	119.9644
28	E	57.0817	29.8770	176.3875	8.6426	119.9716
29	N	53.2458	39.0609	174.8292	8.2214	119.0291
30	N	53.3321	39.1180	174.8955	8.2191	119.7639
31	V	62.5887	32.6221	176.0752	7.9729	120.3817
32	L	54.9579	42.3729	177.0554	8.2218	125.7496
33	S	56.2565	63.2711	0.0000	8.1680	118.2827
34	P	62.8357	32.1011	176.7423	8.2515	123.9002
35	L	53.2311	41.5684	0.0000	8.2432	123.9011
36	P	63.1014	32.1475	177.0680	8.2861	115.8621
37	S	58.5003	63.8341	174.7173	8.2860	115.8637
38	Q	55.8582	29.7038	175.5405	8.3172	122.4035
39	A	52.2456	19.1784	177.8414	8.2462	125.4032

Table 1B – p53 S15D (Continued)						
40	M	55.5839	32.8940	176.2490	8.2745	119.7301
41	D	54.8536	41.3199	176.2204	8.1935	121.1981
42	D	54.6119	40.9724	176.4379	8.1769	120.3699
43	L	55.5275	42.3984	177.3941	8.0291	121.8829
44	M	55.6008	32.6019	175.9193	8.1858	120.5140
45	L	55.0466	42.7556	177.0919	8.0348	123.3578
46	S	56.1416	63.5888	0.0000	8.4580	118.6195
47	P	63.7780	32.0618	176.9902	8.1961	118.9957
48	D	54.9431	41.1265	176.2669	8.1536	119.0033
49	D	54.6060	41.2433	176.3793	8.0372	120.3712
50	I	61.6119	38.9424	176.4557	7.7866	120.3351
51	E	57.0055	30.0844	176.5885	8.2822	123.9294
52	Q	55.7513	29.6656	175.5834	8.0917	120.5804
53	W	57.0659	29.8527	175.5834	7.9417	121.6536
54	F	57.3451	39.8385	175.3647	7.9168	121.6812
55	T	61.4757	69.9499	173.8174	7.9303	116.4534
56	E	56.1731	30.6699	173.7805	8.2410	123.5358
57	D	52.2444	41.1502	0.0000	8.3760	123.7159
58	P	63.3180	32.3569	177.3644	8.3388	109.4867
59	G	44.6275	0.0000	0.0000	8.3389	109.4813
60	P	63.5046	32.2003	177.1036	8.3874	120.0506
61	D	54.4874	41.0426	176.2251	8.3795	120.0538
62	E	56.1031	30.6886	175.7879	8.0461	120.9836
63	A	50.7412	18.1648	0.0000	8.2138	126.7629
64	P	63.0309	32.2621	176.8134	8.4013	122.0626
65	R	55.8704	30.9769	176.2764	8.3990	122.0546
66	M	53.1953	32.1621	0.0000	8.4283	123.4799
67	P	63.0857	32.1011	176.9158	8.4914	121.3346
68	E	56.7174	30.4539	176.1391	8.4782	121.3757
69	A	52.6805	19.4819	176.9609	8.2473	125.5366
70	A	50.4653	18.1598	0.0000	8.1536	125.0023
71	P	62.9392	32.1553	176.7163	8.4202	122.6271
72	R	56.1010	30.8122	175.5538	8.4176	122.6256
73	V	63.4674	33.4683	175.5538	7.6823	125.6816

Table 1C – p53 S15D/T18E

Residue	AA	CA shift	CB	CO shift	H Shift	N shift
1	M	55.5759	32.8942	176.5813	8.4053	121.6560
2	E	56.9143	30.3367	176.0278	8.3573	121.8903
3	E	54.3624	29.8946	0.0000	8.3810	123.6270

Table 1C – p53 S15D/T18E (Continued)						
4	P	63.2092	32.1621	176.9054	8.5079	121.3330
5	Q	55.6055	29.7775	176.0111	8.5236	121.1393
6	S	58.2137	64.0286	173.7677	8.3477	117.8835
7	D	52.3141	41.2364	0.0000	8.4058	123.7205
8	P	63.1625	32.1954	177.1259	8.4848	116.2152
9	S	58.9220	63.8532	174.5537	8.4876	116.2493
10	V	61.8930	32.9347	175.7988	7.8566	121.3188
11	E	54.2153	29.8140	0.0000	8.3116	126.3514
12	P	0.0000	0.0000	0.0000	0.0000	0.0000
13	P	62.6451	32.0700	176.9227	8.3108	122.8046
14	L	55.2673	42.6387	177.3211	8.3109	122.8138
15	D	54.3282	41.1263	177.3903	8.3528	121.2442
16	Q	55.9667	29.7780	176.0484	8.2377	120.5328
17	E	57.0326	30.5836	175.8992	8.4439	122.5301
18	E	56.9301	30.2227	176.3155	8.3379	121.6576
19	F	57.7728	39.3666	175.8913	8.1571	120.7913
20	S	58.7541	63.9510	174.6163	8.0232	117.0966
21	D	54.8938	40.7752	176.8904	8.3206	122.2908
22	L	56.6247	41.8402	178.0820	7.9088	121.2736
23	W	57.7376	28.9727	176.7851	7.8094	119.4128
24	K	56.9792	32.9237	176.2310	7.5378	120.6317
25	L	54.9296	42.3376	177.0612	7.7797	120.8537
26	L	53.0833	41.5550	0.0000	7.8776	123.9104
27	P	63.6788	32.0330	177.4574	8.6836	119.9638
28	E	57.1234	29.9175	176.3876	8.6836	119.9753
29	N	53.1784	39.0220	174.8122	8.2496	119.0426
30	N	53.3626	39.1594	174.8802	8.2492	119.7817
31	V	62.5412	32.6703	176.0746	8.0054	120.4195
32	L	54.9798	42.4052	177.0488	8.2591	125.7796
33	S	56.2147	63.3950	0.0000	8.1973	118.3095
34	P	62.9634	32.1512	176.7336	8.2782	123.9259
35	L	53.1828	41.7080	0.0000	8.2782	123.9193
36	P	63.1295	32.0889	177.0582	8.3120	115.8882
37	S	58.5153	63.7599	176.5813	8.3114	115.8743
38	Q	55.8474	29.6418	175.4731	8.3496	122.4117
39	A	52.2397	19.4542	177.8320	8.2702	125.5554
40	M	55.6439	32.9410	176.2471	8.3018	119.7407
41	D	54.7918	41.2685	176.1961	8.2243	121.2161
42	D	54.7263	41.1094	176.4347	8.2067	120.3840
43	L	55.5401	42.2717	176.1961	8.0268	121.9045

Table 1C – p53 S15D/T18E (Continued)						
44	M	55.4574	32.5493	175.8948	8.2183	120.5232
45	L	54.9907	42.6903	177.0836	8.0556	123.3573
46	S	56.0899	63.5294	0.0000	8.4884	118.6302
47	P	63.7990	32.1105	176.9810	8.1827	119.0138
48	D	54.8901	41.1863	176.2565	8.1830	119.0135
49	D	54.6444	41.2831	176.3542	8.0614	120.3773
50	I	61.6508	38.8872	176.4503	7.8164	120.3435
51	E	57.0440	30.0383	176.5611	8.3121	123.9353
52	Q	55.8800	29.6122	175.5687	8.1107	120.5886
53	W	57.1457	29.8022	175.5687	7.9458	121.6931
54	F	56.9800	39.8785	175.3624	7.9171	121.7278
55	T	61.5081	69.9886	173.8034	7.9570	116.4460
56	E	56.2116	30.7088	173.7677	8.2690	123.5427
57	D	52.3440	41.1546	0.0000	8.4066	123.7159
58	P	63.3500	32.3173	177.3464	8.3677	109.4829
59	G	44.5668	0.0000	0.0000	8.3678	109.4862
60	P	63.4361	32.2378	177.1033	8.4107	120.0724
61	D	54.5390	41.0833	176.1558	8.4098	120.0678
62	E	56.1432	30.7340	175.7813	8.0778	120.9956
63	A	50.6853	18.1082	0.0000	8.2369	126.7709
64	P	62.9652	32.1125	176.7963	8.4271	122.0722
65	R	55.8119	31.0080	176.2755	8.4274	122.0635
66	M	53.2411	32.4045	0.0000	8.4484	123.4874
67	P	63.1348	32.1111	176.8752	8.4850	121.4702
68	E	56.5725	30.4053	175.9484	8.5042	121.3860
69	A	52.4789	19.2970	176.9558	8.2464	125.5947
70	A	50.4086	18.2132	0.0000	8.1882	125.0054
71	P	62.9724	32.1772	176.6941	8.4465	122.6306
72	R	56.0754	30.5836	175.5500	8.4460	122.6031
73	V	63.4998	33.4098	0.0000	7.7120	125.6873

Table 1D – p53 T55D-ND

Residue	AA	CA	CB	CO shift	H Shift	N shift
1	M	55.4517	32.7861	176.0050	8.2932	121.8182
2	E	56.3875	30.4846	176.1178	8.2932	121.8182
3	E	54.2631	29.8224	0.0000	8.3498	123.5811
4	P	63.1631	32.0694	176.9083	8.5239	121.2200
5	Q	55.5455	29.8026	176.0005	8.5254	121.2528
6	S	58.1632	63.9651	173.7503	8.3496	117.9274
7	D	52.1602	41.2686	0.0000	8.4037	123.8319

Table 1D – p53 T55D-ND (Continued)						
8	P	63.1067	63.7744	177.1218	8.4934	116.2845
9	S	58.9151	32.0991	174.5291	8.4924	116.2361
10	V	61.8308	32.8744	175.7957	7.8345	121.2805
11	E	54.1593	29.7686	0.0000	8.3037	126.3371
12	P	0.0000	0.0000	0.0000	0.0000	0.0000
13	P	62.6923	31.9915	176.9129	8.3154	122.6356
14	L	55.2642	42.4140	177.6257	8.3154	122.6334
15	S	58.0875	63.7757	0.0000	8.3009	116.8773
16	Q	55.5703	29.5151	174.6754	8.4586	122.1492
17	E	56.9282	30.1763	176.5902	8.0739	115.0841
18	T	61.9947	69.7958	174.3922	8.0834	115.1243
19	F	57.9948	39.4026	175.8928	8.2162	122.4599
20	S	58.6935	63.7750	174.4911	8.0764	116.8453
21	D	54.8460	40.7541	176.8545	8.2445	122.3319
22	L	56.5207	41.8092	178.0132	7.9131	121.3415
23	W	57.7139	28.9263	176.7392	7.8210	119.5116
24	K	56.8795	32.8641	176.1467	7.5520	120.6033
25	L	54.8951	42.2994	177.0328	7.7961	120.8960
26	L	53.0168	41.5200	0.0000	7.8775	123.8462
27	P	63.6478	31.9767	177.4575	8.6755	119.9918
28	E	57.0687	29.8365	176.3378	8.6759	119.9927
29	N	53.3382	39.0861	174.7961	8.2507	119.6536
30	N	53.3612	39.1175	174.8789	7.9953	120.2934
31	V	62.4952	32.5907	176.0997	7.9963	120.3101
32	L	54.9439	42.3514	177.0720	8.2489	125.5905
33	S	56.1395	63.3798	0.0000	8.1812	118.2264
34	P	62.9403	32.0740	176.6926	8.2657	123.9022
35	L	53.0983	41.6808	0.0000	8.2667	123.8959
36	P	63.0887	32.0233	177.0680	8.3052	115.8557
37	S	58.5203	63.7339	174.7339	8.3054	115.8300
38	Q	55.8769	29.6167	175.5902	8.3511	122.4183
39	A	52.6381	19.2319	177.8414	8.2627	125.2154
40	M	55.6146	32.8667	176.2656	8.2837	119.6583
41	D	54.7939	41.2005	176.2204	8.2175	121.1681
42	D	54.7599	41.0293	176.4361	8.1984	120.5382
43	L	55.5275	42.2176	177.3941	8.0465	121.8275
44	M	55.7924	32.5130	175.9028	8.1928	120.3584
45	L	54.9083	42.6674	177.0257	8.0436	123.0987
46	S	56.0603	63.5421	0.0000	8.4901	118.5967
47	P	63.9587	32.0358	176.9736	8.1791	118.6718
48	D	54.8729	41.1303	176.2338	8.1821	118.8234
49	D	54.6756	41.2441	176.3414	8.0407	120.3801

Table 1D – p53 T55D-ND (Continued)						
50	I	61.5484	38.7560	0.0000	7.7883	120.0346
51	E	0.0000	0.0000	0.0000	0.0000	0.0000
52	Q	0.0000	0.0000	0.0000	0.0000	0.0000
53	W	0.0000	0.0000	0.0000	0.0000	0.0000
54	F	0.0000	0.0000	0.0000	0.0000	0.0000
55	D	0.0000	0.0000	0.0000	0.0000	0.0000
56	E	56.2738	30.4521	173.7640	8.3914	125.2787
57	D	52.8731	41.6391	0.0000	8.3908	125.2900
58	P	63.2830	32.2518	177.3772	8.3589	109.3980
59	G	44.5270	0.0000	0.0000	8.3571	109.4295
60	P	63.4222	32.1642	177.0539	8.4098	120.0027
61	D	54.5204	41.0166	176.1146	8.4098	120.0099
62	E	56.0812	30.6528	175.7382	8.0624	120.7982
63	A	50.6403	18.0868	0.0000	8.2205	126.5899
64	P	62.9159	32.0552	176.7803	8.4285	122.0211
65	R	56.0802	30.9347	176.2764	8.4277	122.0497
66	M	53.1786	32.3284	0.0000	8.4243	123.2581
67	P	63.1631	32.1159	176.9324	8.5239	121.2200
68	E	56.5531	30.2673	176.1060	8.5128	121.1395
69	A	52.2006	19.3874	176.9720	8.2359	125.2833
70	A	50.2803	18.3030	0.0000	8.1866	124.8840
71	P	62.7443	32.0546	176.0428	8.4285	122.0497
72	R	55.9999	30.9141	176.2500	8.4318	122.0497
73	V	61.7556	33.0281	175.3162	8.1255	121.8309
74	A	50.3374	18.3284	0.0000	8.3623	129.7156
75	P	0.0000	0.0000	0.0000	0.0000	0.0000
76	A	0.0000	0.0000	0.0000	0.0000	0.0000
77	P	0.0000	0.0000	0.0000	0.0000	0.0000
78	A	0.0000	0.0000	0.0000	0.0000	0.0000
79	A	0.0000	0.0000	0.0000	0.0000	0.0000
80	P	62.9309	31.9967	176.7947	8.2308	117.2088
81	T	59.6711	69.7505	0.0000	8.2321	117.2526
82	P	62.9429	32.0551	176.5149	8.3056	124.6722
83	A	52.1501	19.3549	177.0134	8.3040	124.6594
84	A	50.3671	18.2195	0.0000	8.1508	124.7676
85	P	62.6749	32.0710	176.2629	8.3173	125.9032
86	A	50.3119	18.1438	0.0000	8.3182	125.9082